A New Approach in Computational Contact Mechanics: The Contact Domain Method

X. Oliver
S. Hartmann
J.C. Cante
R. Weyler
J.A. Hernández

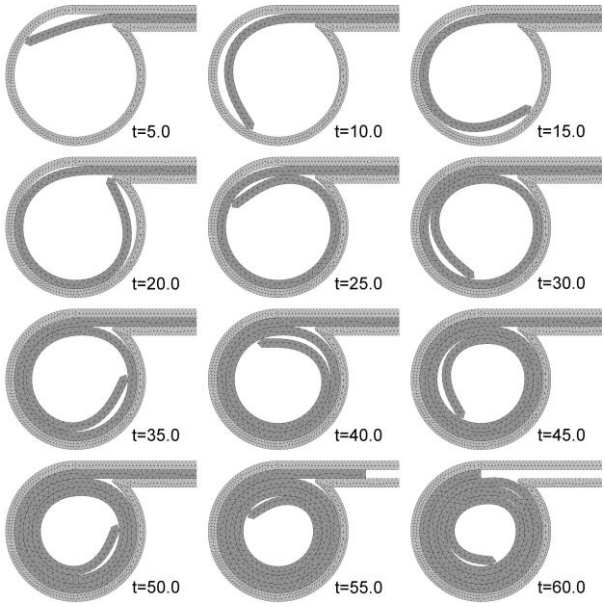

Monograph CIMNE Nº-112, February 2009

A New Approach in Computational Contact Mechanics: The Contact Domain Method

X. Oliver[1]
S. Hartmann[1]
J.C. Cante[2]
R. Weyler[2]
J.A. Hernández[1]

[1]E.T.S. d'Enginyers de Camins, Canals i Ports and
[2]E.T.S. d'Enginyería Industrial i Aeronáutica de Terrassa,
Technical University of Catalonia (UPC)
Campus Nord UPC, Mòdul C-1, c/Jordi Girona 1-3,
08034 Barcelona, Spain

Monograph CIMNE Nº 112, February 2009

INTERNATIONAL CENTER FOR NUMERICAL METHODS IN ENGINEERING
Gran Capitán s/n, 08034 Barcelona, España

INTERNATIONAL CENTER FOR NUMERICAL METHODS IN ENGINEERING
Edificio C1, Campus Norte UPC
Gran Capitán s/n
08034 Barcelona, Spain
www.cimne.upc.es

First edition: February 2009

A NEW APPROACH IN COMPUTATIONAL CONTACT MECHANICS: THE CONTACT DOMAIN METHOD
Monograph CIMNE M112

ISBN: 978-84-96736-62-7

Dep. legal: B-XXXXX-2009

PART 1: THEORETICAL BASIS

Abstract: *This first part of the work presents the theoretical aspects of a new approach to solve two-dimensional large-strain problems in computational contact mechanics. The basic elements of the proposed method are: 1) the use of an updated Lagrangean approach to describe the motion of the contacting bodies, 2) consideration of a two-dimensional contact domain, where the contact/friction restrictions are imposed, and construction of a one layer triangulation in this domain, 3) resorting to a Lagrange multiplier method to impose the contact/friction constraints , 4) an interior penalty procedure, allowing condensation of the Lagrange multipliers, ensuring the stability of the discretized problem and 5) an active set strategy, for determining the subsets of the contact domain were contact/friction conditions have to be applied, based on the concept of effective gaps as suitable entities for extrapolation and prediction purposes.*

Keywords: contact mechanics, domain method, Lagrange multipliers, interior penalty method, effective gaps

1. MOTIVATION

Despite the substantial progress achieved in the last years, simulating technical problems involving contact of various deformable parts is still a challenge in computational contact mechanics. In fact, if we consider the basic two stages of contact/friction algorithms [38] namely: a) the search for the contacting entities in the contacting bodies (contact/friction detection) and b) the imposition of the contact/friction constraints, both stages are highly nonlinear and this results in large computability difficulties in terms of robustness and computational costs. In the following, they are briefly sketched.

One of the main challenges facing contact problems is the nonlinearity induced by the fact that the contacting pairs are not known a priori, which has led to various contributions only focusing on the aspect of contact searching algorithms (e.g. [2], [26], [42], [43], [41], [7], [46], [37]). *Contact/friction* detection is there solved via spatial search algorithms, like grid cells and quadtree/octree search algorithms [38]. In them, a certain number of candidates to become contacted entities (master entities) are compared, in terms of their geometrically position, with another set of candidates to become contacting entities (slave entities). Then, they are paired, at every considered time of the analysis, as candidates to exert mutual contact or friction. When the number of those entities becomes large, as it occurs, for instance, in problems involving many contacting bodies or in general 3D problems, the computational cost involved in those searches can become so large as to make the computational cost unaffordable.

Once the involved entities are determined and paired, some corresponding geometric constraints have to be imposed, namely:

$$g_N^{(i)}(\mathbf{u}) = 0 \quad ; \quad \mathbf{g}_T^{(i)}(\mathbf{u}) = \mathbf{0} \qquad i = (1...n_{pair}) \rightarrow \mathbf{g}(\mathbf{u}) = \mathbf{0} \tag{1}$$

where $\mathbf{u}$ are the displacements of the contacting bodies, N and T stand, respectively, for the normal and tangential associated directions and i stands for one of the n_{pair} pairs of constrained entities grouped in the vector of constraints $\mathbf{g}(\mathbf{u})$.

Here we can distinguish two large families of solution methods that, in turn, give rise to a number of branches, i.e.:

1. *Penalty methods*: the contact/friction constraints, $\mathbf{g}(\mathbf{u}) = \mathbf{0}$ are imposed, at the contacting boundary $\Gamma_{cont.}$, via penalization in a minimizing functional, as

$$\begin{aligned} &\delta\tilde{\Pi}(\mathbf{u}) = \delta[\Pi(\mathbf{u}) + \int_{\Gamma_{cont.}} \frac{1}{2}\varepsilon\left[\mathbf{g}(\mathbf{u})\right]^2 d\Gamma] = 0 \rightarrow \\ &\rightarrow \mathbf{R}(\mathbf{u}) \equiv \mathbf{F}_{\text{int}}(\mathbf{u}) - \mathbf{F}_{ext} + \mathbf{F}_{cont}(\varepsilon\mathbf{g}(\mathbf{u})) = \mathbf{0} \end{aligned} \tag{2}$$

where $\Pi(\mathbf{u})$ and $\tilde{\Pi}(\mathbf{u})$ are, respectively, the original and the penalized minimizing functionals, ε stands for the appropriate set of penalty values, $\mathbf{R}(\mathbf{u})$ are the corresponding residual forces, obtained after the minimization process and the subsequent discretization procedures, and $\mathbf{F}_{\text{int}}$, $\mathbf{F}_{ext}$ and $\mathbf{F}_{cont}$ stand, respectively, for the internal forces, the external forces and the contact forces acting on the contacting bodies. This is a widely used method, because its simplicity and the fact that the number of unknowns of the global problem is not increased by the imposition of the contact/friction restrictions. A negative counterpart is that the effectiveness in the imposition of those constraints relies very much on the appropriate values of the used penalty factors. Either if the stiffness of the contacting bodies is very different or if they evolve along the deformation, finding the correct value of the penalties becomes a tough problem.

2. *Lagrange multiplier methods*: the contact conditions are imposed by introducing new unknowns, the Lagrange multipliers, and new equations in the problem: the contact/friction constraints. The number of Lagrange multipliers is essentially determined by the number of contacting entity pairs. Then, the minimization problem reads:

$$\begin{aligned} &\delta\tilde{\Pi}(\mathbf{u},\boldsymbol{\Lambda}) = \delta[\Pi(\mathbf{u}) + \int_{\Gamma_{cont.}} \boldsymbol{\Lambda}\cdot\mathbf{g}(\mathbf{u})d\Gamma] = 0 \rightarrow \\ &\rightarrow \mathbf{R}(\mathbf{u},\boldsymbol{\Lambda}) \equiv \begin{cases} \mathbf{F}_{\text{int}}(\mathbf{u}) - \mathbf{F}_{ext} + \mathbf{F}_{cont}(\boldsymbol{\Lambda},\mathbf{u}) &= \mathbf{0} \\ \mathbf{F}_{\boldsymbol{\Lambda}}(\mathbf{g}(\mathbf{u})) &= \mathbf{0} \end{cases} \end{aligned} \tag{3}$$

where $\mathbf{R}(\mathbf{u},\boldsymbol{\Lambda})$ is the residual vector, and $\boldsymbol{\Lambda} = \left\{\lambda^{(1)},....,\lambda^{(n_{pair})}\right\}$ is the vector of Lagrange multipliers. In addition, the Hessian of equations (3) has the following structure:

$$\mathbf{K} \equiv \frac{\partial^2\mathbf{R}(\mathbf{u},\boldsymbol{\Lambda})}{\partial\mathbf{u}\otimes\partial\boldsymbol{\Lambda}} = \begin{bmatrix} \mathbf{K}_{uu} & \mathbf{K}_{u\lambda} \\ \mathbf{K}_{\lambda u} & \mathbf{K}_{\lambda\lambda} \end{bmatrix} \equiv \begin{bmatrix} \dfrac{\partial(\mathbf{F}_{\text{int}} + \mathbf{F}_{cont})}{\partial\mathbf{u}} & \dfrac{\partial\mathbf{F}_{cont}}{\partial\boldsymbol{\Lambda}} \\ \dfrac{\partial\mathbf{F}_{\boldsymbol{\Lambda}}}{\partial\mathbf{u}} & \mathbf{0} \end{bmatrix} \tag{4}$$

and, thus, the linearized form of $\mathbf{R}(\mathbf{u},\boldsymbol{\Lambda})$ reads:

$$\mathbf{R}(\mathbf{u}+\Delta\mathbf{u},\boldsymbol{\Lambda}+\Delta\boldsymbol{\Lambda}) = \mathbf{R}(\mathbf{u},\boldsymbol{\Lambda}) + \underbrace{\begin{bmatrix} \mathbf{K}_{uu} & \mathbf{K}_{u\lambda} \\ \mathbf{K}_{\lambda u} & \mathbf{0} \end{bmatrix}}_{\mathbf{K}} \begin{bmatrix} \Delta\mathbf{u} \\ \Delta\boldsymbol{\Lambda} \end{bmatrix} \tag{5}$$

where the Hessian $\mathbf{K}$ in equation (5) is a sparse matrix due to the appearance of matrices $\mathbf{K}_{u\lambda}$ and $\mathbf{K}_{\lambda u}$. In addition, the null character of matrix $\mathbf{K}_{\lambda\lambda}$ precludes direct condensation (elimination) of the unknowns, $\Delta\boldsymbol{\Lambda}$, in equation

(5) in the context of an iterative (Newton-Raphson) procedure to solve the problem. This translates into high computational solution costs, since the extended system in equations (5) is large and sparse. In addition, if the corresponding BBL conditions are not fulfilled [19], it can often translate into instabilities in the results after discretization. These are challenges posed by Lagrange multiplier methods.

Another important aspect is the utilized discretization strategy. Many existing contact formulations developed in the past use a specific collocation method to enforce the contact constraints at some discrete points. The most popular discretization method used for large deformation contact problems is the so-called node-to-segment approach, where a specific node on the *slave side* must not penetrate the opposing *master side* segment. Early applications of this strategy date back to the works of Hughes et al. [20] and Hallquist [12]. On this basis several extensions and generalizations have been proposed (e.g. [13], [40], [2], [21]). Although the node-to-segment discretization approach is quite popular, the lack of robustness of these models is still a limitation in certain applications, especially when large tangential relative displacements come into play. Due to the spatial approximation with finite elements, an unsmooth representation of the real geometry could emerge, having edges between neighboring elements, which will cause jumps in the contact forces once a slave node slides off the contacting master segment. To overcome these deficiencies various smoothing algorithms have been proposed (e.g. [36], [28], [39], [30], [35]).
Due to the aforementioned drawbacks of the node-to-segment discretization strategy, the research for so-called segment-to-segment methods became quite active in recent years. This approach was first introduced by Simo et al. [34] for geometrical linear problems. Similar segment-to-segment formulations have been proposed by Papadopoulos and Taylor [29] as well as Zavarise and Wriggers [45]. Recently many segment-to-segment contact algorithms were proposed on basis of the mortar method, which was originally introduced as a domain decomposition method ([3], [4], [5]). Introducing the continuity condition at the interfaces in integral form, the mortar method has been successfully applied to various large deformation contact problems ([31], [32], [44], [8], [9], [10], [14], [15], [17]). Even though these algorithms preserve optimal convergence rates, they suffer from the quite expensive quadrature problem. As the Lagrange multiplier space is typically defined only on one boundary of the two bodies coming into contact, it is necessary to integrate basis functions defined on two different surface meshes. This leads to a quite expensive search for defining the appropriate contact segments in order to perform the numerical quadrature ([31], [32]).
No matter whether using a node-to-segment or a segment-to-segment contact discretization strategy, nearly all of the proposed methods have in common, that they project somehow one contact-surface/point (*slave*) onto the other contact-surface (*master*), to formulate the necessary contact conditions. Therefore, the contact problem is defined on a subdomain, which is usually one dimension lower than the domain of the contacting bodies.

This work is focused to describe a new approach to computational contact problems intending to overcome the drawbacks of the preceding methodologies. The main elements of the approach are the following:

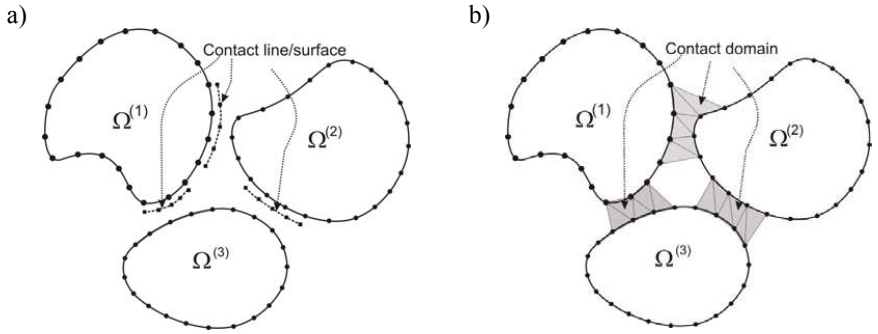

Figure 1: Imposition of contact constraints on the contacting bodies: a) classical method, b) contact domain method

1) An efficient, simple and fast method for pairing the contacting entities. In this sense, the concept of *contact domain*, is introduced as a geometric entity: a manifold with the same dimension than the contacting bodies (i.e.: 2D for two-dimensional bodies and 3D for three-dimensional bodies), which is constructed via a Delaunay triangulation of a single layer [11] taking the nodes placed in the boundary of the contacting bodies as vertices of the triangulation.
2) In order to facilitate the construction and use of this contact domain, *an updated Lagrangean description* [23] *of the motion* of the contacting bodies is used in the mechanical setting.
3) Unlike in more standard procedures, where the contact/friction constrains are imposed on the basis of projections onto manifolds which are one dimension smaller than the contacting bodies (the contact lines/surfaces, see Figure 1a)), the contact/friction constraints are imposed on a manifold of the same dimension than the contacting bodies: the aforementioned contact domain (see Figure 1b)). Thus, the introduction of a Lagrange multiplier space on this contact domain does not lead to the difficulty of integration of products of finite element basis functions on different surface grids.
4) As for the imposition of the contact/friction conditions at the contact domain, a finite element format is adopted and the standard Lagrange multiplier method is modified. By resorting to an *interior penalty procedure* [1], the resulting system (5) is made λ*-solvable* (i.e. allowing condensation of the Lagrange multipliers) in a consistent manner, this resulting in large computability benefits.

In the following, the approach is presented for two-dimensional problems, although no assumption is made in terms of the kinematics. Therefore, full large strains can be undergone by the contacting bodies.

2. GEOMETRICAL ASPECTS

2.1. Geometrical description of the contact domain

Let us consider two contacting bodies whose motion is described by means of an *updated Lagrangean approach* [23]. Let $[t_n, t_{n+1}]$ be the current time interval, of length $\Delta t_{n+1} = t_{n+1} - t_n$, $\Omega_n^{(1)}$ and $\Omega_n^{(2)}$ are the reference (material) configurations, and $\Omega_{n+1}^{(1)}$ and

$\Omega_{n+1}^{(2)}$ are the corresponding spatial configurations. The incremental motion $\boldsymbol{\varphi}_{n+1}$ is then defined by:

$$\begin{aligned} &\boldsymbol{\varphi}_{n+1}(\mathbf{x}_n) : (\Omega_n^{(1)} \cup \Omega_n^{(2)}) \to (\Omega_{n+1}^{(1)} \cup \Omega_{n+1}^{(2)}) \\ &\mathbf{x}_{n+1} = \boldsymbol{\varphi}_{n+1}(\mathbf{x}_n) = \mathbf{x}_n + \mathbf{u}_{n+1} \\ &\mathbf{u}_{n+1} = \boldsymbol{\varphi}_{n+1}(\mathbf{x}_n) - \mathbf{x}_n = \mathbf{x}_{n+1} - \mathbf{x}_n \end{aligned} \tag{6}$$

where $\mathbf{x}_n$ and $\mathbf{x}_{n+1}$ stand, respectively, for the initial (material) and final (spatial) positions (coordinates) of a given particle in the considered time interval, and $\mathbf{u}_{n+1}$ are the corresponding incremental displacements. For the sake of simplicity subscripts $(\bullet)_n$ referring to the reference configuration will be omitted, whenever no confusion is induced, in the subsequent derivations, so that entities with no time subscript will denote material entities associated to time t_n (i.e. $\Omega_n^{(1)}$, $\Omega_n^{(2)}$ will be denoted as $\Omega^{(1)}$, $\Omega^{(2)}$).

Let then $\Omega^{(1)}$ and $\Omega^{(2)}$ be the domains occupied by the bodies at the reference configuration, $\partial\Omega^{(1)}$, $\partial\Omega^{(2)}$ being the corresponding domain boundaries with outward normal $\boldsymbol{\nu}^{(1)}$ and $\boldsymbol{\nu}^{(2)}$, respectively. Let us also consider the so-called *contact domain* D, with boundary, ∂D joining part of the boundaries $\partial\Omega^{(1)}$ and $\partial\Omega^{(2)}$ i.e: $\Gamma_D^{(1)} \subset \partial\Omega^{(1)}$ and $\Gamma_D^{(2)} \subset \partial\Omega^{(2)}$, see Figure 2. We will assume that $\Gamma_D^{(1)}$ and $\Gamma_D^{(2)}$ are *large enough to contain those parts of* $\partial\Omega^{(1)}$ *and* $\partial\Omega^{(2)}$ *that are coming into contact* at the end of the time step.

Let us also consider a local system of orthogonal curvilinear coordinates (N,T) parametrizing the contact domain in such a way that (see Figure 2) :

$$D := \left\{ \mathbf{x}_n(N,T) \mid N^- < N < N^+ \;;\; T^- < T < T^+ \right\} \tag{7}$$

where $N^- - N^+$ and $T^- - T^+$ are measures of the width and the length, respectively, of the contact domain D.

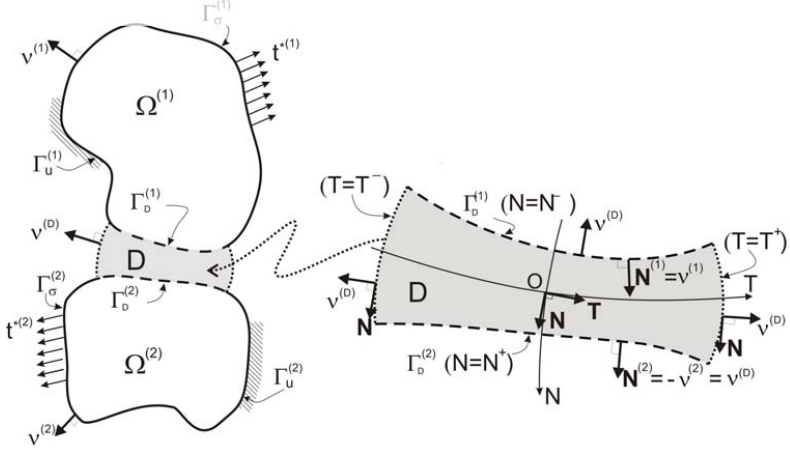

Figure 2: Geometrical definition of the material contact domain, D, between two contacting bodies $\Omega^{(1)}$ and $\Omega^{(2)}$.

Associated to that system of coordinates, one can define the orthogonal unit vectors $\mathbf{N}$ and $\mathbf{T}$, the physical basis of the system, tangent to the coordinate lines at every point and defined through:

$$\mathbf{e}_N = \frac{\partial \mathbf{x}_n(N,T)}{\partial N} \;:\; \mathbf{N} = \frac{\mathbf{e}_N}{\|\mathbf{e}_N\|}$$
$$\mathbf{e}_T = \frac{\partial \mathbf{x}_n(N,T)}{\partial T} \;:\; \mathbf{T} = \frac{\mathbf{e}_T}{\|\mathbf{e}_T\|} \tag{8}$$

The above definitions imply a sense on $\mathbf{N}$ and $\mathbf{T}$. In fact, if $\Omega^{(1)}$ and $\Omega^{(2)}$, are considered, respectively, the *master and the slave contacting bodies,* the sense of $\mathbf{N}$ is defined *as pointing from* $\Gamma_D^{(1)}$ *to* $\Gamma_D^{(2)}$ (see Figure 2.) i.e.:

$$\boldsymbol{\nu}^{(1)}(\mathbf{x}) = \mathbf{N}(\mathbf{x}) \overset{def}{=} \mathbf{N}^{(1)}(\mathbf{x}) \quad \forall \mathbf{x} \in \Gamma_D^{(1)}$$
$$\boldsymbol{\nu}^{(2)}(\mathbf{x}) = -\mathbf{N}(\mathbf{x}) \overset{def}{=} -\mathbf{N}^{(2)}(\mathbf{x}) \quad \forall \mathbf{x} \in \Gamma_D^{(2)} \tag{9}$$

Also for the sake of simplicity, it will be assumed that the curvature of the N and T coordinate lines is small. This is not a relevant restriction in view of the discretized (piecewise linear) geometry endowed to the contact domain D (see Section 5.1 below and REMARK 5-1). In consequence, it will be assumed that:

$$\frac{\partial \mathbf{N}}{\partial N} \approx \mathbf{0} \;;\; \frac{\partial \mathbf{T}}{\partial N} \approx \mathbf{0}$$
$$\frac{\partial \mathbf{N}}{\partial T} \approx \mathbf{0} \;;\; \frac{\partial \mathbf{T}}{\partial T} \approx \mathbf{0} \tag{10}$$

In addition, although the motion $\boldsymbol{\varphi}(\mathbf{x})$, in equation (6), is only defined in the domains $\Omega_n^{(1)} \cup \Omega_n^{(2)}$, we endow the domain D with an extension of the incremental displacement field, $\mathbf{u}_{n+1}^{(D)}$, *for the only purpose of supplying a mathematical expression to the physical entity of the gap* (see Section 2.2). To this end, we assign to the points in the domain D a displacement field, $\mathbf{u}_{n+1}^{(D)}(N,T)$, linearly interpolated in the N direction from the corresponding mechanical displacements at the contacting boundaries: $\mathbf{u}_{n+1}^{(1)}$, at $\Gamma_D^{(1)}$, and $\mathbf{u}_{n+1}^{(2)}$, at $\Gamma_D^{(2)}$, i.e.:

$$\mathbf{x}_{n+1} = \boldsymbol{\varphi}_{n+1}^{(D)}(\mathbf{x}_n) = \mathbf{x}_n + \mathbf{u}_{n+1}^{(D)} \qquad \forall \mathbf{x}_n \in D$$
$$\mathbf{u}_{n+1}^{(D)}(N,T) = A^{(1)}(N)\,\mathbf{u}_{n+1}^{(1)}(T) + A^{(2)}(N)\,\mathbf{u}_{n+1}^{(2)}(T)$$
$$A^{(1)}(N) = \frac{N^+ - N}{N^+ - N^-} \;\;;\;\; A^{(2)}(N) = \frac{N - N^-}{N^+ - N^-} \tag{11}$$

Then, the normal, $u_{N_{n+1}}^{(D)}$, and tangent, $u_{T_{n+1}}^{(D)}$, physical components of the displacement field at D are defined through:

$$\mathbf{u}_{n+1}^{(D)}(N,T) = u_{N_{n+1}}^{(D)}\mathbf{N} + u_{T_{n+1}}^{(D)}\mathbf{T}$$
$$u_{N_{n+1}}^{(D)} = \mathbf{u}_{n+1}^{(D)} \cdot \mathbf{N} \;\;;\;\; u_{T_{n+1}}^{(D)} = \mathbf{u}_{n+1}^{(D)} \cdot \mathbf{T} \tag{12}$$

REMARK 2-1. From the geometrical point of view the contact domain D, defined in equation (7), can be ill defined. Typically, if the two contacting bodies are already in contact at the beginning of the time step (therefore in the reference configuration), then the width measure of the contact domain is null ($N^+ - N^- = 0$). This translates into possible singularities in the

formulation above (for instance in equation (11)). As a way to avoid such singularities a *regularized contact domain,* at the reference configuration, could be assumed in terms of a (very small) positive regularization parameter such that, in the case of initial contact, the minimum width of the contact domain D is made larger than that regularization parameter:

$$\min_{T\in[T^-,T^+]}\left[\int_{N^-}^{N^+} dS(N,T)\right]\geq k>0 \tag{13}$$

However, it can be shown that the final numerical solution procedure of the problem can be made independent of the value of such parameter which can be eventually null (see equations (122), REMARK 5-3 below and section 4.3 in the second part of this work [16]).

2.2. Gap definitions

Let us consider the contact domain, D, at the material configuration, and its convected spatial domain, $D_{n+1}=\boldsymbol{\varphi}_{n+1}^{(D)}(D)$, (see Figure 3), where the corresponding normal/tangent unit vectors, $(\mathbf{n},\mathbf{t})$, and curvilinear coordinate lines are defined. Notice that, by construction, the spatial contacting boundaries $\Gamma_{D_{n+1}}^{(1)}$ and $\Gamma_{D_{n+1}}^{(2)}$ are convected from the material ones ($\Gamma_{D_{n+1}}^{(1)}=\boldsymbol{\varphi}_{n+1}^{(D)}(\Gamma_D^{(1)})$ and $\Gamma_{D_{n+1}}^{(2)}=\boldsymbol{\varphi}_{n+1}^{(D)}(\Gamma_D^{(2)})$). The same happens for the *tangential* coordinate lines ($\Gamma_{n+1}^{(t)}=\varphi_{n+1}^{(D)}(\Gamma^{(T)})$), but not for the normal coordinate lines $\Gamma_{n+1}^{(n)}\neq\boldsymbol{\varphi}_{n+1}^{(D)}(\Gamma^{(N)})$, since $\boldsymbol{\varphi}_{n+1}^{(D)}$ does not necessarily preserve orthogonality.

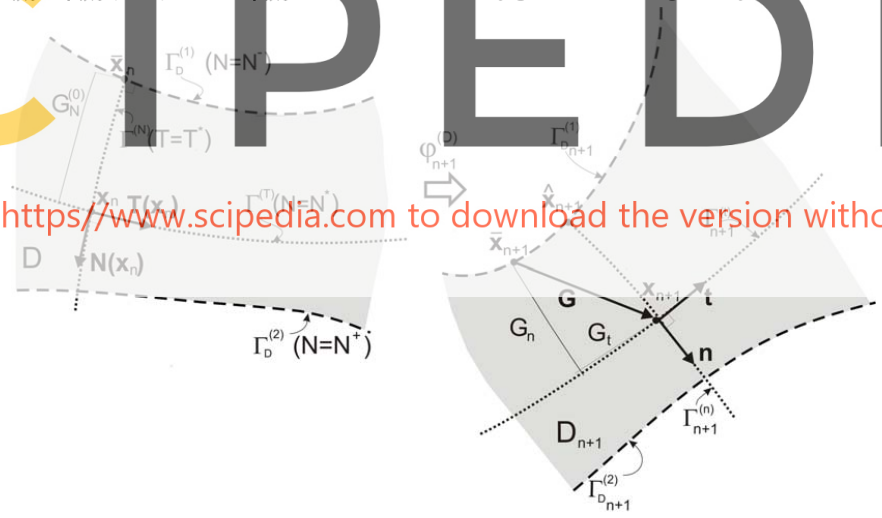

Figure 3: Gap definition in the contact domain

Therefore, the normal $\mathbf{n}$ can be computed as the normalized vector convected of $\mathbf{N}$ [6]:

$$\mathbf{n}=\frac{\mathbf{F}_{n+1}^{-T}\cdot\mathbf{N}}{\left\|\mathbf{F}_{n+1}^{-T}\cdot\mathbf{N}\right\|} \tag{14}$$
$$\mathbf{F}_{n+1}=\boldsymbol{\varphi}_{n+1}^{(D)}\otimes\nabla_{\mathbf{x}_n}=\mathbf{1}+\nabla\mathbf{u}_{n+1}^{(D)}(\mathbf{x}_n)$$

where $(\bullet)^{-T} \equiv \left[(\bullet)^{-1}\right]^T$, $\mathbf{F}_{n+1}$ is the gradient of deformation tensor, $\mathbf{1}$ stands for the second order unit tensor and $\nabla(\square)$ stand for the gradient (i.e.: $\left[\nabla(\square)\right]_{ij} = \partial(\square)_i / \partial x_j$). The tangent vector $\mathbf{t}$ can then be computed as the anti-clockwise rotated vector orthogonal to $\mathbf{n}$.

2.2.1 Geometric gap

Let us now consider a given material point $\mathbf{x}_n \in D$, defined by the material curvilinear coordinate values (N^*, T^*), its corresponding *projected* point on $\Gamma_D^{(1)}$ along the same N-coordinate line, $\overline{\mathbf{x}}_n(N^-, T^*) \in \Gamma_D^{(1)}$ and their respective convected points, $\mathbf{x}_{n+1} = \boldsymbol{\varphi}_{n+1}^{(D)}(\mathbf{x}_n)$ and $\overline{\mathbf{x}}_{n+1} = \boldsymbol{\varphi}_{n+1}^{(D)}(\overline{\mathbf{x}}_n)$ (see Figure 3). Let us also consider the length, $G_N^{(0)}$, of the curvilinear segment of the N-coordinate line $\Gamma^{(N)}$, joining the points $\mathbf{x}_n$ and $\overline{\mathbf{x}}_n$:

$$\begin{aligned} G_N^{(0)}(N^*, T^*) &= \int_{N=N^-}^{N=N^*} d\Gamma^{(N)}(N, T^*) \\ d\Gamma^{(N)}(N, T^*) &= \left\| d\mathbf{x}_n(N, T^*) \right\| = (d\mathbf{x}_n \cdot d\mathbf{x}_n)^{\frac{1}{2}} \end{aligned} \tag{15}$$

The *initial gap vector* $\mathbf{G}^{(0)}(\mathbf{x}_n)$ is then defined as:

$$\mathbf{G}^{(0)}(\mathbf{x}_n) = G_N^{(0)} \mathbf{N}(\mathbf{x}_n) \tag{16}$$

Therefore, one can write:

$$\begin{aligned} \mathbf{x}_n &= \overline{\mathbf{x}}_n + \int_{N^-}^{N^*} d\mathbf{x}_n(N, T^*) = \overline{\mathbf{x}}_n + \int_{N^-}^{N^*} \mathbf{N} d\Gamma^{(N)} = \\ &\cong \overline{\mathbf{x}}_n + \mathbf{N} \underbrace{\int_{N^-}^{N^*} d\Gamma^{(N)}}_{G_N^{(0)}} = \overline{\mathbf{x}}_n + G_N^{(0)} \mathbf{N} \end{aligned} \tag{17}$$

where the hypothesis in equation (10) has been considered. The *final gap vector*, $\mathbf{G}(\mathbf{x}_n)$, is then defined as:

$$\begin{aligned} \mathbf{G}(\mathbf{x}_n) &= \mathbf{x}_{n+1} - \overline{\mathbf{x}}_{n+1} = \boldsymbol{\varphi}_{n+1}^{(D)}(\mathbf{x}_n) - \boldsymbol{\varphi}_{n+1}^{(D)}(\overline{\mathbf{x}}_n) = \\ &= \boldsymbol{\varphi}_{n+1}^{(D)}(\overline{\mathbf{x}}_n + G_N^{(0)} \mathbf{N}) - \boldsymbol{\varphi}_{n+1}^{(D)}(\overline{\mathbf{x}}_n) \end{aligned} \tag{18}$$

where equation (17) has been used. Now, considering the Taylor's expansion

$$\boldsymbol{\varphi}_{n+1}^{(D)}(\overline{\mathbf{x}}_n + G_N^{(0)} \mathbf{N}) = \boldsymbol{\varphi}_{n+1}^{(D)}(\overline{\mathbf{x}}_n) + \nabla \boldsymbol{\varphi}_{n+1}^{(D)} \cdot (G_N^{(0)} \mathbf{N}) \tag{19}$$

where the higher order terms are identically zero due to equation (11), substitution of equation (19) into equation (18) yields:

$$\begin{aligned} \mathbf{G}(\mathbf{x}_n) &= \boldsymbol{\varphi}_{n+1}^{(D)}(\overline{\mathbf{x}}_n + G_N^{(0)} \mathbf{N}) - \boldsymbol{\varphi}_{n+1}^{(D)}(\overline{\mathbf{x}}_n) = \\ &= \nabla \boldsymbol{\varphi}_{n+1}^{(D)} \cdot (G_N^{(0)} \mathbf{N}) = (\mathbf{1} + \nabla \mathbf{u}_{n+1}^{(D)}) \cdot \mathbf{N} G_N^{(0)} \\ &= (\mathbf{N} + \nabla \mathbf{u}_{n+1}^{(D)} \cdot \mathbf{N}) G_N^{(0)} \end{aligned} \tag{20}$$

where equations (6) and (14) have been used. Finally, the normal and tangential gaps are defined as the respective components of $\mathbf{G}(\mathbf{x}_n)$ in the local spatial basis $(\mathbf{n}(\mathbf{x}_{n+1}), \mathbf{t}(\mathbf{x}_{n+1}))$:

$$G_n(\mathbf{u}_{n+1}^{(D)}) = \mathbf{n}(\mathbf{x}_n + \mathbf{u}_{n+1}^{(D)}) \cdot (\mathbf{N} + \nabla \mathbf{u}_{n+1}^{(D)} \cdot \mathbf{N}) G_N^{(0)}$$
$$G_t(\mathbf{u}_{n+1}^{(D)}) = \mathbf{t}(\mathbf{x}_n + \mathbf{u}_{n+1}^{(D)}) \cdot (\mathbf{N} + \nabla \mathbf{u}_{n+1}^{(D)} \cdot \mathbf{N}) G_N^{(0)} \quad (21)$$

REMARK 2-2. The normal gap G_n in equation (21) does not exactly match its classical definition [22, 38], considered as the minimum distance from $\mathbf{x}_{n+1}$ to the closest point $\hat{\mathbf{x}}_{n+1}$ in the master contact boundary $\Gamma_{D_{n+1}}^{(1)}$ (see Figure 3). However, both definitions tend to each other in *any* of the following scenarios:

- As $\Gamma_{D_{n+1}}^{(1)}$ is smooth, which is implicitly assumed in equations (10).
- As the incremental tangential gap G_t is small, that is connatural to the adopted updated Lagrangean approach.

REMARK 2-3. Unlike in mortar or node to segment contact methods, *the gaps are here defined for all points of the contact domain* D and not only for the points in the possible contacting boundaries $\Gamma_D^{(1)}$ and $\Gamma_D^{(2)}$. This is a very distinguishing feature of this approach in comparison with alternative ones. However, it is also clear from that definition that, imposition of a null normal gap in some domain $D^{(N)} \subset D$ (see equation (45) below), implies also imposition of contact, at the boundaries $\Gamma_D^{(1)}$ and $\Gamma_D^{(2)}$ of that domain, in the classical sense (see Figure 3).

2.2.2 Normalized gap

From the results in equations (21) it appears that the initial gap $G_N^{(0)}$ plays a role of *scale length* in both the normal and tangential gaps G_n and G_t. Therefore one could define

$$g_n(\mathbf{u}_{n+1}^{(D)}) = \frac{G_n}{G_N^{(0)}} = \mathbf{n}(\mathbf{x}_n + \mathbf{u}_{n+1}^{(D)}) \cdot (\mathbf{N} + \nabla \mathbf{u}_{n+1}^{(D)} \cdot \mathbf{N})$$
$$g_t(\mathbf{u}_{n+1}^{(D)}) = \frac{G_t}{G_N^{(0)}} = \mathbf{t}(\mathbf{x}_n + \mathbf{u}_{n+1}^{(D)}) \cdot (\mathbf{N} + \nabla \mathbf{u}_{n+1}^{(D)} \cdot \mathbf{N}) \quad (22)$$

where the dimensionless entities g_n and g_t are *the normalized gaps,* or the values of *the final gaps per unit of the initial normal gap*. In order to warranty a bounded definition of the values in equations (22) the considerations in REMARK 2-1, about the positive width of the regularized contact domain and, therefore, the nonzero values of the normal gap G_N^0, are recalled.

REMARK 2-4. Notice that, since $G_N^{(0)}(\mathbf{x}_n) > 0 \quad \forall \mathbf{x}_n \in D$, the imposition of the contact condition $G_n(\mathbf{x}_n) \geq 0 \quad \forall \mathbf{x}_n \in D$ is completely equivalent to $g_n(\mathbf{x}_n) \geq 0 \quad \forall \mathbf{x}_n \in D$. Also, $sign(g_t(\mathbf{x}_n)) = sign(G_t(\mathbf{x}_n)) \quad \forall \mathbf{x}_n \in D$.
Therefore, the normalized gaps in equation (22) provide all the information that is going to be required from the actual geometrical gaps, in equations (21), and they could be considered suitable *contact indicators*. In consequence, in subsequent sections *the contact restrictions will be imposed*

in terms of the normalized gaps in equations (22) instead of the geometrical gaps.

REMARK 2-5. The normalized gap definitions in equations (22) display a highly nonlinear dependence on the displacement field, $\mathbf{u}_{n+1}^{(D)}$, through the nonlinear dependence of $\mathbf{n}(\mathbf{u}_{n+1}^{(D)})$ and $\mathbf{t}(\mathbf{u}_{n+1}^{(D)})$ on the current displacements (see equations (14)). This translates into large analytical complexities and inherited difficulties for linearization of the resulting formulation. This is the reason why simplified (linearized) expressions of those gap definitions are explored in next paragraphs.

2.2.3 Linear normalized gap

The first alternative consists of substituting the spatial basis $(\mathbf{n},\mathbf{t})$ in equations (22) by the material one, $(\mathbf{N},\mathbf{T})$, giving rise to the following normal and tangential gap definitions:

$$\begin{aligned} g_N(\mathbf{u}_{n+1}^{(D)}) &= \mathbf{N}\cdot(\mathbf{N}+\nabla\mathbf{u}_{n+1}^{(D)}\cdot\mathbf{N}) = (\mathbf{1}+\mathbf{N}\cdot\nabla\mathbf{u}_{n+1}^{(D)}\cdot\mathbf{N}) \\ g_T(\mathbf{u}_{n+1}^{(D)}) &= \mathbf{T}\cdot(\mathbf{N}+\nabla\mathbf{u}_{n+1}^{(D)}\cdot\mathbf{N}) = \mathbf{T}\cdot\nabla\mathbf{u}_{n+1}^{(D)}\cdot\mathbf{N} \end{aligned} \tag{23}$$

which exhibit linear dependence with respect to the current incremental displacement field $\mathbf{u}_{n+1}^{(D)}$. Although this definition keeps consistency, since the spatial and material basis tend to each other as the time step length $\Delta t_{n+1} = t_{n+1} - t_n$ is reduced, its adoption could affect the accuracy of the results, for moderate time step lengths, in a non-negligible manner.

2.2.4 Extrapolation based normalized gap

Let us consider the following *prediction* of the current incremental displacement field:

$$\tilde{\mathbf{u}}_{n+1}^{(D)} = \frac{\Delta t_{n+1}}{\Delta t_n}\mathbf{u}_n^{(D)} \tag{24}$$

where $\mathbf{u}_n^{(D)}$ and $\Delta t_n = t_n - t_{n-1}$ stand, respectively, for the incremental displacements and time step length in the previous time step $[t_{n-1}, t_n]$. Expression (24) corresponds to a first order approximation of $\tilde{\mathbf{u}}_{n+1}^{(D)}$ to $\mathbf{u}_{n+1}^{(D)}$ in the Taylor's expansion along time:

$$\begin{aligned} \mathbf{x}_{n+1} &= \mathbf{x}(t_n+\Delta t_{n+1}) = \mathbf{x}(t_n) + \dot{\mathbf{x}}(t_n)\Delta t_{n+1} + \mathcal{O}(\Delta t_{n+1}^2) = \\ &= \mathbf{x}_n + \frac{\mathbf{u}_n^{(D)}}{\Delta t_n}\Delta t_{n+1} + \mathcal{O}(\Delta t_{n+1}^2) \Rightarrow \\ \mathbf{u}_{n+1}^{(D)} &= \mathbf{x}_{n+1} - \mathbf{x}_n = \frac{\Delta t_{n+1}}{\Delta t_n}\mathbf{u}_n^{(D)} + \mathcal{O}(\Delta t_{n+1}^2) = \tilde{\mathbf{u}}_{n+1}^{(D)} + \mathcal{O}(\Delta t_{n+1}^2) \end{aligned} \tag{25}$$

The corresponding predictions of the spatial normal and tangent vectors and the gradient of deformation tensor, according to equations (14) read:

$$\begin{aligned} \tilde{\mathbf{n}}(\mathbf{u}_n^{(D)}) &= \frac{\tilde{\mathbf{F}}_{n+1}^{-T}\cdot\mathbf{N}}{\left\|\tilde{\mathbf{F}}_{n+1}^{-T}\cdot\mathbf{N}\right\|} \quad ; \quad \tilde{\mathbf{t}}\cdot\tilde{\mathbf{n}} = 0 \\ \tilde{\mathbf{F}}_{n+1}(\mathbf{u}_n^{(D)}) &= \mathbf{1} + \nabla_{\mathbf{x}_n}\tilde{\mathbf{u}}_{n+1}^{(D)}(\mathbf{x}_n) \end{aligned} \tag{26}$$

Then, substitution of equation (26) into equation (22) yields:

$$\begin{aligned}\tilde{g}_n(\mathbf{u}_{n+1}^{(D)}) &= \tilde{\mathbf{n}}(\mathbf{u}_n^{(D)})\cdot(\mathbf{N}+\nabla\mathbf{u}_{n+1}^{(D)}\cdot\mathbf{N})\\ \tilde{g}_t(\mathbf{u}_{n+1}^{(D)}) &= \tilde{\mathbf{t}}(\mathbf{u}_n^{(D)})\cdot(\mathbf{N}+\nabla\mathbf{u}_{n+1}^{(D)}\cdot\mathbf{N})\end{aligned} \tag{27}$$

where *the linear dependence of the gaps* on the current value of the displacement field, $\mathbf{u}_{n+1}^{(D)}$, is emphasized. The gap definitions in equations (27) combine this linear dependence, when compared with expressions (21), with a higher (first order) approximation of the couple $(\tilde{\mathbf{n}},\tilde{\mathbf{t}})$, when compared with expressions (23), and they will be the ones considered from now on.

REMARK 2-6. Due to the independence of $\tilde{\mathbf{n}}$ and $\tilde{\mathbf{t}}$, in equations (26) and (27), on the current displacements $\mathbf{u}_{n+1}^{(D)}$, the Gâteaux variation [33] of the gaps defined in equation (27) read:

$$\begin{aligned}\delta\tilde{g}_n(\mathbf{u}_{n+1}^{(D)}) &= \underbrace{\delta(\tilde{\mathbf{n}}(\mathbf{u}_n^{(D)})\cdot\mathbf{N})}_{=\mathbf{0}}+\tilde{\mathbf{n}}\cdot\nabla\delta\mathbf{u}_{n+1}^{(D)}\cdot\mathbf{N}=\tilde{\mathbf{n}}\cdot\nabla\delta\mathbf{u}_{n+1}^{(D)}\cdot\mathbf{N}\\ \delta\tilde{g}_t(\mathbf{u}_{n+1}^{(D)}) &= \underbrace{\delta(\tilde{\mathbf{t}}(\mathbf{u}_n^{(D)})\cdot\mathbf{N})}_{=\mathbf{0}}+\tilde{\mathbf{t}}\cdot\nabla\delta\mathbf{u}_{n+1}^{(D)}\cdot\mathbf{N}=\tilde{\mathbf{t}}\cdot\nabla\delta\mathbf{u}_{n+1}^{(D)}\cdot\mathbf{N}\end{aligned} \tag{28}$$

which are linear expressions (see also REMARK 2-5). As it will be shown in subsequent sections, these facts simplify, without a substantial loss of accuracy, the analytical derivations using those gap definitions, instead of the ones in equations (21).

3. THE FRICTIONLESS PROBLEM

3.1. Inequality constrained boundary value problem

Now let us consider the following boundary value problem at the time interval $[t_n,t_{n+1}]$

FIND:

$$\begin{cases}\mathbf{u}(\mathbf{x}_n,t_{n+1})\equiv\mathbf{u}(\mathbf{x}_n): & \Omega^{(1)}\cup\Omega^{(2)}\to\mathsf{R}^2\\ \lambda_N(T,t_{n+1})\equiv\lambda_N(T): & [T^-,T^+]\to\mathsf{R}\end{cases} \tag{29}$$

FULFILLING:

Momentum equation
$$\underbrace{\mathbf{P}\cdot\nabla}_{DIV\,\mathbf{P}}+\mathbf{b}=\mathbf{0}\quad in\quad \Omega\equiv\Omega^{(1)}\cup\Omega^{(2)} \tag{30}$$

Constitutive model
$$\mathbf{P}=\boldsymbol{\Sigma}(\mathbf{u})\quad in\quad \Omega\equiv\Omega^{(1)}\cup\Omega^{(2)} \tag{31}$$

Dirichlet's boundary conditions
$$\mathbf{u}=\mathbf{u}^*\quad in\quad \Gamma_u\equiv\Gamma_u^{(1)}\cup\Gamma_u^{(2)} \tag{32}$$

Neumann's boundary conditions
$$\mathbf{P}\cdot\boldsymbol{\nu}=\mathbf{t}^*\quad in\quad \Gamma_{\boldsymbol{\sigma}}\equiv\Gamma_\sigma^{(1)}\cup\Gamma_\sigma^{(2)} \tag{33}$$

Lagrange multiplier identification
$$P_{\tilde{n}N}\equiv\tilde{\mathbf{n}}\cdot\mathbf{P}\cdot\mathbf{N}=\lambda_N\quad in\quad \Gamma_D\equiv\Gamma_D^{(1)}\cup\Gamma_D^{(2)} \tag{34}$$

Kuhn/Tucker/Karush conditions

$$\tilde{g}_n \geq 0 \quad ; \quad \lambda_N \leq 0 \qquad \lambda_N \tilde{g}_n = 0 \quad in \quad D \tag{35}$$

where $\mathbf{P}(\mathbf{x}_n, t_{n+1})$ is the first Piola-Kirchoff stress tensor [6], related to the current incremental displacements via the constitutive model $\boldsymbol{\Sigma}$, $\mathbf{b}(\mathbf{x}_n, t_{n+1})$ are the body forces, $\mathbf{u}^*(\mathbf{x}_n, t_{n+1})$ are the prescribed displacements, $\mathbf{t}^*(\mathbf{x}_n, t_{n+1})$ are the prescribed boundary tractions and λ_N is a parameter (the normal Lagrange multiplier) defined in all points of the contact domain, D, whose value at the boundaries, $\Gamma_D^{(1)} \cup \Gamma_D^{(2)}$, is made equal to the component $P_{\bar{n}N}$, of $\mathbf{P}$, in equation (34). The inequality equations (35) are the classical Karush /Kuhn/Tucker conditions [38] in terms of the normalized gap and the Lagrange multiplier.

3.2. Equality constrained boundary value problem

Let us now assume that the material boundaries of the two bodies that are going to be in contact at the end of the time interval, $\Gamma_N^{(1)}$ and $\Gamma_N^{(2)}$ (see Figure 4), are *known in advance* (at the beginning of the time interval), so that the corresponding *active contact domain*, $D^{(N)} \subset D$, is also known. This procedure to know (or to predict) in advance the active contact domain, is part of the *active set strategy* described in section 5.2. Let us then *define* the *active* part of the contact domain D as (see Figure 4):

$$\begin{aligned} D^{(N)} &:= \left\{ \mathbf{x}_n(N,T) \mid \lambda_N(\mathbf{x}_n) < 0 \right\} = \\ &= \left\{ \mathbf{x}_n(N,T) \mid N^- < N < N^+ \;\; ; \;\; T_N^- < T < T_N^+ \right\} \end{aligned} \tag{36}$$

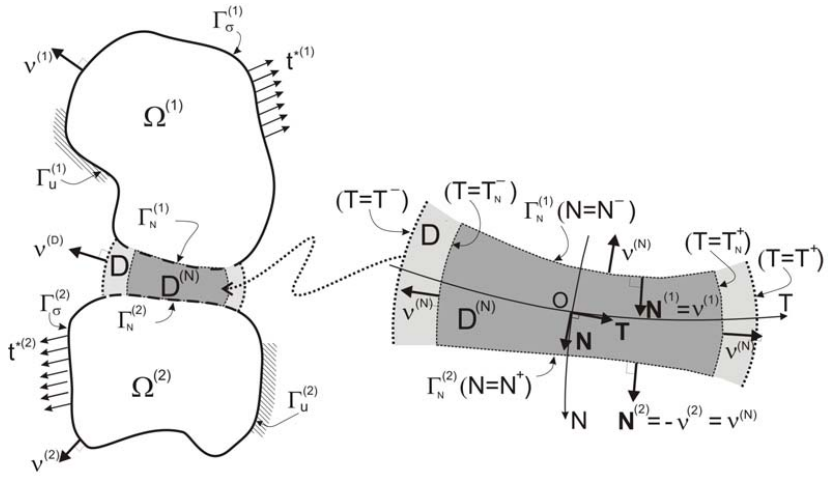

Figure 4: Geometrical definition of the active normal contact domain $D^{(N)}$.

In view of the definition in equation (36) and from the equality $\lambda_N \tilde{g}_n = 0$ in equation (35):

$$\left.\begin{array}{l} \lambda_N(\mathbf{x}_n) < 0 \\ \lambda_N \tilde{g}_n = 0 \end{array}\right\} \Rightarrow \tilde{g}_n(\mathbf{x}_n) = 0 \quad \forall \mathbf{x}_n \in D^{(N)} \tag{37}$$

which shows that a *null normal gap has to be imposed at the active contact domain* $D^{(N)}$. In addition, in view of the inequality $\lambda_N \leq 0$ in equation (35), and the definition of the active contact domain $D^{(N)}$ in equation (36), at its complementary part $D \setminus D^{(N)}$ it has to be fulfilled:

$$\lambda_N(\mathbf{x}_n) = 0 \quad \forall \mathbf{x}_n \in D \setminus D^{(N)} \tag{38}$$

Therefore the Lagrange multiplier λ_N is automatically solved at $D \setminus D^{(N)}$, and *this domain can be excluded from the original problem* that now reads:

$$\begin{array}{l} \textit{FIND}: \\ \left\{\begin{array}{ll} \mathbf{u}(\mathbf{x}_n, t_{n+1}) \equiv \mathbf{u}(\mathbf{x}_n): & \Omega^{(1)} \cup \Omega^{(2)} \rightarrow \mathsf{R}^2 \\ \lambda_N(T, t_{n+1}) \equiv \lambda_N(T): & [T_N^-, T_N^+] \rightarrow \mathsf{R}^- \end{array}\right. \end{array} \tag{39}$$

Momentum equation	$\underbrace{\mathbf{P} \cdot \boldsymbol{\nabla}}_{DIV\,\mathbf{P}} + \mathbf{b} = \mathbf{0} \quad in \quad \Omega \equiv \Omega^{(1)} \cup \Omega^{(2)}$	(40)
Constitutive model	$\mathbf{P} = \boldsymbol{\Sigma}(\mathbf{u}) \quad in \quad \Omega \equiv \Omega^{(1)} \cup \Omega^{(2)}$	(41)
Dirichlet's boundary conditions	$\mathbf{u} = \mathbf{u}^* \quad in \quad \Gamma_u \equiv \Gamma_u^{(1)} \cup \Gamma_u^{(2)}$	(42)
Neumann's boundary conditions	$\mathbf{P} \cdot \boldsymbol{\nu} = \mathbf{t}^* \quad in \quad \Gamma_{\boldsymbol{\sigma}} \equiv \Gamma_\sigma^{(1)} \cup \Gamma_\sigma^{(2)}$	(43)
Lagrange multiplier identification	$P_{\tilde{n}N} \equiv \tilde{\mathbf{n}} \cdot \mathbf{P} \cdot \mathbf{N} = \lambda_N \quad in \quad \Gamma_N \equiv \Gamma_N^{(1)} \cup \Gamma_N^{(2)}$	(44)
Constraint condition	$\tilde{g}_n = 0 \quad in \quad D^{(N)}$	(45)

In contrast with equations (35) now equation (45) is an equality constraint that determines a null value for the normal gap, $\tilde{g}_n$, defined in equation (27), at all points of the active contact domain $D^{(N)}$, thus imposing the contact along the boundaries $\Gamma_N^{(1)}$ and $\Gamma_N^{(2)}$ (see REMARK 2-3).

> **REMARK 3-1**. For the sake of simplicity in the subsequent derivations, the quasi-static case (null acceleration) has been considered in equations (30) or (40). However, the presented approach is fully valid for the dynamic case, with the only modification of correcting the body forces term with inertial

effects, as $\hat{\mathbf{b}}(\mathbf{x}_n, t_{n+1}) = \mathbf{b} - \rho\,\mathbf{a}$, in terms of the density $\rho(\mathbf{x}_n, t_{n+1})$ and the acceleration $\mathbf{a}(\mathbf{x}_n, t_{n+1})$.

3.3. Variational problem

Although it is not a requirement for the proposed approach, for the sake of simplicity, from now on we will consider that the material of the contacting bodies follows a hyperelastic model so that:

$$\mathbf{P} = \partial_{\mathbf{F}} \Psi(\mathbf{F}) \quad in \quad \Omega \tag{46}$$

and, therefore, that there exists the functional:

$$\begin{aligned} &\Pi(\mathbf{u}, \lambda_N) = \Pi_{\text{int}} - \Pi_{ext} + \Pi_{cont}(\mathbf{u}, \lambda_N) \\ &\Pi_{\text{int}}(\mathbf{u}) = \int_\Omega \Psi(\mathbf{F}(\mathbf{u}))\, d\Omega \\ &\Pi_{ext}(\mathbf{u}) = \int_\Omega \mathbf{u} \cdot \mathbf{b}\, d\Omega + \int_{\Gamma_\sigma} \mathbf{u} \cdot \mathbf{t}^*\, d\Gamma \\ &\Pi_{cont}(\mathbf{u}, \lambda_N) = \int_{D^{(N)}} \lambda_N \tilde{g}_n(\mathbf{u})\, dD \end{aligned} \tag{47}$$

where Π is the potential energy functional of the hyperelastic bodies in terms of the internal, Π_{int}, and the external, Π_{ext}, potential energies and the potential energy associated to the contact Π_{cont}. Let us then consider the following variational problem:

$$\begin{aligned} &GIVEN: \\ &V := \left\{ \boldsymbol{\eta}(\mathbf{x}) \in H^1(\Omega) \;;\; \boldsymbol{\eta}(\mathbf{x})|_{\Gamma_u} = \mathbf{u}^* \right\} \\ &\mathbf{L} := \left\{ \mu_N(T) \in L^2([T_N^-, T_N^+]) \;\;;\;\; \mu_N < 0 \right\} \\ &V^0 := \left\{ \boldsymbol{\eta}(\mathbf{x}) \in H^1(\Omega) \;;\; \boldsymbol{\eta}(\mathbf{x})|_{\Gamma_u} = \mathbf{0} \right\} \\ &FIND \\ &\mathbf{u}(\mathbf{x}_n) \in V \quad ; \quad \lambda_N(\mathbf{x}_n) \in \mathbf{L} \\ &FULFILLING: \end{aligned} \tag{48}$$

$$\begin{aligned} \delta\Pi(\mathbf{u}, \lambda_N, \delta\mathbf{u}, \delta\lambda_N) = &\delta\Pi_{\text{int}}(\mathbf{u}, \delta\mathbf{u}) - \delta\Pi_{ext}(\mathbf{u}, \delta\mathbf{u}) + \delta\Pi_{cont}(\mathbf{u}, \lambda_N, \delta\mathbf{u}, \delta\lambda_N) = 0 \\ &\forall \delta\mathbf{u} \in V^0 \quad ; \quad \forall \delta\lambda_N \in \mathbf{L} \end{aligned} \tag{49}$$

where, in equation (49) $\delta\Pi$ stands for the classical Gâteaux variation [33]. Taking into account that from equations (46), (47) and (14),

$$\delta\Pi_{\text{int}}(\mathbf{u},\delta\mathbf{u}) = \int_\Omega \delta\Psi(\mathbf{F}(\mathbf{u}))d\Omega = \int_\Omega \partial_{\mathbf{F}}\Psi(\mathbf{F}(\mathbf{u})\cdot\delta\mathbf{F}d\Omega = \\ = \int_\Omega \mathbf{P}:\nabla\delta\mathbf{u}d\Omega \tag{50}$$

standard algebraic manipulations of equations (47) to (50), taking also into account equations (28), lead to the following two variational equations:

Virtual work principle:

$$\delta\Pi_u(\mathbf{u},\lambda_N,\delta\mathbf{u}) \equiv \int_\Omega \mathbf{P}(\mathbf{u}):\nabla\delta\mathbf{u}\,d\Omega - (\int_\Omega \delta\mathbf{u}\cdot\mathbf{b}d\Omega + \int_{\Gamma_\sigma}\delta\mathbf{u}\cdot\mathbf{t}^* d\Gamma) + \\ + \int_{D^{(N)}} \tilde{\mathbf{n}}\cdot\nabla\delta\mathbf{u}\cdot\mathbf{N}\,\lambda_N dD = 0 \qquad \forall\delta\mathbf{u}\in V^0 \tag{51}$$

Constraint variational equation:

$$\delta\Pi_\lambda(\mathbf{u},\delta\lambda_N) \equiv \int_{D^{(N)}} \delta\lambda_N\,\tilde{g}_n(\mathbf{u})dD = 0 \qquad \forall\delta\lambda_N \in \mathbf{L} \tag{52}$$

REMARK 3-2. It can be proven (see Appendix I) that:

- Equations (40) to (44) are the Euler-Lagrange equations of the variational principle (51).
- Equation (45) is the Euler-Lagrange equation of the variational equation (52).

Therefore, the variational problem above is the weak form of the boundary value problem in section 3.2.

3.4. Spatial discretization

Let us consider a Galerkin-based finite element discretization of the contacting bodies $\Omega^{(1)}$ and $\Omega^{(2)}$, in Figure 2, and the corresponding triangulation in the contact domain $D^{(N)}$ (see also Figure 1). Let then $\mathbf{u}^h(\mathbf{d}) = \sum_i N_i\mathbf{d}_i$ and $\lambda_N^h(\mathbf{\Lambda}) = \sum_j \Phi_j\Lambda_{N_j}$ be the corresponding interpolated fields in terms of the interpolation functions N_i, at the domains $\Omega^{(1)}$, $\Omega^{(2)}$ and $D^{(N)}$, and Φ_j appropriately defined in the domain $D^{(N)}$,

$$\{\mathbf{d}\} = [\mathbf{d}_1,...,\mathbf{d}_{n_u}]^T \quad ; \quad \{\mathbf{\Lambda}\} = [\Lambda_{N_1},...,\Lambda_{N_{n_\lambda}}]^T \tag{53}$$

being the arrays of the corresponding discrete values of the solution. The discretized counterpart of the variational equations (51) and (52) reads

Virtual work principle:

$$\delta\Pi_u^h(\mathbf{d},\mathbf{\Lambda},\delta\mathbf{d}) \equiv \int_\Omega \mathbf{P}(\mathbf{u}^h(\mathbf{d})):\nabla\delta\mathbf{u}^h(\delta\mathbf{d})d\Omega - \\ -\int_\Omega \delta\mathbf{u}^h(\delta\mathbf{d})\cdot\mathbf{b}d\Omega - \int_{\Gamma_\sigma}\delta\mathbf{u}^h(\delta\mathbf{d})\cdot\mathbf{t}^* d\Gamma + \\ + \int_{D^{(N)}} \tilde{\mathbf{n}}\cdot\nabla\delta\mathbf{u}^h(\delta\mathbf{d})\cdot\mathbf{N}\,\lambda_N^h(\mathbf{\Lambda})\,dD = 0 \qquad \forall\delta\mathbf{d} \tag{54}$$

Constraint variational equation:

$$\delta\Pi_\lambda^h(\mathbf{d},\delta\mathbf{\Lambda}) \equiv \int_{D^{(N)}} \delta\lambda_N^h(\delta\mathbf{\Lambda})\,\tilde{g}_n(\mathbf{u}^h(\mathbf{d}))dD = 0 \qquad \forall\delta\mathbf{\Lambda} \tag{55}$$

Solving the variational equations (54) and (55) leads to the nonlinear system of equations:

$$\left.\begin{array}{ll} \delta\Pi_u^h(\mathbf{d},\boldsymbol{\Lambda},\delta\mathbf{d})=0 & \forall\delta\mathbf{d} \\ \delta\Pi_\lambda^h(\mathbf{d},\delta\boldsymbol{\Lambda})=0 & \forall\delta\boldsymbol{\Lambda} \end{array}\right\} \quad \Rightarrow \quad \left\{\begin{array}{l} \mathbf{R}_u^h(\mathbf{d},\boldsymbol{\Lambda})=\mathbf{0} \\ \mathbf{R}_\lambda^h(\mathbf{d})=\mathbf{0} \end{array}\right. \tag{56}$$

where $\mathbf{R}_u^h(\mathbf{d},\boldsymbol{\Lambda})$ and $\mathbf{R}_\lambda^h(\mathbf{d})$ are the residuals of the discretized problem, which in the context of an iterative solution method, based on a linearized sequence of solutions (i.e. the Newton-Raphson method), have to be made equal to zero.

3.5. Problem linearization

Linearization of equations (56) reads:

$$\begin{bmatrix} \mathbf{R}_u^h(\mathbf{d},\boldsymbol{\Lambda}) \\ \mathbf{R}_\lambda^h(\mathbf{d}) \end{bmatrix} + \begin{bmatrix} \dfrac{\partial\mathbf{R}_u^h(\mathbf{d},\boldsymbol{\Lambda})}{\partial\mathbf{d}} & \dfrac{\partial\mathbf{R}_u^h(\mathbf{d},\boldsymbol{\Lambda})}{\partial\boldsymbol{\Lambda}} \\ \dfrac{\partial\mathbf{R}_\lambda^h(\mathbf{d})}{\partial\mathbf{d}} & \mathbf{0} \end{bmatrix} \begin{bmatrix} \Delta\mathbf{d} \\ \Delta\boldsymbol{\Lambda} \end{bmatrix} = \begin{bmatrix} \mathbf{0} \\ \mathbf{0} \end{bmatrix} \tag{57}$$

where the Hessian (stiffness matrix) of the linearized problem reads:

$$\begin{bmatrix} \dfrac{\partial\mathbf{R}_u^h(\mathbf{d},\boldsymbol{\Lambda})}{\partial\mathbf{d}} & \dfrac{\partial\mathbf{R}_u^h(\mathbf{d},\boldsymbol{\Lambda})}{\partial\boldsymbol{\Lambda}} \\ \dfrac{\partial\mathbf{R}_\lambda^h(\mathbf{d})}{\partial\mathbf{d}} & \mathbf{0} \end{bmatrix} \equiv \begin{bmatrix} \mathbf{K}_{uu} & \mathbf{K}_{u\lambda} \\ \mathbf{K}_{\lambda u} & \mathbf{K}_{\lambda\lambda} \end{bmatrix} \tag{58}$$

> **REMARK 3-3.** Notice the similarities of the stiffness matrix in equation (58) with the one in equation (4). As in there, the null character of the matrix $\mathbf{K}_{\lambda\lambda}$ precludes the λ-solvability (condensation of $\Delta\boldsymbol{\Lambda}$) in equation (57). Most importantly: the problem can be prone to exhibit instabilities if the BBL condition is not fulfilled by the used discretizations.

3.6. Lambda-solvability. Interior penalty method

In order to overcome the problems mentioned in REMARK 3-3 a procedure that can be inserted in the context of the *Nitsche method* [25] or the *interior penalty methods* [1, 18, 24] is proposed. The procedure can be considered as a generalization of the stabilization method presented in [18] for the linear kinematics case. A generalization to the present setting, considering the proposed contact domain method and large strain kinematics, is made here.

The motivation of the method is equation (44):

$$P_{\tilde{n}N} \equiv \tilde{\mathbf{n}}\cdot\mathbf{P}\cdot\mathbf{N} = \lambda_N \quad in \quad \Gamma_N \equiv \Gamma_N^{(1)} \cup \Gamma_N^{(2)} \tag{59}$$

which is one of the Euler-Lagrange equations emerging from the *first variational equation* (the Virtual Work Principle) in equation (51) (see REMARK 3-2). Then, equation (59) is inserted in weak form *in the second variational* equation (52).

3.6.1 Modified variational problem

The resulting modified variational equations (51)-(52) read:

Virtual work principle:

$$\delta\Pi_u(\mathbf{u},\lambda_N,\delta\mathbf{u}) \equiv \int_\Omega \mathbf{P}(\mathbf{u}):\nabla\delta\mathbf{u}\,d\Omega - \left(\int_\Omega \delta\mathbf{u}\cdot\mathbf{b}\,d\Omega + \int_{\Gamma_\sigma}\delta\mathbf{u}\cdot\mathbf{t}^*\,d\Gamma\right) + \\ + \int_{D^{(N)}} \tilde{\mathbf{n}}\cdot\nabla\delta\mathbf{u}\cdot\mathbf{N}\,\lambda_N\,dD = 0 \qquad \forall\delta\mathbf{u}\in V^0 \tag{60}$$

Modified constraint variational equation:

$$\delta\Pi_\lambda(\mathbf{u},\lambda_N,\delta\lambda_N) \equiv \int_{D^{(N)}}\delta\lambda_N\,\tilde{g}_n(\mathbf{u})\,dD + \\ + \underbrace{\int_{\Gamma_N}\delta\lambda_N\,\tau(P_{\tilde{n}N}(\mathbf{u})-\lambda_N)\,d\Gamma}_{\text{additional term}} = 0 \quad \forall\delta\lambda_N\in L \tag{61}$$

where, in equation (61), τ is a suitable parameter introduced in order to adjust the dimension of the additional term.

> **REMARK 3-4.** The role of τ could be also regarded as that of a penalty factor, penalizing the term $(P_{\tilde{n}N}(\mathbf{u})-\lambda_N)$ in equation (61). This motivates the character of *interior penalty method* of the proposed procedure. However, since that penalized term is part of the Euler-Lagrange equations of (60), mesh refinement will automatically force the penalized term to tend to zero. Therefore, the procedure could be qualified as a *consistent penalty method*, and, unlike in non-consistent penalty methods, the penalty factor τ can be made small (or even very small) without affecting, necessarily, the quality of the obtained results.

The effects of the proposed procedure on the features of the final discretized problem are crucial. Now after mesh discretization, as displayed in Section 3.4, the discrete variational equations read:

$$\left.\begin{aligned}\delta\Pi_u^h(\mathbf{d},\boldsymbol{\Lambda},\delta\mathbf{d}) = 0 \qquad \forall\delta\mathbf{u}\\ \delta\Pi_\lambda^h(\mathbf{d},\boldsymbol{\Lambda},\delta\boldsymbol{\Lambda}) = 0 \qquad \forall\delta\boldsymbol{\Lambda}\end{aligned}\right\} \;\Rightarrow\; \left\{\begin{aligned}\mathbf{R}_u^h(\mathbf{d},\boldsymbol{\Lambda}) = \mathbf{0}\\ \mathbf{R}_\lambda^h(\mathbf{d},\boldsymbol{\Lambda}) = \mathbf{0}\end{aligned}\right. \tag{62}$$

where now, in contrast with equations (55)-(56), the dependence of $\delta\Pi_\lambda^h$:

$$\delta\Pi_\lambda^h(\mathbf{d},\boldsymbol{\Lambda},\delta\boldsymbol{\Lambda}) \equiv \int_{D^{(N)}}\delta\lambda_N^h(\delta\boldsymbol{\Lambda})\,\tilde{g}_n(\mathbf{u}^h(\mathbf{d}))\,dD + \\ + \underbrace{\int_{\Gamma_N}\delta\lambda_N^h(\delta\boldsymbol{\Lambda})\,\tau\,(P_{\tilde{n}N}(\mathbf{u}^h(\mathbf{d}))-\lambda_N^h(\boldsymbol{\Lambda}))\,d\Gamma}_{\text{additional term}} = 0 \quad \forall\delta\boldsymbol{\Lambda} \tag{63}$$

on the vector of discrete Lagrange multipliers $\boldsymbol{\Lambda}$ is emphasized.

In consequence the corresponding residual vectors $\mathbf{R}_u^h$ and $\mathbf{R}_\lambda^h$, obtained from equation (62) will depend, *both*, on the *two* set of variables $(\mathbf{d},\boldsymbol{\Lambda})$ and their linearization yields:

$$\begin{bmatrix}\mathbf{R}_u^h(\mathbf{d},\boldsymbol{\Lambda})\\ \mathbf{R}_\lambda^h(\mathbf{d},\boldsymbol{\Lambda})\end{bmatrix} + \begin{bmatrix}\mathbf{K}_{uu} & \mathbf{K}_{u\lambda}\\ \mathbf{K}_{\lambda u} & \mathbf{K}_{\lambda\lambda}\end{bmatrix}\begin{bmatrix}\Delta\mathbf{d}\\ \Delta\boldsymbol{\Lambda}\end{bmatrix} = \begin{bmatrix}\mathbf{0}\\ \mathbf{0}\end{bmatrix}$$

$$\begin{bmatrix}\mathbf{K}_{uu} & \mathbf{K}_{u\lambda}\\ \mathbf{K}_{\lambda u} & \mathbf{K}_{\lambda\lambda}\end{bmatrix} = \begin{bmatrix}\dfrac{\partial\mathbf{R}_u^h(\mathbf{d},\boldsymbol{\Lambda})}{\partial\mathbf{d}} & \dfrac{\partial\mathbf{R}_u^h(\mathbf{d},\boldsymbol{\Lambda})}{\partial\boldsymbol{\Lambda}}\\ \dfrac{\partial\mathbf{R}_\lambda^h(\mathbf{d},\boldsymbol{\Lambda})}{\partial\mathbf{d}} & \dfrac{\partial\mathbf{R}_\lambda^h(\mathbf{d},\boldsymbol{\Lambda})}{\partial\boldsymbol{\Lambda}}\end{bmatrix} \tag{64}$$

with a full Hessian (stiffness matrix) in the linearized problem. The advantages of the problem displayed in equations (64) with respect to the one in equations (57) are mainly two:

- The vector $\Delta\boldsymbol{\Lambda}$ can be condensed in equation (64) giving rise to the following solution scheme:

a) *Condensation of $\Delta\boldsymbol{\Lambda}$ and solution of the displacement problem*

$$\begin{cases} \underbrace{\left[\mathbf{K}_{uu} - \mathbf{K}_{u\lambda}\cdot\mathbf{K}_{\lambda\lambda}^{-1}\cdot\mathbf{K}_{\lambda u}\right]}_{=\mathbf{K}_u^*}\cdot\Delta\mathbf{d} = \\ = -\mathbf{R}_u^h + \underbrace{\mathbf{K}_{u\lambda}\cdot\mathbf{K}_{\lambda\lambda}^{-1}\cdot\mathbf{R}_\lambda^h}_{\mathbf{R}_{cont.}} \Rightarrow \\ \mathbf{K}_u^*\cdot\Delta\mathbf{d} = -\mathbf{R}_u^h + \mathbf{R}_{cont.} \rightarrow \Delta\mathbf{d} \end{cases} \tag{65}$$

b) *Solution of the Lagrange multipliers*

$$\Delta\boldsymbol{\Lambda} = -\mathbf{K}_{\lambda\lambda}^{-1}\cdot\left[\mathbf{R}_\lambda^h + \mathbf{K}_{\lambda u}\cdot\Delta\mathbf{d}\right] \tag{66}$$

Indeed, since the structure of $\mathbf{K}_{\lambda\lambda}$ is banded (even diagonal in the final proposed implementation (see Section 5.2)) the operations involved in the condensation are very immediate. The resulting problem, in the stage a) above, involves only the displacement unknowns $\Delta\mathbf{d}$, which, once solved, allow computing $\Delta\boldsymbol{\Lambda}$ in stage b). This condensation based procedure exhibits optimal features, in terms of the computational efficiency and simplicity of implementation, in comparison with the one-block solution of system (64).

- Possible instabilities due to the unbalance of the chosen discrete spaces for $\mathbf{u}^h$ and λ_N^h (not fulfilling the BBL condition) in the original problem are removed. In reference [18] the stability of the procedure, for the linear kinematics and classical contact method cases is proven. Although a similar analysis for the procedure in the present setting is not available yet, the authors can report that, after a large variety of simulation examples, no instability has been found in any case, even for very small values of the penalty parameter τ in equation (61).

4. EXTENSION TO THE FRICTIONAL CASE

Frictional effects require some additional elements in the formulation presented in Section 3, namely (see Figure 5):

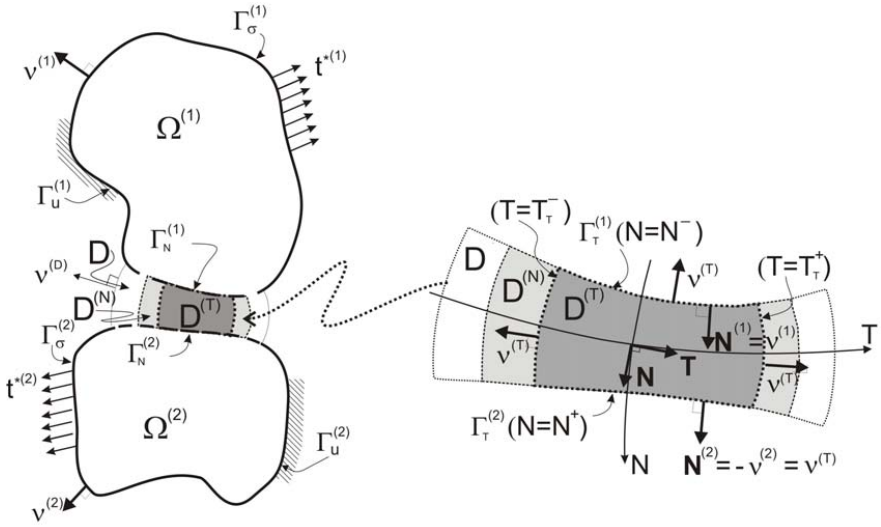

Figure 5: Geometrical definition of the contact domain for the frictional case, accounting for the stick condition (in $D^{(T)}$) and the slip condition (in $D^{(N)} \setminus D^{(T)}$).

1) Considering the part of the active contact domain $D^{(N)}$ where the tangential sliding is precluded. We will consider a subset of the contact domain, *the stick domain* $D^{(T)} \subset D^{(N)}$, where, at the end of the time step , $[t_n, t_{n+1}]$, both the normal and the tangential gaps are precluded (*the stick condition* [22, 38]). As established in section 2.2.4 and in REMARK 2-4 and REMARK 2-6, this condition will be imposed in terms of the normalized gaps in equation (27), namely:

$$\left.\begin{aligned} \tilde{g}_n(\mathbf{x}_n, t_{n+1}) \equiv \tilde{g}_n(\mathbf{x}_n) = 0 \\ \tilde{g}_t(\mathbf{x}_n, t_{n+1}) \equiv \tilde{g}_t(\mathbf{x}_n) = 0 \end{aligned}\right\} \quad \forall \mathbf{x} \in D^{(T)} \tag{67}$$

2) Accounting for the friction effects in the complementary part $D^{(N)} \setminus D^{(T)}$ of $D^{(T)}$ with respect to the active contact domain $D^{(N)}$. This is done via the following constraints defining *the slip conditions:*

$$\left.\begin{aligned} \tilde{g}_n(\mathbf{x}_n, t_{n+1}) \equiv \tilde{g}_n(\mathbf{x}_n) = 0 \\ T(\mathbf{x}_n, t_{n+1}) \equiv T(\mathbf{x}_n) = \mu\, sign(\tilde{g}_t) \left| P_{\tilde{n}N} \right| \end{aligned}\right\} \quad \forall \mathbf{x}_n \in D^{(N)} \setminus D^{(T)} \tag{68}$$

where the classical Coulomb's friction law has been used in terms of a *friction stress*, $T(\tilde{g}_t(\mathbf{x}_n), P_{\tilde{n}N}(\mathbf{x}_n))$, the friction coefficient μ, the sign of the tangential gap in equation (27), $sign(\tilde{g}_t)$, and the normal stress to the slip plane $P_{\tilde{n}N}$.

The plasticity-like format of the Coulomb's friction law in equation (68) will be used here, based on the following ingredients [33, 38]:

1) Slip/yield function definition:

$$F^{slip} \equiv |T| - \mu |P_{\tilde{n}N}| \tag{69}$$

2) *Evolution of the tangential gap*

$$\tilde{g}_t = \gamma \frac{\partial F^{slip}}{\partial T} = \gamma sign(T) \tag{70}$$

3) *Karush/ Kuhn/Tucker conditions*

$$\gamma \geq 0 \quad ; \quad F^{slip} \leq 0 \quad ; \quad \gamma F^{slip} = 0 \tag{71}$$

were $\gamma = |\tilde{g}_t|$ is the slip/plastic multiplier. From equations (69) to (71) it can be readily checked that *for the stick/elastic case* ($F^{slip} < 0$):

$$\left.\begin{array}{r} F^{slip} < 0 \\ \gamma F^{slip} = 0 \end{array}\right\} \Rightarrow \gamma = 0 \left.\begin{array}{r} \\ \\ \tilde{g}_t = \gamma sign(T) \end{array}\right\} \Rightarrow \tilde{g}_t = 0 \tag{72}$$

matching equation (67), whereas *for the slip/(plastic) case* ($F^{slip} = 0$):

$$\left.\begin{array}{l} F^{slip} \equiv |T| - \mu |P_{\tilde{n}N}| = 0 \\ sign(\tilde{g}_t) = sign(\underbrace{\gamma}_{\geq 0}) \cdot sign(T) = sign(T) \\ T = sign(T)|T| \end{array}\right\} \Rightarrow T = \mu sign(\tilde{g}_t)|P_{\tilde{n}N}| \tag{73}$$

which matches equation (68).

4.1. Inequality constrained boundary value problem

The frictional contact problem can then be written as:

$$FIND: \begin{cases} \mathbf{u}(\mathbf{x}_n, t_{n+1}) \equiv \mathbf{u}(\mathbf{x}_n): & \Omega^{(1)} \cup \Omega^{(2)} \to \mathbb{R}^2 \\ \lambda_N(T, t_{n+1}) \equiv \lambda_N(T): & (T^-, T^+) \to \mathbb{R} \\ \lambda_T(T, t_{n+1}) \equiv \lambda_T(T): & (T^-, T^+) \to \mathbb{R} \end{cases} \tag{74}$$

$FULFILLING$:

Momentum Equation

$$\underbrace{\mathbf{P} \cdot \nabla}_{DIV\,\mathbf{P}} + \mathbf{b} = \mathbf{0} \quad in \quad \Omega \equiv \Omega^{(1)} \cup \Omega^{(2)} \tag{75}$$

Constitutive model

$$\mathbf{P} = \boldsymbol{\Sigma}(\mathbf{u}) \quad in \quad \Omega \equiv \Omega^{(1)} \cup \Omega^{(2)} \tag{76}$$

Dirichlet's boundary conditions

$$\mathbf{u} = \mathbf{u}^* \quad in \quad \Gamma_u \equiv \Gamma_u^{(1)} \cup \Gamma_u^{(2)} \tag{77}$$

Neumann's boundary conditions

$$\mathbf{P} \cdot \mathbf{v} = \mathbf{t}^* \quad in \quad \Gamma_{\boldsymbol{\sigma}} \equiv \Gamma_\sigma^{(1)} \cup \Gamma_\sigma^{(2)} \tag{78}$$

Coulomb's friction law

$$\left.\begin{array}{l} F^{slip} \equiv |\lambda_T| - \mu |\lambda^N| \\ \tilde{g}_t = \gamma sign(\lambda_T) \end{array}\right\} \quad in \;\; D \tag{79}$$

Lagrange multiplier identification

$$\left.\begin{array}{l} P_{\tilde{n}N} \equiv \tilde{\mathbf{n}} \cdot \mathbf{P} \cdot \mathbf{N} = \lambda_N \\ P_{\tilde{t}N} \equiv \tilde{\mathbf{t}} \cdot \mathbf{P} \cdot \mathbf{N} = \lambda_T \end{array}\right\} \Rightarrow in \;\; \Gamma_D \equiv \Gamma_D^{(1)} \cup \Gamma_D^{(2)} \tag{80}$$

$$\left.\begin{array}{lll} \tilde{g}_n \geq 0 \;\; ; \;\; \lambda_N \leq 0 \;\; ; \;\; \lambda_N \tilde{g}_n = 0 \\ \gamma \geq 0 \;\; ; \;\; F^{slip} \leq 0 \;\; ; \;\; \gamma F^{slip} = 0 \end{array}\right\} \; in \; D \tag{81}$$

Kuhn/Tucker/Karush conditions

where $\lambda_T = P_{tN}$ in equations (79) can be identified as the friction stress T in equations (69) and (70).

4.2. Equality constrained boundary value problem

Similarly to what has been stated in section 3.2, it will be assumed that both the domains $D^{(N)}$ and $D^{(T)}$ *are known* (or predicted) *in advance* as a result of an active set strategy (see section 5.2) based on the following criteria (see Figure 5):

$$\begin{aligned} D^{(N)} &:= \left\{ \mathbf{x}_n(N,T) \;|\; \lambda_N(\mathbf{x}_n) < 0 \right\} = \\ &= \left\{ \mathbf{x}_n(N,T) \;|\; N^- < N < N^+ \;\; ; \; T_N^- < T < T_N^+ \right\} \end{aligned} \tag{82}$$

$$\begin{aligned} D^{(T)} &:= \left\{ \mathbf{x}_n(N,T) \;|\; F^{slip}(\mathbf{x}_n) < 0 \right\} = \\ &= \left\{ \mathbf{x}_n(N,T) \;|\; N^- < N < N^+ \;\; ; \; T_T^- < T < T_T^+ \right\} \end{aligned} \tag{83}$$

REMARK 4-1. The definition of the active contact domain in equation (82) implies *that a null normal gap has to be imposed in the contact domain* $D^{(N)}$ (see equation (37)):

$$\tilde{g}_n(\mathbf{x}_n) = 0 \quad \forall \mathbf{x}_n \in D^{(N)} \tag{84}$$

In addition, the definition of the active stick domain in equation (83), based on the condition $F^{slip}(\mathbf{x}_n) < 0$, implies, in view of equation (72), that

$$\tilde{g}_t(\mathbf{x}_n) = 0 \quad \forall \mathbf{x}_n \in D^{(T)} \tag{85}$$

which displays the fact *that a null tangential gap* ($\tilde{g}_t = 0$) *has to be imposed at the stick domain* $D^{(T)}$.

Again, in view of the definitions of the active domains in equations (82) and (83), equations (79) and (81) provide the following trivial solutions for λ_N and λ_T in the complementary domains $D \setminus D^{(N)}$ and $D \setminus D^{(T)}$:

$$\left.\begin{array}{l} \lambda_N(\mathbf{x}_n) \geq 0 \;\; \forall \mathbf{x}_n \in D \\ \lambda_N(\mathbf{x}_n) < 0 \Leftrightarrow \mathbf{x}_n \in D^{(N)} \end{array}\right\} \Rightarrow \lambda_N(\mathbf{x}_n) = 0 \;\; \forall \mathbf{x}_n \in D \setminus D^{(N)} \tag{86}$$

$$\left.\begin{array}{l} F^{slip}(\mathbf{x}_n) \leq 0 \;\; \forall \mathbf{x}_n \in D \\ F^{slip}(\mathbf{x}_n) < 0 \Leftrightarrow \mathbf{x}_n \in D^{(T)} \end{array}\right\} \Rightarrow F^{slip}(\mathbf{x}_n) = 0 \;\; \forall \mathbf{x}_n \in D \setminus D^{(T)} \tag{87}$$

and, operating on equation (87), in view of equations (69) and (70):

$$\left.\begin{array}{l} F^{slip}(\mathbf{x}_n) \equiv \left|\lambda_T\right| - \mu\left|\lambda_N\right| = 0 \;\Rightarrow\; \left|\lambda_T\right| = \mu\left|\lambda_N\right| \\ sign(\tilde{g}_T) = sign(\underbrace{\gamma}_{\geq 0}) \cdot sign(\lambda_T) = sign(\lambda_T) \\ \lambda_T = sign(\lambda_T)\left|\lambda_T\right| \end{array}\right\} \Rightarrow$$
$$\Rightarrow \lambda_T = T\ (\tilde{g}_t, \lambda_N) = sign(\tilde{g}_t)\mu\left|\lambda_N\right| \quad \forall \mathbf{x}_n \in D \setminus D^{(T)} \tag{88}$$

Equations (86) and (88) provide a closed form solution for the Lagrange multipliers λ_N and λ_T at the complementary domains $D \setminus D^{(N)}$ and $D \setminus D^{(T)}$. Therefore, these domains *can be excluded from the original problem* that now reads:

$$FIND: \begin{cases} \mathbf{u}(\mathbf{x}_n, t_{n+1}) \equiv \mathbf{u}(\mathbf{x}_n): & \Omega^{(1)} \cup \Omega^{(2)} \to \mathsf{R}^2 \\ \lambda_N(T, t_{n+1}) \equiv \lambda_N(T): & (T_N^-, T_N^+) \to \mathsf{R}^- \\ \lambda_T(T, t_{n+1}) \equiv \lambda_T(T): & (T_T^-, T_T^-) \to \mathsf{R} \end{cases} \tag{89}$$

FULFILLING:

Momentum Equation
$$\underbrace{\mathbf{P} \cdot \nabla}_{DIV\,\mathbf{P}} + \mathbf{b} = \mathbf{0} \quad in \quad \Omega \equiv \Omega^{(1)} \cup \Omega^{(2)} \tag{90}$$

Constitutive model
$$\mathbf{P} = \boldsymbol{\Sigma}(\mathbf{u}) \quad in \quad \Omega \equiv \Omega^{(1)} \cup \Omega^{(2)} \tag{91}$$

Dirichlet's boundary conditions
$$\mathbf{u} = \mathbf{u}^* \quad in \quad \Gamma_u \equiv \Gamma_u^{(1)} \cup \Gamma_u^{(2)} \tag{92}$$

Neumann's boundary conditions
$$\mathbf{P} \cdot \boldsymbol{\nu} = \mathbf{t}^* \quad in \quad \Gamma_{\boldsymbol{\sigma}} \equiv \Gamma_\sigma^{(1)} \cup \Gamma_\sigma^{(2)} \tag{93}$$

Coulomb's friction law
$$T = \mu\ sign(\tilde{g}_t)\left|\lambda_N\right| \quad in \quad D^{(N)} \setminus D^{(T)} \tag{94}$$

Lagrange multiplier identification
$$\begin{cases} P_{\tilde{n}N} \equiv \tilde{\mathbf{n}} \cdot \mathbf{P} \cdot \mathbf{N} = \lambda_N & in \quad \Gamma_N \equiv \Gamma_N^{(1)} \cup \Gamma_N^{(2)} \\ P_{\tilde{t}N} \equiv \tilde{\mathbf{t}} \cdot \mathbf{P} \cdot \mathbf{N} = \lambda_T & in \quad \Gamma_T \equiv \Gamma_T^{(1)} \cup \Gamma_T^{(2)} \end{cases} \tag{95}$$

Friction stress identification
$$P_{\tilde{t}N} = T \quad in \quad \Gamma_N \cap \partial(D^{(N)} \setminus D^{(T)}) \tag{96}$$

Constraint conditions
$$\begin{cases} \tilde{g}_n = 0 & in \quad D^{(N)} \\ \tilde{g}_t = 0 & in \quad D^{(T)} \end{cases} \tag{97}$$

where now equations (97) *are equality constraints* in terms of the normal and the tangential normalized gaps $\tilde{g}_n$ and $\tilde{g}_t$, respectively.

4.3. Variational problem

The variational form of the boundary value problem in equations (89) to (97) reads:

$$
\begin{aligned}
&\textit{GIVEN}: \\
&V := \left\{ \boldsymbol{\eta}(\mathbf{x}) \in H^1(\Omega) \;;\; \boldsymbol{\eta}(\mathbf{x})|_{\Gamma_u} = \mathbf{u}^* \right\} \\
&\mathbf{L}_N := \left\{ \mu_N(T) \in L^2([T_N^-, T_N^+]) \;\;;\;\; \mu_N < 0 \right\} \\
&\mathbf{L}_T := \left\{ \mu_T(T) \in L^2([T_T^-, T_T^+]) \right\} \\
&V^0 := \left\{ \boldsymbol{\eta}(\mathbf{x}) \in H^1(\Omega) \;;\; \boldsymbol{\eta}(\mathbf{x})|_{\Gamma_u} = \mathbf{0} \right\} \\
&\textit{FIND} \\
&\mathbf{u}(\mathbf{x}_n) \in V \quad ; \quad \lambda_N(\mathbf{x}_n) \in \mathbf{L}_N \quad ; \quad \lambda_T(\mathbf{x}_n) \in \mathbf{L}_T \\
&\textit{FULFILLING}:
\end{aligned}
\tag{98}
$$

$$
\begin{aligned}
&\delta\Pi(\mathbf{u}, \lambda_N, \lambda_T, \delta\mathbf{u}, \delta\lambda_N, \delta\lambda_T) = \delta\Pi_{\text{int}}(\mathbf{u}, \delta\mathbf{u}) - \delta\Pi_{ext}(\mathbf{u}, \delta\mathbf{u}) + \\
&\qquad\qquad + \delta\Pi_{cont}(\mathbf{u}, \lambda_N, \lambda_T, \delta\mathbf{u}, \delta\lambda_N, \delta\lambda_T) = 0 \\
&\forall \delta\mathbf{u} \in V^0 \quad ; \quad \forall \delta\lambda_N \in \mathbf{L}_N \quad ; \quad \forall \delta\lambda_T \in \mathbf{L}_T
\end{aligned}
\tag{99}
$$

which can be decomposed into the three following variational equations:

Virtual work principle:

$$
\begin{cases}
\delta\Pi_u(\mathbf{u}, \lambda_N, \lambda_T, \delta\mathbf{u}) \equiv \int_\Omega \mathbf{P}(\mathbf{u}) : \nabla\delta\mathbf{u}\, d\Omega - \left(\int_\Omega \delta\mathbf{u} \cdot \mathbf{b} d\Omega + \int_{\Gamma_\sigma} \delta\mathbf{u} \cdot \mathbf{t}^* d\Gamma \right) \\
\qquad + \int_{D^{(N)}} \tilde{\mathbf{n}} \cdot \nabla\delta\mathbf{u} \cdot \mathbf{N}\, \lambda_N dD + \int_{D^{(T)}} \tilde{\mathbf{t}} \cdot \nabla\delta\mathbf{u} \cdot \mathbf{N}\, \lambda_T dD \; + \\
\qquad + \int_{D^{(N)} \setminus D^{(T)}} \tilde{\mathbf{t}} \cdot \nabla\delta\mathbf{u} \cdot \mathbf{N} T \; dD = 0 \qquad \forall \delta\mathbf{u} \in V^0
\end{cases}
\tag{100}
$$

Constraint variational equations:

$$
\begin{cases}
\delta\Pi_{\lambda_N}(\mathbf{u}, \delta\lambda_N) \equiv \int_{D^{(N)}} \delta\lambda_N\, \tilde{g}_n(\mathbf{u}) dD = 0 \qquad \forall \delta\lambda_N \in \mathbf{L}_N \\
\delta\Pi_{\lambda_T}(\mathbf{u}, \delta\lambda_T) \equiv \int_{D^{(T)}} \delta\lambda_T\, \tilde{g}_t(\mathbf{u}) dD = 0 \qquad \forall \delta\lambda_T \in \mathbf{L}_T
\end{cases}
\tag{101}
$$

REMARK 4-2. In Appendix I, it is proven that:

- Equations (90) to (96) are the Euler-Lagrange equations of the virtual work principle (100).
- Equations (97) are the Euler-Lagrange equations of the constraint variational equations (101).

Therefore the variational problem above is the weak form of the boundary value problem in equations (89) to (97).

REMARK 4-3. *Pseudo-mechanical stresses*

Let us construct the following tensor $\mathbf{P}^*(\mathbf{u}, \lambda_N, \lambda_T)$ *defined at the domain* $\Omega^{(1)} \cup \Omega^{(2)} \cup D^{(N)}$ *occupied by the contacting bodies plus the active contact domain* $D^{(N)}$ by means of:

$$\mathbf{P}^*(\mathbf{u},\lambda_N,\lambda_T)=\begin{cases}\mathbf{P}(\mathbf{u})=\dfrac{\partial\Psi(\mathbf{F})}{\partial\mathbf{F}} & in \quad \Omega\equiv\Omega^{(1)}\cup\Omega^{(2)}\\ \lambda_N\tilde{\mathbf{n}}\otimes\mathbf{N}+\lambda_T\tilde{\mathbf{t}}\otimes\mathbf{N} & in \quad D^{(T)}\\ \lambda_N\tilde{\mathbf{n}}\otimes\mathbf{N}+\mathcal{T}\ \tilde{\mathbf{t}}\otimes\mathbf{N} & in \quad D^{(N)}\setminus D^{(T)}\end{cases} \tag{102}$$

Then, after some straightforward operations, the variational equation (100) can be written as:

$$\delta\Pi_u(\mathbf{u},\lambda_N,\lambda_T,\delta\mathbf{u})\equiv\underbrace{\int_{\Omega\cup D^{(N)}\cup D^{(T)}}\mathbf{P}^*:\nabla\delta\mathbf{u}\,d\Omega}_{\delta\Pi^*_{\text{int}}}-\underbrace{(\int_\Omega\delta\mathbf{u}\cdot\mathbf{b}d\Omega+\int_{\Gamma_\sigma}\delta\mathbf{u}\cdot\mathbf{t}^*d\Gamma)}_{\delta\Pi_{ext}}=0 \tag{103}$$
$$\forall\delta\mathbf{u}\in\mathcal{V}^0$$

which recalls the classical format of the virtual work principle in terms of the pseudo mechanical stress tensor $\mathbf{P}^*$ defined in equation (102). This motivates the name *virtual work principle* supplied to equations (100). The concept of pseudo-mechanical stresses, has been also used by the authors in a previous work based on penalization of the contact constraints [27].

4.4. Lambda-solvability.

Due to reasons similar to those displayed in section 3.6, the discretized version of the variational equations (100) and (101) does not allow condensation of the Lagrange multipliers λ_N and λ_T and can suffer from instabilities. A modification of the constraint variational equations (101), similar to the one in section 3.6, based on an interior penalty procedure, leads to the following modified variational equations:

Virtual work principle:

$$\begin{cases}\delta\Pi_u(\mathbf{u},\lambda_N,\lambda_T,\delta\mathbf{u})\equiv\int_\Omega\mathbf{P}(\mathbf{u}):\nabla\delta\mathbf{u}\,d\Omega-(\int_\Omega\delta\mathbf{u}\cdot\mathbf{b}d\Omega+\int_{\Gamma_\sigma}\delta\mathbf{u}\cdot\mathbf{t}^*d\Gamma)+\\ \qquad+\int_{D^{(N)}}\tilde{\mathbf{n}}\cdot\nabla\delta\mathbf{u}\cdot\mathbf{N}\,\lambda_N dD+\int_{D^{(T)}}\tilde{\mathbf{t}}\cdot\nabla\delta\mathbf{u}\cdot\mathbf{N}\,\lambda_T dD\ +\\ \qquad+\int_{D^{(N)}\setminus D^{(T)}}\tilde{\mathbf{t}}\cdot\nabla\delta\mathbf{u}\cdot\mathbf{N}\,\mathcal{T}\ dD\ =0 \qquad \forall\delta\mathbf{u}\in\mathcal{V}^0\\ (\mathcal{T}\ (\lambda_N)\ =\mu\ sign(\tilde{g}_t)\left|\lambda_N\right|)\end{cases} \tag{104}$$

Modified constraint variational equations:

$$\begin{cases}\delta\Pi_{\lambda_N}(\mathbf{u},\lambda_N,\delta\lambda_N)\equiv\int_{D^{(N)}}\delta\lambda_N\,\tilde{g}_n(\mathbf{u})dD+\\ \qquad+\underbrace{\int_{\Gamma_N}\delta\lambda_N\tau(P_{\tilde{n}N}(\mathbf{u})-\lambda_N)d\Gamma}_{\text{additional term}}=0 \quad \forall\delta\lambda_N\in\mathbf{L}_{\mathrm{N}}\\ \delta\Pi_{\lambda_T}(\mathbf{u},\lambda_T,\delta\lambda_T)\equiv\int_{D^{(T)}}\delta\lambda_T\,\tilde{g}_t(\mathbf{u})dD+\\ \qquad+\underbrace{\int_{\Gamma_T}\delta\lambda_T\tau(P_{\tilde{t}N}(\mathbf{u})-\lambda_T)d\Gamma}_{\text{additional term}}=0 \quad \forall\delta\lambda_T\in\mathbf{L}_{\mathrm{T}}\end{cases} \tag{105}$$

where the additional terms in the variational equations (105) emerge from a consistent penalty based imposition of equations (95), which, in turn, are stated in weak form in the virtual work principle (104), i.e.:

$$\begin{aligned}\lambda_N &= P_{\tilde{n}N} \equiv \tilde{\mathbf{n}} \cdot \mathbf{P} \cdot \mathbf{N} \qquad in \quad \Gamma_N \equiv \Gamma_N^{(1)} \cup \Gamma_N^{(2)} \\ \lambda_T &= P_{\tilde{t}N} \equiv \tilde{\mathbf{t}} \cdot \mathbf{P} \cdot \mathbf{N} \qquad in \quad \Gamma_T \equiv \Gamma_T^{(1)} \cup \Gamma_T^{(2)}\end{aligned} \tag{106}$$

4.5. Spatial discretization. Linearization

Let $\mathbf{u}^h(\mathbf{d}) = \sum_i N_i \mathbf{d}_i$, $\lambda_N^h(\mathbf{\Lambda}_N) = \sum_j \Phi_j \Lambda_{N_j}$ and $\lambda_T^h(\mathbf{\Lambda}_T) = \sum_j \Phi_j \Lambda_{T_j}$ be , respectively, the discretized displacement, normal and tangent Lagrange multiplier fields, interpolated in terms of the shape functions N_i, defined at the domains $\Omega^{(1)}$, $\Omega^{(2)}$ and $D^{(N)}$, and the interpolation functions Φ_j defined in the domains $D^{(N)}$ and $D^{(T)}$ (see Figure 5). Let

$$\{\mathbf{d}\} = [\mathbf{d}_1, ..., \mathbf{d}_{n_u}]^T \quad ; \quad \{\mathbf{\Lambda}_N\} = [\Lambda_{N_1}, ..., \Lambda_{N_{n_N}}]^T \quad ; \quad \{\mathbf{\Lambda}_T\} = [\Lambda_{T_1}, ..., \Lambda_{T_{n_T}}]^T \tag{107}$$

be the arrays of the corresponding discrete values of the solution. The discretized counterpart of the variational equations (104) and (52) reads:

Virtual work principle:

$$\begin{cases} \delta\Pi_u^h(\mathbf{d}, \mathbf{\Lambda}_N, \mathbf{\Lambda}_T, \delta\mathbf{d}) \equiv \int_\Omega \mathbf{P}(\mathbf{u}^h(\mathbf{d})) : \nabla \delta\mathbf{u}^h(\delta\mathbf{d}) d\Omega - \\ \qquad - \int_\Omega \delta\mathbf{u}^h(\delta\mathbf{d}) \cdot \mathbf{b} d\Omega - \int_{\Gamma_\sigma} \delta\mathbf{u}^h(\delta\mathbf{d}) \cdot \mathbf{t}^* d\Gamma + \\ \qquad + \int_{D^{(N)}} \tilde{\mathbf{n}} \cdot \nabla \delta\mathbf{u}^h(\delta\mathbf{d}) \cdot \mathbf{N} \, \lambda_N^h(\mathbf{\Lambda}_N) \, dD + \\ \qquad + \int_{D^{(T)}} \tilde{\mathbf{t}} \cdot \nabla \delta\mathbf{u}^h(\delta\mathbf{d}) \cdot \mathbf{N} \, \lambda_T^h(\mathbf{\Lambda}_T) \, dD + \\ \qquad + \int_{D^{(N)} \setminus D^{(T)}} \tilde{\mathbf{t}} \cdot \nabla \delta\mathbf{u}^h(\delta\mathbf{d}) \cdot \mathbf{N} \, T \, (\mathbf{\Lambda}_N) dD \; = 0 \end{cases} \tag{108}$$

Constraint variational equations:

$$\begin{cases} \delta\Pi_{\lambda_N}^h(\mathbf{d}, \mathbf{\Lambda}_N, \delta\mathbf{\Lambda}_N) \equiv \int_{D^{(N)}} \delta\lambda_N^h(\delta\mathbf{\Lambda}_N) \tilde{g}_n(\mathbf{u}^h(\mathbf{d})) dD \\ \qquad + \int_{\Gamma_N} \delta\lambda_N^h(\delta\mathbf{\Lambda}_N) \tau(P_{\tilde{n}N}(\mathbf{u}^h(\mathbf{d})) - \lambda_N(\mathbf{\Lambda}_N) d\Gamma = 0 \qquad \forall \delta\mathbf{\Lambda}_N \\ \delta\Pi_{\lambda_T}^h(\mathbf{d}, \mathbf{\Lambda}_T, \delta\mathbf{\Lambda}_T) \equiv \int_{D^{(T)}} \delta\lambda_T^h(\delta\mathbf{\Lambda}_T) \tilde{g}_t(\mathbf{u}^h(\mathbf{d})) dD \\ \qquad + \int_{\Gamma_T} \delta\lambda_T^h(\delta\mathbf{\Lambda}_T) \tau(P_{\tilde{t}N}(\mathbf{u}^h(\mathbf{d})) - \lambda_T(\mathbf{\Lambda}_T) d\Gamma = 0 \qquad \forall \delta\mathbf{\Lambda}_T \end{cases} \tag{109}$$

Solving the variational equations (108) and (109) leads to the nonlinear system of equations:

$$\left.\begin{array}{ll} \delta\Pi_u^h(\mathbf{d}, \mathbf{\Lambda}, \delta\mathbf{d}) = 0 & \forall \delta\mathbf{d} \\ \delta\Pi_{\lambda_N}^h(\mathbf{d}, \mathbf{\Lambda}_N, \delta\mathbf{\Lambda}_N) = 0 & \forall \delta\mathbf{\Lambda}_N \\ \delta\Pi_{\lambda_T}^h(\mathbf{d}, \mathbf{\Lambda}_T, \delta\mathbf{\Lambda}_T) = 0 & \forall \delta\mathbf{\Lambda}_T \end{array}\right\} \quad \Rightarrow \quad \begin{cases} \mathbf{R}_u^h(\mathbf{d}, \mathbf{\Lambda}_N, \mathbf{\Lambda}_T) = \mathbf{0} \\ \mathbf{R}_{\lambda_N}^h(\mathbf{d}, \mathbf{\Lambda}_N) = \mathbf{0} \\ \mathbf{R}_{\lambda_T}^h(\mathbf{d}, \mathbf{\Lambda}_T) = \mathbf{0} \end{cases} \tag{110}$$

Linearization of the residuals in (110) yields:

$$\begin{bmatrix} \mathbf{R}_u^h(\mathbf{d},\boldsymbol{\Lambda}_N,\boldsymbol{\Lambda}_T) \\ \mathbf{R}_{\lambda_N}^h(\mathbf{d},\boldsymbol{\Lambda}_N) \\ \mathbf{R}_{\lambda_T}^h(\mathbf{d},\boldsymbol{\Lambda}_T) \end{bmatrix} + \begin{bmatrix} \mathbf{K}_{uu} & \mathbf{K}_{u\lambda_N} & \mathbf{K}_{u\lambda_T} \\ \mathbf{K}_{\lambda_N u} & \mathbf{K}_{\lambda_N\lambda_N} & \mathbf{0} \\ \mathbf{K}_{\lambda_T u} & \mathbf{0} & \mathbf{K}_{\lambda_T\lambda_T} \end{bmatrix} \begin{bmatrix} \Delta\mathbf{d} \\ \Delta\boldsymbol{\Lambda}_N \\ \Delta\boldsymbol{\Lambda}_T \end{bmatrix} = \begin{bmatrix} \mathbf{0} \\ \mathbf{0} \\ \mathbf{0} \end{bmatrix}$$

$$\begin{bmatrix} \mathbf{K}_{uu} & \mathbf{K}_{u\lambda_N} & \mathbf{K}_{u\lambda_T} \\ \mathbf{K}_{\lambda_N u} & \mathbf{K}_{\lambda_N\lambda_N} & \mathbf{0} \\ \mathbf{K}_{\lambda_T u} & \mathbf{0} & \mathbf{K}_{\lambda_T\lambda_T} \end{bmatrix} = \begin{bmatrix} \dfrac{\partial\mathbf{R}_u^h}{\partial\mathbf{d}} & \dfrac{\partial\mathbf{R}_u^h}{\partial\boldsymbol{\Lambda}_N} & \dfrac{\partial\mathbf{R}_u^h}{\partial\boldsymbol{\Lambda}_T} \\ \dfrac{\partial\mathbf{R}_{\lambda_N}^h}{\partial\mathbf{d}} & \dfrac{\partial\mathbf{R}_{\lambda_N}^h}{\partial\boldsymbol{\Lambda}_N} & \mathbf{0} \\ \dfrac{\partial\mathbf{R}_{\lambda_T}^h}{\partial\mathbf{d}} & \mathbf{0} & \dfrac{\partial\mathbf{R}_{\lambda_T}^h}{\partial\boldsymbol{\Lambda}_T} \end{bmatrix} \tag{111}$$

Finally, the linear system (111) can be solved by condensation of the Lagrange multipliers in the two following stages:

a) *Condensation of $\Delta\boldsymbol{\Lambda}$ and solution of the displacement problem*

$$\begin{cases} \underbrace{\left[\mathbf{K}_{uu} - \mathbf{K}_{u\lambda_N}\cdot\mathbf{K}_{\lambda_N\lambda_N}^{-1}\cdot\mathbf{K}_{\lambda_N u} - \mathbf{K}_{u\lambda_T}\cdot\mathbf{K}_{\lambda_T\lambda_T}^{-1}\cdot\mathbf{K}_{\lambda_T u}\right]}_{=\mathbf{K}_u^*}\cdot\Delta\mathbf{d} = \\ -\mathbf{R}_u^h + \underbrace{\mathbf{K}_{u\lambda_N}\cdot\mathbf{K}_{\lambda_N\lambda_N}^{-1}\cdot\mathbf{R}_{\lambda_N}^h}_{\mathbf{R}_{cont\text{-}N}} + \underbrace{\mathbf{K}_{u\lambda_T}\cdot\mathbf{K}_{\lambda_T\lambda_T}^{-1}\cdot\mathbf{R}_{\lambda_T}^h}_{\mathbf{R}_{cont\text{-}N}} \Rightarrow \\ \mathbf{K}_u^*\cdot\Delta\mathbf{d} = -\mathbf{R}_u^h + \mathbf{R}_{cont\text{-}N} + \mathbf{R}_{cont\text{-}T} \rightarrow \Delta\mathbf{d} \end{cases} \tag{112}$$

b) *Solution of the Lagrange multipliers*

$$\begin{cases} \Delta\boldsymbol{\Lambda}_N = -\mathbf{K}_{\lambda_N\lambda_N}^{-1}\cdot\left[\mathbf{R}_{\lambda_N}^h + \mathbf{K}_{\lambda_N u}\cdot\Delta\mathbf{d}\right] \\ \Delta\boldsymbol{\Lambda}_T = -\mathbf{K}_{\lambda_T\lambda_T}^{-1}\cdot\left[\mathbf{R}_{\lambda_T}^h + \mathbf{K}_{\lambda_T u}\cdot\Delta\mathbf{d}\right] \end{cases} \tag{113}$$

5. DETERMINATION OF THE CONTACT/FRICTION DOMAIN. ACTIVE SET STRATEGY

The problems described in sections 3.2 and 4.2 are equality-constraint problems. There, it is assumed that the domains $D^{(N)}$ and $D^{(T)}$, defined in equations (82) and (83), are known in advance. In this section, a specific methodology to determine those domains at the current time step, based on an active set strategy, is presented.

5.1. Contact domain mesh. Numerical gaps

Let us consider that a finite element mesh in the contacting bodies is available at the beginning of the time step $[t_n, t_{n+1}]$. Let us also assume a triangulation, D^h, of the contact domain D in Figure 2 is constructed featuring (see Figure 6):

- There is a unique layer of triangles along the width of D^h (therefore, there are no internal vertices in the triangulation).
- The vertices of the triangles match exactly boundary nodes of the finite element meshes at the contacting bodies.

The specific procedure for the construction of this triangulation is detailed in Part 2 of this work [16].

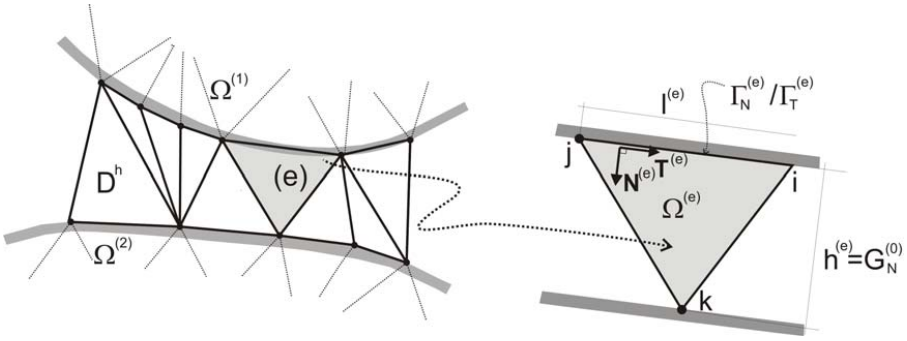

Figure 6: Triangularization of the contact domain

Let us now consider that triangulation as a finite element mesh, and that the displacement field $\mathbf{u}_{n+1}^{(D)}$ is linearly interpolated at the interior of D^h as:

$$\begin{aligned}
&\mathbf{u}_{n+1}^{h}(\mathbf{x}_n) = \sum_{i=1}^{n_{vert}} N_i(\mathbf{x}_n)\,\mathbf{d}_i \\
&\mathbf{u}_{n+1}^{(e)}(\mathbf{x}_n) = \bar{\mathbf{N}}^{(e)}(\mathbf{x}_n)\,\mathbf{d}^{(e)} \quad \forall \mathbf{x}_n \in \Omega^{(e)} \\
&\mathbf{d}^{(e)} = \left[\mathbf{d}_1, \mathbf{d}_2, \mathbf{d}_3\right]^T
\end{aligned} \tag{114}$$

where $n_{vert.}$ stands for the number of vertices (nodes) of the triangulation, N_i are the standard linear interpolation functions [47], $\mathbf{d}_i$ are *the nodal displacements at the vertices,* and $\mathbf{d}^{(e)}$ and $\bar{\mathbf{N}}^{(e)}$ are the elemental displacement vector and the elemental interpolation matrix of a typical element e, respectively.

> **REMARK 5-1.** Notice that this piece-wise linear interpolation is an approach of the linear interpolation in equation (11). In addition, the normal $\mathbf{N} \equiv \mathbf{N}^{(e)}$ is defined in an element-wise constant manner inside every element (see Figure 6). Due to this, and to the linear character of the interpolated displacement field, its gradient $\nabla \mathbf{u}_{n+1}^{h}$ is constant inside the element, and so are the tensor $\mathbf{F}_{n+1}^{h}$ in equations (14), the extrapolated based normal $\tilde{\mathbf{n}}$ in equation (26) and the normalized gaps in equations (27) i.e.:
>
> $$\left.\begin{aligned}
> &\tilde{\mathbf{n}}(\mathbf{x}_n) \equiv \tilde{\mathbf{n}}^{(e)} \\
> &\tilde{g}_n(\mathbf{x}_n) \equiv \tilde{g}_n^{(e)} \\
> &\tilde{g}_t(\mathbf{x}_n) \equiv \tilde{g}_t^{(e)}
> \end{aligned}\right\} = (\text{constant}) \quad \forall \mathbf{x}_n \in \Omega^{(e)} \tag{115}$$

In turn, the interpolation of the Lagrange multipliers λ_N and λ_T is based on element-wise constant interpolation functions $\Phi^{(e)}$. This reads:

$$\begin{aligned}
&\lambda_N(\mathbf{x}_n) = \sum_{e=1}^{n_{triang.}} \Phi^{(e)}(\mathbf{x}_n)\Lambda_N^{(e)} \quad ; \quad \lambda_T = \sum_{e=1}^{n_{triang.}} \Phi^{(e)}(\mathbf{x}_n)\Lambda_T^{(e)} \\
&\Phi^{(e)}(\mathbf{x}_n) = \begin{cases} 1 & \forall \mathbf{x}_n \in \Omega^{(e)} \\ 0 & \forall \mathbf{x}_n \notin \Omega^{(e)} \end{cases}
\end{aligned} \tag{116}$$

where the elemental support of the interpolation functions, $\Phi^{(e)}(\mathbf{x}_n)$, allows a decoupled, element-by-element, solution of the variational equations (108) and (109) i.e.:

$$\begin{aligned}
&\delta\Pi^h_{\lambda_N^{(e)}}(\mathbf{d},\Lambda_N^{(e)},\delta\Lambda_N^{(e)}) \equiv \\
&\quad \int_{\Omega^{(e)}} \delta\Lambda_N^{(e)}\, \tilde{g}_n^{(e)} d\Omega + \int_{\Gamma_N^{(e)}} \delta\Lambda_N^{(e)} \tau^{(e)} (P_{\tilde{n}N}^{(e)} - \Lambda_N^{(e)}) d\Gamma = 0 \\
&\quad \forall \delta\Lambda_N^{(e)} \quad \forall e \in D^{(N)} \subset D^h \\
&\delta\Pi^h_{\lambda_T^{(e)}}(\mathbf{d},\Lambda_T^{(e)},\delta\Lambda_T^{(e)}) \equiv \\
&\quad \int_{\Omega^{(e)}} \delta\Lambda_T^{(e)}\, \tilde{g}_t^{(e)} d\Omega + \int_{\Gamma_T^{(e)}} \delta\Lambda_T^{(e)} \tau^{(e)} (P_{\tilde{t}N}^{(e)} - \Lambda_T^{(e)}) d\Gamma = 0 \\
&\quad \forall \delta\Lambda_T^{(e)} \quad \forall e \in D^{(T)} \subset D^h
\end{aligned} \tag{117}$$

Their solution reads:

$$\begin{aligned}
&\int_{\Omega^{(e)}} \tilde{g}_n^{(e)} d\Omega + \int_{\Gamma_N^{(e)}} \tau^{(e)} (P_{\tilde{n}N}^{(e)} - \Lambda_N^{(e)}) d\Gamma = 0 \quad \forall e \in D^{(N)} \subset D^h \\
&\int_{\Omega^{(e)}} \tilde{g}_t^{(e)} d\Omega + \int_{\Gamma_T^{(e)}} \tau^{(e)} (P_{\tilde{t}N}^{(e)} - \Lambda_T^{(e)}) d\Gamma = 0 \quad \forall e \in D^{(T)} \subset D^h
\end{aligned} \tag{118}$$

If the elemental stress measures $P_{\tilde{n}N}^{(e)}$ and $P_{\tilde{t}N}^{(e)}$ are assumed constant along the elemental boundary $\Gamma_N^{(e)}$ or $\Gamma_T^{(e)}$, see Figure 6, and obtained from the adjacent element in the corresponding contacting body, integration of equations (118) yields:

$$\begin{aligned}
&\tilde{g}_n^{(e)} \Omega^{(e)} + \tau^{(e)} (P_{\tilde{n}N}^{(e)} - \Lambda_N^{(e)}) l^{(e)} = \frac{\tilde{G}_n^{(e)}}{G_N^0} \Omega^{(e)} + \tau^{(e)} (P_{\tilde{n}N}^{(e)} - \Lambda_N^{(e)}) l^{(e)} = 0 \quad \forall e \in D^{(N)} \\
&\tilde{g}_t^{(e)} \Omega^{(e)} + \tau^{(e)} (P_{\tilde{t}N}^{(e)} - \Lambda_T^{(e)}) l^{(e)} = \frac{\tilde{G}_t^{(e)}}{G_N^0} \Omega^{(e)} + \tau^{(e)} (P_{\tilde{t}N}^{(e)} - \Lambda_T^{(e)}) l^{(e)} = 0 \quad \forall e \in D^{(T)}
\end{aligned} \tag{119}$$

And, taking into account the definition of the normalized gaps in equations (22),

$$\begin{aligned}
\tilde{G}_n^{(e)}(\mathbf{u}_{n+1}^{(e)}) &= \tilde{G}_n(\mathbf{x}_k) = \tilde{g}_n^{(e)} G_N^{(0)}(\mathbf{x}_k) = \tilde{\mathbf{n}}^{(e)} \cdot (\mathbf{N} + \nabla \mathbf{u}_{n+1}^{(e)} \cdot \mathbf{N}) G_N^{(0)} \\
\tilde{G}_t^{(e)}(\mathbf{u}_{n+1}^{(e)}) &= \tilde{G}_t(\mathbf{x}_k) = \tilde{g}_t^{(e)} G_N^{(0)}(\mathbf{x}_k) = \tilde{\mathbf{t}}^{(e)} \cdot (\mathbf{N} + \nabla \mathbf{u}_{n+1}^{(e)} \cdot \mathbf{N}) G_N^{(0)}
\end{aligned} \tag{120}$$

In equation (120) $\tilde{G}_n^{(e)} = \tilde{G}_n(\mathbf{x}_k)$ and $\tilde{G}_t^{(e)} = \tilde{G}_t(\mathbf{x}_k)$ are the (extrapolation based) normal and tangential gaps, respectively, *at the end of the current time step*, for the vertex (node) k (see Figure 6). Now taking into account the expression of the area of the elemental triangle ($\Omega^{(e)} = (1/2) G_N^{(0)} l^{(e)}$), straightforward operations in equations (120) yield:

$$\left.\begin{aligned}
G_n^{num.}(\mathbf{u}_{n+1}^{(e)}) &\equiv \tilde{G}_n^{(e)} + 2\tau^{(e)} (P_{\tilde{n}N}^{(e)} - \Lambda_N^{(e)}) \\
G_t^{num.}(\mathbf{u}_{n+1}^{(e)}) &\equiv \tilde{G}_t^{(e)} + 2\tau^{(e)} (P_{\tilde{t}N}^{(e)} - \Lambda_T^{(e)})
\end{aligned}\right\} \quad \forall e \in D^h \tag{121}$$

which, after substitution in equations (119) yield the following *numerical constraint equations*:

$$\begin{aligned}
G_n^{num.}(\mathbf{u}_{n+1}^{(e)}) &= 0 \quad \forall e \in D^{(N)} \\
G_t^{num.}(\mathbf{u}_{n+1}^{(e)}) &= 0 \quad \forall e \in D^{(T)}
\end{aligned} \tag{122}$$

REMARK 5-2. Equations (122) are computed as the sum of the actual *geometric gaps*, $\tilde{G}_n^{(e)}$ and $\tilde{G}_t^{(e)}$, plus the additional term penalized by the

elemental penalty value $\tau^{(e)}$ in equation (121). *A null value of* $\tau^{(e)}$ *will translate* into a numerical gap equal to the geometrical gap*, and*, therefore, *into an exact imposition of the node* (k) *to segment* (i,j) *contact in every element* (e) *of the contact domain mesh* (see Figure 6). Small non-zero values of $\tau^{(e)}$, necessary for the lambda-solvability issues, will perturb slightly that exact imposition of the geometrical constraints. Additionally, mesh refinement will also make the penalized terms $(P_{\tilde{n}N}^{(e)} - \Lambda_N^{(e)})$ and $(P_{\tilde{t}N}^{(e)} - \Lambda_T^{(e)})$ tend to zero, according to equations (80), and, again, the numerical and geometrical gaps will coincide, regardless the size of the penalty value $\tau^{(e)}$ (consistent penalty).

REMARK 5-3. Notice that the final constraint equations (122) are independent of the value of the initial normal gap $G_N^{(0)}$, which could eventually be null, as it was anticipated in REMARK 2-1. In fact, *the only relevant aspect for determination of the effective gaps in a given element* (e) *of the contact domain,* (see Figure 6), *is the connectivity of the three nodes* (i,j,k) *of the element.* This will be conveniently recalled for numerical implementation purposes in the second part of this work [16].

5.2. Active set strategy.

From the definition of the numerical gaps in equation (121), and accounting for equations (122), one can solve for the elemental normal and tangential Lagrange multipliers as:

$$\begin{aligned} \Lambda_N^{(e)} &= P_{\tilde{n}N}^{(e)} + \frac{1}{2\tau^{(e)}} \tilde{G}_n^{(e)}(\mathbf{u}_{n+1}^{(e)}) \quad \forall e \in D^{(N)} \\ \Lambda_T^{(e)} &= P_{\tilde{t}N}^{(e)} + \frac{1}{2\tau^{(e)}} \tilde{G}_t^{(e)}(\mathbf{u}_{n+1}^{(e)}) \quad \forall e \in D^{(T)} \end{aligned} \tag{123}$$

where the role of $\tau^{(e)} > 0$ to allow for the, element by element, *lambda solvability* is clearly displayed.

5.2.1. Effective gaps

By multiplying equations (123) times $2\tau^{(e)}$ one gets the, from now on termed, *effective gaps*:

$$\begin{aligned} \bar{G}_n^{(e)}(\mathbf{u}_{n+1}^{(e)}) &\equiv \tilde{G}_n^{(e)} + 2\tau^{(e)} P_{\tilde{n}N}^{(e)} = 2\tau^{(e)} \Lambda_N^{(e)} \quad \forall e \in D^{(N)} \\ \bar{G}_t^{(e)}(\mathbf{u}_{n+1}^{(e)}) &\equiv \tilde{G}_t^{(e)} + 2\tau^{(e)} P_{\tilde{t}N}^{(e)} = 2\tau^{(e)} \Lambda_T^{(e)} \quad \forall e \in D^{(T)} \end{aligned} \tag{124}$$

REMARK 5-4. The most relevant features of the so defined effective gaps $\bar{G}_n^{(e)}$ and $\bar{G}_t^{(e)}$ are:

- For $\tau^{(e)} > 0$ *they have the same sign* then the lambda multipliers, $\Lambda_N^{(e)}$ and $\Lambda_T^{(e)}$ i.e.:

$$\left.\begin{aligned} sign(\bar{G}_n^{(e)}(\mathbf{u}_{n+1}^{(e)})) &= sign(\Lambda_N^{(e)}) \\ sign(\bar{G}_t^{(e)}(\mathbf{u}_{n+1}^{(e)})) &= sign(\Lambda_T^{(e)}) \end{aligned}\right\} \quad \forall e \in D^h \tag{125}$$

  Therefore, they are *displacement-based* indicators of the sign of the Lagrange multipliers.

- They are constructed on the basis of values of geometrical gaps, $\tilde{G}_n^{(e)}$ and $\tilde{G}_t^{(e)}$, and contact (friction) stresses $P_{\tilde{n}N}^{(e)}$, $P_{\tilde{t}N}^{(e)}$. Due to this, they exhibit suitable *smoothness properties* along situations involving change of the contact/friction scenario, i.e: contact-to-release and stick-to-slip. This fact will crucially used in the specific algorithm for determining the active contact/friction sets (see also REMARK 5-5 below).

5.2.2. *Inequality constraints. Active constraints indicators.*

According to the definitions of the active domains $D^{(N)}$ and $D^{(T)}$, in equations (82) and (83), $\Lambda_N^{(e)} < 0$ and $F^{slip^{(e)}} < 0$ are being taken, respectively, as indicators for the element e to belong to $D^{(N)}$ or to $D^{(T)}$ i.e.:

$$\begin{aligned} &\Lambda_N^{(e)} < 0 \quad \Leftrightarrow e \in D^{(N)} \\ &F^{slip^{(e)}} < 0 \;\Leftrightarrow e \in D^{(T)} \end{aligned} \tag{126}$$

Now, in view of equations (125)

$$e \in D^{(N)} \Leftrightarrow \begin{cases} \Lambda_N^{(e)} < 0 \\ sign(\Lambda_N^{(e)}) = sign(\bar{G}_n^{(e)}) \end{cases} \Leftrightarrow \bar{G}_n^{(e)} < 0 \tag{127}$$

In addition, in Appendix II it is shown that $D^{(T)} \subset D^{(N)}$. Then, from the definition of F^{slip} in equation (79) and equations (126), and (123):

$$\begin{aligned} & e \in D^{(N)} \Rightarrow F^{slip^{(e)}} = \left\{ \left|\Lambda_T^{(e)}\right| - \mu \left|\Lambda_N^{(e)}\right| < 0 \right\} \Rightarrow \\ & \Rightarrow | P_{\tilde{t}N}^{(e)} + \frac{1}{2\tau^{(e)}} \tilde{G}_t^{(e)} | - \mu | P_{\tilde{n}N}^{(e)} + \frac{1}{2\tau^{(e)}} \tilde{G}_n^{(e)} | = \\ & \frac{1}{2\tau^{(e)}} (| \tilde{G}_t^{(e)} + 2\tau^{(e)} P_{\tilde{t}N}^{(e)} | - \mu | \tilde{G}_n^{(e)} + 2\tau^{(e)} P_{\tilde{n}N}^{(e)} |) = \\ & \frac{1}{2\tau^{(e)}} (| \bar{G}_t^{(e)} | - \mu | \bar{G}_n^{(e)} |) < 0 \Leftrightarrow | \bar{G}_t^{(e)} | - \mu | \bar{G}_n^{(e)} | < 0 \end{aligned} \tag{128}$$

where the fact that $\tau^{(e)} > 0$ and equations (124) (only defined in $D^{(N)}$ and $D^{(T)}$), have been considered. Then, from equations (127) and (128) we obtain the following suitable (displacement based) active constraint indicators $\beta_N^{(e)}$ and $\beta_T^{(e)}$:

$$\begin{aligned} &e \in D^{(N)} \Leftrightarrow \beta_N^{(e)}(\mathbf{u}_{n+1}) \overset{def}{=} \bar{G}_n^{(e)} < 0 \\ &e \in D^{(T)} \Leftrightarrow \beta_T^{(e)}(\mathbf{u}_{n+1}) \overset{def}{=} | \bar{G}_t^{(e)} | - \mu | \bar{G}_n^{(e)} | < 0 \end{aligned} \tag{129}$$

5.2.3. *Active set strategy. Iterative algorithm*

Let us first assume that the only reason for non-linearity of the problem lies in the non linear dependence of the active constraint indicators $\beta_N^{(e)}(\mathbf{u}_{n+1})$ and $\beta_T^{(e)}(\mathbf{u}_{n+1})$ on the displacement field. Then, in the current time step $[t_n, t_{n+1}]$ the iterative algorithm in Box 1 is proposed for determining the active contact/friction element set.

DATA:	$(\bar{G}_n^{(e)})_n, (\bar{G}_n^{(e)})_{n-1}$ $(\bar{G}_t^{(e)})_n, (\bar{G}_t^{(e)})_{n-1}$ → Effective gaps at the end of the previous time steps (n, n - 1) $\Delta\bar{G}_n^{(e)} = (\bar{G}_n^{(e)})_n - (\bar{G}_n^{(e)})_{n-1}$ $\Delta\bar{G}_t^{(e)} = (\bar{G}_t^{(e)})_n - (\bar{G}_t^{(e)})_{n-1}$ $D^h \rightarrow$ Contact domain triangularization for the current time step
1) Initialization:	$\bar{G}_n^{(e)^{(0)}} = (\bar{G}_n^{(e)})_n + \frac{\Delta t_{n+1}}{\Delta t_n}(\Delta\bar{G}_n^{(e)})_n$ $\bar{G}_t^{(e)^{(0)}} = (\bar{G}_t^{(e)})_n + \frac{\Delta t_{n+1}}{\Delta t_n}(\Delta\bar{G}_t^{(e)})_n$ → Effective gap extrapolation for iteration zero $i = 0 \rightarrow$ Iteration counter
2) Compute active sets:	For i ≠ 0 compute $\mathbf{u}_{n+1}^{(i)} = \bar{\mathbf{N}}\,\mathbf{d}_{n+1}^{(i)}$, $\bar{G}_n^{(e)}(\mathbf{u}_{n+1}^{(i)})$, $\bar{G}_t^{(e)}(\mathbf{u}_{n+1}^{(i)})$ Compute $\beta_N^{(e)}(\bar{G}_n^{(e)^{(i)}})$, $\beta_T^{(e)}(\bar{G}_t^{(e)^{(i)}})$ *Loop* $\forall e \in D^h$ *if* $\beta_N^{(e)} < 0 \rightarrow e \in D^{(N)^{(i)}}$ *if* $\beta_T^{(e)} < 0 \rightarrow e \in D^{(T)^{(i)}}$ *end loop* → $D^{(N)^{(i)}}, D^{(T)^{(i)}}$ *if* $i = 0 \rightarrow$ Go to step 4
3) Check convergence of the active sets:	if $D^{(N)^{(i)}} = D^{(N)^{(i-1)}}$ and $D^{(T)^{(i)}} = D^{(T)^{(i-1)}} \rightarrow$ *EXIT*
4) Solve the equality constrained problem:	$i = i + 1$ $\mathbf{K}\,\mathbf{d}_{n+1}^{(i)} = \mathbf{f}_{n+1} \rightarrow \mathbf{d}_{n+1}^{(i)} \rightarrow$ Go to step 2

Box 1: Algorithm for determination of the contact/friction active sets

The algorithm ends with converged active sets, $D^{(N)}$ and $D^{(T)}$ fulfilling equations (126) to (128), and a displacement field $\mathbf{u}_{n+1}(\mathbf{d}_{n+1})$ fulfilling equations (129) and the equality constrained problem in equations (108) and (109).

For the mechanical non-linear case, the algorithm in Box 1 can be combined, as an internal or an external loop, with the Newton-Raphson iterations.

> **REMARK 5-5.** The computational effectiveness of the active set strategy presented in Box 1, relies crucially on the appropriate prediction of the active set made in the iteration zero, so that, in most cases, the algorithm converges in a unique iteration. This is based on *the good predictive properties of the extrapolation for the effective gaps* $\bar{G}_n^{(e)^{(0)}}$ and $\bar{G}_t^{(e)^{(0)}}$ made in the initialization stage, which, in turn, is based on the smoothness of those entities along the process (see REMARK 5-4).

6. CONCLUDING REMARKS

Along this work, a new approach to solve computational contact mechanic problems has been presented. In this first part, the theoretical aspects of the approach have been described for two-dimensional problems, including the frictionless and frictional cases and considering large strain kinematics in the contacting bodies. The approach presents some relevant distinguishing features with respect to more classical ones, namely:

- The use of a two-dimensional domain, *the contact domain*, generated via a Delaunay triangulation to join the contacting bodies. The computationally costly node-to-segment or segment-to-segment searches are replaced here by that triangulation, which implicitly provides anticipated information about the contacting entities.
- Related to the previous point an updated Lagrangean approach [23] is used to describe the motion of the involved bodies. Therefore, the reference configuration is updated, to the converged one, at the end of every time step. This translates, in a natural manner, into the proximity of the contacting bodies in the reference configuration, which allows an effective exploitation of the proposed triangularization procedure.
- The contact/friction restrictions are then imposed on that contact domain by means of appropriated definitions of the gaps, and the corresponding variational equations, via Lagrange-multiplier procedures. The Lagrange multipliers are then made condensable via an interior penalty method, which, in addition, provides stability to the mixed displacement-Lagrange multiplier problem. The problem can then be reduced to a displacement-based problem and the Lagrange multipliers, which are computed in closed form, can be interpreted in the classical sense as specific stress components at the contacting boundaries.
- Determination of the active contact/friction sets in the contact domain is made via an *active set strategy*. The concept of *effective gap*s, as mechanical entities involving the geometrical gaps and the contact stresses exhibiting suitable smoothness properties for predictive strategies, is introduced and used for such purposes.

Details on the numerical and implementation aspects of the approach, as well as numerical simulations and comparison studies to prove its computational efficiency are provided in the second part of this work [16].

Acknowledgements

Financial support from the Spanish Ministry of Science and Technology through grant BIA2005-09250-C03-03 is gratefully acknowledged. The second author also acknowledges the support of the German Research Foundation through grant HA 5433|1-1.

REFERENCES

[1] Arnold D.N. An interior penalty finite element method with discontinuous elements. *SIAM J. Numer. Anal.* **19**, 742--760, 1982.

[2] Benson D.,Hallquist J. A single surface contact algorithm for the post-buckling analysis of shell structures. *Computer Methods in Applied Mechanics and Engineering*. **78**, 141-163, 1990.

[3] Bernardi C.,Debit N.,Maday Y. Coupling Finite Elements and Spectral Methods: First Results. *Mathematics of Computation*. **54**, 21-39, 1990.

[4] Bernardi C.,Maday Y.,Patera A., Domain decomposition by the mortar element method, in *Asymptotic and Numerical Methods for Partial Differential Equations with Critical Parameters*, H. Kasper and M. Garby, Eds. Dordrecht, Netherlands: Kluwer Academic Publisher, 1993, pp. 269-286.

[5] Bernardi C.,Maday Y.,Patera A., A new nonconforming approach to domain decomposition: the mortar element method, in *Nonlinear partial differential equations and their applications - Collège de France Seminar*, vol. XI, H. Brezis and J. Lions, Eds.: Longman, Harlow, 1994, pp. 13-51.

[6] Bonet J.,Wood R.D. *Non linear continuum mechanics for finite element analysis*. Cambridge, UK: Cambridge University Press, 1997.

[7] Bruneel H.C.J.,De Rycke I. QuickTrace: a fast algorithm to detect contact. *International Journal for Numerical Methods in Engineering*. **54**, 299-316, 2002.

[8] Fischer K.A., Mortar Type Methods Applied to Nonlinear Contact Mechanics, Ph.D. Thesis, Research Report F05/2, Institut für Baumechanik und Numerische Mechanik, Universtität Hannover, Germany. 2005.

[9] Fischer K.A.,Wriggers P. Frictionless 2D Contact formulations for finite deformations based on the mortar method. *Computational Mechanics*. **36**, 226-244, 2005.

[10] Fischer K.A.,Wriggers P. Mortar based frictional contact formulation for higher order interpolations using the moving friction cone. *Computer Methods in Applied Mechanics and Engineering*. **195**, 5020-5036, 2006.

[11] George P.L. *Automatic Mesh Generation, Applications to Finite Methods*. New York: Wiley, 1991.

[12] Hallquist J., An implicit, finite-deformation, finite element code for analysing the static and dynamic response of two-dimensional solids, Technical Report UCRL-52678, University of California, Lawrence Livermore National Laboratory 1979.

[13] Hallquist J.,Goudreau G.,Benson D. Sliding interfaces with contact-impact in large-scale Lagrangian computations. *Computer Methods in Applied Mechanics and Engineering*. **51**, 107-137, 1985.

[14] Hartmann S., Kontaktanalyse dünnwandiger Strukturen bei großen Deformationen, Ph.D. Thesis, Report No 49, Institut für Baustatik, Universität Stuttgart, Germany 2007.

[15] Hartmann S.,Brunssen S.,Ramm E.,Wohlmuth B. Unilateral non-linear dynamic contact of thin-walled structures using a primal-dual active set strategy. *International Journal for Numerical Methods in Engineering*. **70**, 883-912, 2007.

[16] Hartmann S.,Oliver J.,Weyler R.,Cante J.C.,Hernández J. A new approach in computational contact mechanics: the contact domain method. Part 2: numerical

aspects. *Computer Methods in Applied Mechanics and Engineering*. **(submitted)**, 2009.

[17] Hartmann S.,Ramm E. A mortar based contact formulation for non-linear dynamics using dual Lagrange multipliers. *Finite Elements in Analysis and Design*. **44**, 245-258, 2008.

[18] Heintz P.,Hansbo P. Stabilized Lagrange multiplier method for bilateral elastic contact with friction. *Comput. Methods Appl. Mech. Engrg.* **195**, 4323-4333, 2006.

[19] Hughes J.R. *The Finite Element Method. Linear Static and Dynamic Finite Element Analysis*: Prentice-Hall, Englewood Cliffs, New Jersey, USA, 1987.

[20] Hughes T.,Taylor R.,Kanoknukulchai W., A finite element method for large displacement contact and impact problems, in *Formulations and Computational Algorithms in FE Analysis*, K. Bathe, Ed. Boston: MIT Press, 1977, pp. 468-495.

[21] Laursen T., Formulation and treatment of frictional contact problems using finite elements, Ph.D. Thesis, Technical Report No. 92-6, Stanford University, USA 1992.

[22] Laursen T.A. *Computational Contact and Impact Mechanics*: Springer, 2002.

[23] Malvern L.E.E. *Introduction to the Mechanics of a Continuous Medium* Prentice-Hall, 1997.

[24] Montlaur A.,Fernandez-Mendez S.,Huerta A. Discontinuous Galerkin methods for the Stokes equations using divergence-free approximations. *Int. J. Numer. Meth. Fluids*. **(submitted)**, 2007.

[25] Nitsche J. Über ein Variationsprinzip zur Lösung von Dirichlet-Problemen bei Verwendung von Teilräumen, die keinen Randbedingungen unterworfen sind. *Abhandlungen in der Mathematik an der Universität Hamburg*. **36**, 9-15, 1971.

[26] Oldenburg M.,Larsgunnar N. The position code algorithm for contact searching. *International Journal for Numerical Methods in Engineering*. **37**, 359-386, 1994.

[27] Oliver J.,Cante J.C.,Weyler R.,González C.,Hernández J. Particle finite element methods in solid mechanics problems. in *Computational Plasticity*, E. Oñate and R. Owen, Eds.: Springer, 2007.

[28] Padmanabhan V.,Laursen T. A framework for development of surface smoothing procedures in large deformation frictional contact analysis. *Finite Elements in Analysis and Design*. **37**, 173-198, 2001.

[29] Papadopoulos P.,R. T. A mixed formulation for the finite element solution of contact problems. *Computer Methods in Applied Mechanics and Engineering*. **94**, 373-389, 1992.

[30] Puso M.,Laursen T. A 3d contact smoothing method using gregory patches. *International Journal for Numerical Methods in Engineering*. **54**, 1161-1194, 2002.

[31] Puso M.,Laursen T. A mortar segment-to-segment contact method for large deformation solid mechanics. *Computer Methods in Applied Mechanics and Engineering*. **193**, 601-629, 2004.

[32] Puso M.,Laursen T. A mortar segment-to-segment frictional contact method for large deformations. *Computer Methods in Applied Mechanics and Engineering*. **193**, 4891-4913, 2004.

[33] Simo J.,Hughes T.H.R. *Computational Inelasticity*. New York: Springer-Verlag, 1998.

[34] Simo J.,Wriggers P.,R. T. A perturbed Lagrangian formulation for the finite element solution of contact problems. *Computer Methods in Applied Mechanics and Engineering*. **50**, 163-180, 1985.
[35] Stadler M.,Holzapfel G. Subdivision schemes for smooth contact surfaces of arbitrary mesh topology in 3d. *International Journal for Numerical Methods in Engineering*. **60**, 1161-1195, 2004.
[36] Taylor R.,Wriggers P., Smooth surface discretization for large deformation frictionless contact, Technical Report UCB/SEMM-99-04, University of California, Berkeley, 1999.
[37] Wang S.P.,Nakamacki E. The inside-outside contact search algorithm for finite element analysis. *International Journal for Numerical Methods in Engineering*. **40**, 3665-3685, 1997.
[38] Wriggers P. *Computational Contact Mechanics*. 2nd ed. New York: Springer Berlin / Heidelberg, 2006.
[39] Wriggers P.,Krstulovic-Opera L.,Korelc J. Smooth c1-interpolations for two-dimensional frictional contact problems. *International Journal for Numerical Methods in Engineering*. **51**, 2001.
[40] Wriggers P.,Vu Van T.,Stein E. Finite element formulation of large deformation impact-contact problems with friction. *Computers and Structures*. **37**, 319-331, 1990.
[41] Wu J.-H.,Juang C.H.,Lin H.-M. Vertex-to-face contact searching algorithm for three dimensional frictionless contact problems. *International Journal for Numerical Methods in Engineering*. **63**, 876-897, 2005.
[42] Yang B.,Laursen T. A contact searching algorithm including bounding volume trees applied to finite sliding mortar formulations. *Computational Mechanics*. **41**, 189-205, 2008.
[43] Yang B.,Laursen T. A large deformation mortar formulation of self contact with finite sliding. *Computer Methods in Applied Mechanics and Engineering*. **197**, 756-772, 2008.
[44] Yang B.,Laursen T.,Meng X. Two dimensional mortar contact methods for large deformation frictional sliding. *International Journal for Numerical Methods in Engineering*. **62**, 1183-1225, 2005.
[45] Zavarise G.,Wriggers P. A segment-to-segment contact strategy. *Mathematical and Computer Modelling*. **28**, 497-515, 1998.
[46] Zhong Z.-H.,Nilsson L. A contact searching algorithm for general contact problems. *Computers and Structures*. **33**, 197-209, 1989.
[47] Zienkiewicz O.C.,Taylor R.L. *The Finite Element Method*. Oxford UK: Butterworth-Heinemann, 2000.

APPENDIX I.

EQUIVALENCE OF THE VARIATIONAL AND THE BOUNDARY VALUE PROBLEMS FOR THE FRICTIONAL CASE

From the variational equation (100):

$$\delta\Pi_u(\mathbf{u},\lambda_N,\lambda_T,\delta\mathbf{u}) \equiv \underbrace{\int_\Omega \mathbf{P}(\mathbf{u}):\nabla\delta\mathbf{u}d\Omega - (\int_\Omega \delta\mathbf{u}\cdot\mathbf{b}d\Omega + \int_{\Gamma_\sigma}\delta\mathbf{u}\cdot\mathbf{t}^* d\Gamma)}_{(I)} +$$
$$+\underbrace{\int_{D^{(N)}}\tilde{\mathbf{n}}\cdot\nabla\delta\mathbf{u}\cdot\mathbf{N}\,\lambda_N dD}_{(II)} + \underbrace{\int_{D^{(T)}}\tilde{\mathbf{t}}\cdot\nabla\delta\mathbf{u}\cdot\mathbf{N}\,\lambda_T dD}_{(III)} \tag{130}$$
$$+\underbrace{\int_{D^{(N)}\setminus D^{(T)}}\tilde{\mathbf{t}}\cdot\nabla\delta\mathbf{u}\cdot\mathbf{N}T\;dD}_{(IV)} = 0 \qquad \forall\delta\mathbf{u}\in V^0$$

integration by parts yields of the term (I) yields:

$$\begin{aligned}(I) = &\int_\Omega \mathbf{P}(\mathbf{u}):\nabla\delta\mathbf{u}d\Omega - (\int_\Omega \delta\mathbf{u}\cdot\mathbf{b}d\Omega + \int_{\Gamma_\sigma}\delta\mathbf{u}\cdot\mathbf{t}^* d\Gamma) = \\ &= -\int_\Omega \delta\mathbf{u}\cdot(DIV\,\mathbf{P})d\Omega + \int_{\partial\Omega}(\delta\mathbf{u}\cdot\mathbf{P})\cdot\boldsymbol{\nu}\,d\Gamma - \\ &-(\int_\Omega \delta\mathbf{u}\cdot\mathbf{b}d\Omega + \int_{\Gamma_\sigma}\delta\mathbf{u}\cdot\mathbf{t}^* d\Gamma) = \\ &= -\int_\Omega \delta\mathbf{u}\cdot(DIV\,\mathbf{P}+\mathbf{b})\,d\Omega + \int_{\Gamma_\sigma}\delta\mathbf{u}\cdot(\mathbf{P}\cdot\boldsymbol{\nu}-\mathbf{t}^*)\,d\Gamma + \\ &+\int_{\Gamma_D^{(1)}}\delta\mathbf{u}^{(1)}\cdot\mathbf{P}\cdot\mathbf{N}^{(1)}\,d\Gamma - \int_{\Gamma_D^{(2)}}\delta\mathbf{u}^{(2)}\cdot\mathbf{P}\cdot\mathbf{N}^{(2)}\,d\Gamma\end{aligned} \tag{131}$$

where the divergence theorem over the domain $\Omega\equiv\Omega^{(1)}\cup\Omega^{(2)}$ with Neuman's boundary $\Gamma_\sigma\equiv\Gamma_\sigma^{(1)}\cup\Gamma_\sigma^{(2)}$ has been applied (see Figure 5). In addition, the term (II) in equation (130) can be written:

$$\begin{aligned}(II) = &\int_{D^{(N)}}\tilde{\mathbf{n}}\cdot\nabla\delta\mathbf{u}\cdot\mathbf{N}\,\lambda_N dD = \int_{D^{(N)}}\nabla\cdot((\delta\mathbf{u}\cdot\tilde{\mathbf{n}})\otimes\mathbf{N})\lambda_N dD = \\ &= -\int_{D^{(N)}}(\delta\mathbf{u}\cdot\tilde{\mathbf{n}})(\mathbf{N}\cdot\nabla\lambda_N)\,dD + \int_{\partial D^{(N)}}(\delta\mathbf{u}\cdot\tilde{\mathbf{n}})\lambda_N(\mathbf{N}\cdot\boldsymbol{\nu}^D)\,d\Gamma = \\ &= -\int_{D^{(N)}}(\delta\mathbf{u}\cdot\tilde{\mathbf{n}})\;\underbrace{(\nabla\lambda_N\cdot\mathbf{N})}_{\frac{\partial\lambda_N(T)}{\partial N}=0}\;dD + \int_{\partial D^{(N)}}(\delta\mathbf{u}\cdot\tilde{\mathbf{n}})\lambda_N(\mathbf{N}\cdot\boldsymbol{\nu}^D)\,d\Gamma = \\ &= -\int_{\Gamma_N^{(1)}}\delta\mathbf{u}^{(1)}\cdot(\lambda_N\tilde{\mathbf{n}}^{(1)})\,d\Gamma + \int_{\Gamma_N^{(2)}}\delta\mathbf{u}^{(2)}\cdot(\lambda_N\tilde{\mathbf{n}}^{(2)})\,d\Gamma\end{aligned} \tag{132}$$

where, equations (10) ($\nabla\mathbf{N}\cong\mathbf{0}$), the divergence theorem in the domain $D^{(N)}$, the condition $\frac{\partial\lambda_N}{\partial N}=0$ (from the definition of equation (89)) and the senses of the normal in Figure 5 have been applied. Similarly, for the domain $D^{(T)}$ and the term (III) in equation (130):

$$\begin{aligned}(III) = &\int_{D^{(T)}}\tilde{\mathbf{t}}\cdot\nabla\delta\mathbf{u}\cdot\mathbf{N}\,\lambda_T dD = \int_{D^{(T)}}\nabla\cdot((\delta\mathbf{u}\cdot\tilde{\mathbf{t}})\otimes\mathbf{N})\lambda_T dD = \\ &= -\int_{D^{(T)}}(\delta\mathbf{u}\cdot\tilde{\mathbf{t}})(\mathbf{N}\cdot\nabla\lambda_T)\,dD + \int_{\partial D^{(T)}}(\delta\mathbf{u}\cdot\tilde{\mathbf{t}})\lambda_T(\mathbf{N}\cdot\boldsymbol{\nu}^D)\,d\Gamma = \\ &= -\int_{D^{(T)}}(\delta\mathbf{u}\cdot\tilde{\mathbf{t}})\;\underbrace{(\nabla\lambda_T\cdot\mathbf{N})}_{\frac{\partial\lambda_T(T)}{\partial N}=0}\;dD + \int_{\partial D^{(T)}}(\delta\mathbf{u}\cdot\tilde{\mathbf{t}})\lambda_T(\mathbf{N}\cdot\boldsymbol{\nu}^D)\,d\Gamma = \\ &= -\int_{\Gamma_T^{(1)}}\delta\mathbf{u}^{(1)}\cdot(\lambda_T\tilde{\mathbf{t}}^{(1)})\,d\Gamma + \int_{\Gamma_T^{(2)}}\delta\mathbf{u}^{(2)}\cdot(\lambda_T\tilde{\mathbf{t}}^{(2)})\,d\Gamma\end{aligned} \tag{133}$$

Finally, for the term (IV) in equation (130):

$$
\begin{aligned}
(IV) &= \int_{D^{(N)}\setminus D^{(T)}} \tilde{\mathbf{t}}\cdot\nabla\delta\mathbf{u}\cdot\mathbf{N}T \; dD = \int_{D^{(N)}\setminus D^{(T)}} \nabla\cdot((\delta\mathbf{u}\cdot\tilde{\mathbf{t}})\otimes\mathbf{N})T \; dD = \\
&= -\int_{D^{(N)}\setminus D^{(T)}} (\delta\mathbf{u}\cdot\tilde{\mathbf{t}})(\mathbf{N}\cdot\nabla T \;) dD + \int_{\partial(D^{(N)}\setminus D^{(T)})} (\delta\mathbf{u}\cdot\tilde{\mathbf{t}})T \;\; (\mathbf{N}\cdot\boldsymbol{\nu}^D)\, d\Gamma = \\
&= -\int_{D^{(N)}\setminus D^{(T)}} (\delta\mathbf{u}\cdot\tilde{\mathbf{t}}) \underbrace{(\underbrace{\nabla T \;\cdot\mathbf{N}}_{\frac{\partial T}{\partial N}\;(\lambda_N)})}_{} dD + \int_{\partial(D^{(N)}\setminus D^{(T)})} (\delta\mathbf{u}\cdot\tilde{\mathbf{t}})T \;\; (\mathbf{N}\cdot\boldsymbol{\nu}^D)\, d\Gamma = \\
&= -\int_{D^{(N)}\setminus D^{(T)}} (\delta\mathbf{u}\cdot\tilde{\mathbf{t}}) \frac{dT}{d\lambda_N} \underbrace{\frac{\partial\lambda_N}{\partial N}}_{=0} dD + \int_{\partial(D^{(N)}\setminus D^{(T)})} (\delta\mathbf{u}\cdot\tilde{\mathbf{t}})T \;\; (\mathbf{N}\cdot\boldsymbol{\nu}^D)\, d\Gamma = \\
&= -\int_{\Gamma_N^{(1)}\cap\partial(D^{(N)}\setminus D^{(T)})} \delta\mathbf{u}^{(1)}\cdot(T \;\; \tilde{\mathbf{t}}^{(1)})\, d\Gamma + \int_{\Gamma_N^{(2)}\cap\partial(D^{(N)}\setminus D^{(T)})} \delta\mathbf{u}^{(2)}\cdot(T \;\; \tilde{\mathbf{t}}^{(2)})\, d\Gamma
\end{aligned}
\tag{134}
$$

where the dependence of T on λ_N in equation (104) has been exploited. Substitution of equations (131) to (134) into equation (130) yields:

$$
\begin{aligned}
&\delta\Pi_u(\mathbf{u},\lambda_N,\lambda_T,\delta\mathbf{u}) = 0 \;\; \forall\delta\mathbf{u} \;\; in \;\; \Omega \Rightarrow \\
&\Rightarrow DIV\,\mathbf{P} + \mathbf{b} = \mathbf{0} \quad in \;\; \Omega \equiv \Omega^{(1)} \cup \Omega^{(2)}
\end{aligned}
\tag{135}
$$

which matches equation (90). Then

$$
\begin{aligned}
&\delta\Pi_u(\mathbf{u},\lambda_N,\lambda_T,\delta\mathbf{u}) = 0 \;\; \forall\delta\mathbf{u} \;\; in \;\; \Gamma_\sigma \Rightarrow \\
&\Rightarrow \mathbf{P}\cdot\boldsymbol{\nu} - \mathbf{t}^* = \mathbf{0} \quad in \;\; \Gamma_\sigma \equiv \Gamma_\sigma^{(1)} \cup \Gamma_\sigma^{(2)}
\end{aligned}
\tag{136}
$$

fulfilling equation (93). On the other hand

$$
\begin{aligned}
&\delta\Pi_u(\mathbf{u},\lambda_N,\lambda_T,\delta\mathbf{u}) = 0 \;\; \forall\delta\mathbf{u} \;\; in \;\; \Gamma_N \equiv \Gamma_N^{(1)} \cup \Gamma_N^{(2)} \Rightarrow \\
&\Rightarrow \left.\begin{array}{l}
\mathbf{P}\cdot\mathbf{N}^{(1)} - (\lambda_N\tilde{\mathbf{n}}^{(1)} + \lambda_T\tilde{\mathbf{t}}^{(1)}) = \mathbf{0} \quad in \;\; \Gamma_T^{(1)} \\
\mathbf{P}\cdot\mathbf{N}^{(1)} - (\lambda_N\tilde{\mathbf{n}}^{(1)} + T \;\tilde{\mathbf{t}}^{(1)}) = \mathbf{0} \quad in \;\; \Gamma_N^{(1)} \cap \partial(D^{(N)} \setminus D^{(T)}) \\
\mathbf{P}\cdot\mathbf{N}^{(2)} - (\lambda_N\tilde{\mathbf{n}}^{(2)} + \lambda_T\tilde{\mathbf{t}}^{(2)}) = \mathbf{0} \quad in \;\; \Gamma_T^{(2)} \\
\mathbf{P}\cdot\mathbf{N}^{(2)} - (\lambda_N\tilde{\mathbf{n}}^{(2)} + T \;\tilde{\mathbf{t}}^{(2)}) = \mathbf{0} \quad in \;\; \Gamma_N^{(2)} \cap \partial(D^{(N)} \setminus D^{(T)})
\end{array}\right\} \Rightarrow \\
&\Rightarrow \begin{cases}
\tilde{\mathbf{n}}\cdot\mathbf{P}\cdot\mathbf{N} = \lambda_N \quad in \;\; \Gamma_N \equiv \Gamma_N^{(1)} \cup \Gamma_N^{(2)} \\
\tilde{\mathbf{t}}\cdot\mathbf{P}\cdot\mathbf{N} = \lambda_T \quad in \;\; \Gamma_T \equiv \Gamma_T^{(1)} \cup \Gamma_T^{(2)} \\
\tilde{\mathbf{t}}\cdot\mathbf{P}\cdot\mathbf{N} = T \quad in \;\; \Gamma_N \cap \partial(D^{(N)} \setminus D^{(T)})
\end{cases}
\end{aligned}
\tag{137}
$$

corresponding to equations (95) and (96).

Let us now consider, the assumed linear interpolation of the displacements in equation (11) leading to:

$$
\frac{\partial\mathbf{u}_{n+1}^{(D)}}{\partial N} = \frac{1}{N^+ - N^-}(\mathbf{u}_{n+1}^{(2)}(T) - \mathbf{u}_{n+1}^{(2)}(T)) = \frac{\partial\mathbf{u}_{n+1}^{(D)}}{\partial N}(T)
\tag{138}
$$

Let us also assume that, similarly to equation (10),

$$
\left.\begin{array}{lll}
\dfrac{\partial\mathbf{N}}{\partial N} \cong \mathbf{0} & ; & \dfrac{\partial\mathbf{T}}{\partial N} \cong \mathbf{0} \\
\dfrac{\partial\tilde{\mathbf{n}}}{\partial N} \cong \mathbf{0} & ; & \dfrac{\partial\tilde{\mathbf{t}}}{\partial N} \cong \mathbf{0}
\end{array}\right\} \Rightarrow \begin{array}{lll}
\mathbf{N} = \mathbf{N}(T) & ; & \mathbf{T} = \mathbf{T}(T) \\
\tilde{\mathbf{n}} = \tilde{\mathbf{n}}(T) & ; & \tilde{\mathbf{t}} = \tilde{\mathbf{t}}(T)
\end{array}
\tag{139}
$$

Then, from the normalized gap definitions in equation (27), and equations (138) and (139):

$$\tilde{g}_n(N,T) = \tilde{\mathbf{n}}(\mathbf{u}_n^{(D)}) \cdot (\mathbf{N} + \nabla \mathbf{u}_{n+1}^{(D)} \cdot \mathbf{N}) = \tilde{\mathbf{n}}(T) \cdot (\mathbf{N}(T) + \frac{\partial \mathbf{u}_{n+1}^{(D)}}{\partial N}(T)) = \tilde{g}_n(T)$$
$$\tilde{g}_t(N,T) = \tilde{\mathbf{t}}(\mathbf{u}_n^{(D)}) \cdot (\mathbf{N} + \nabla \mathbf{u}_{n+1}^{(D)} \cdot \mathbf{N}) = \tilde{\mathbf{t}}(T) \cdot (\mathbf{N}(T) + \frac{\partial \mathbf{u}_{n+1}^{(D)}}{\partial N}(T)) = \tilde{g}_t(T) \tag{140}$$

displaying that the normalized gaps are constant along the same coordinate line N. Now, from the first variational equation (101):

$$\delta\Pi_{\lambda_N}(\mathbf{u}, \delta\lambda_N) \equiv \int_{D^{(N)}} \delta\lambda_N \, \tilde{g}_n(\mathbf{u}) dD = 0 \qquad \forall \delta\lambda_N \in \mathbf{L}_N \tag{141}$$

one obtains, in view of equations (140):

$$\int_{D^{(N)}} \delta\lambda_N \, \tilde{g}_n(\mathbf{u}) dD = \int_{T_N^-}^{T_N^+} \delta\lambda_N(T) \tilde{g}_n(T) [\int_{N^-}^{N^+} dN] dT =$$
$$= \underbrace{(N^+ - N^-)}_{\neq 0} \int_{T_N^-}^{T_N^+} \delta\lambda_N(T) \tilde{g}_n(T) dT = 0 \quad \forall \delta\lambda_N \in \mathbf{L}_N \Rightarrow \tag{142}$$
$$\tilde{g}_n(T) = 0 \quad \forall T \in [T_N^-, T_N^+] \Rightarrow \tilde{g}_n(\mathbf{x}_n) = 0 \quad \forall \mathbf{x}_n \in D^{(N)}$$

where the definition of $D^{(N)}$ in equation (82) has been exploited. Therefore, the first equation (97) is fulfilled. Similarly, from the second equation (101):

$$\delta\Pi_{\lambda_T}(\mathbf{u}, \delta\lambda_T) \equiv \int_{D^{(T)}} \delta\lambda_T \, \tilde{g}_t(\mathbf{u}) dD = 0 \qquad \forall \delta\lambda_T \in \mathbf{L}_T \tag{143}$$

$$\int_{D^{(T)}} \delta\lambda_T \, \tilde{g}_t(\mathbf{u}) dD = \int_{T_T^-}^{T_T^+} \delta\lambda_T(T) \tilde{g}_t(T) [\int_{N^-}^{N^+} dN] dT =$$
$$= \underbrace{(N^+ - N^-)}_{\neq 0} \int_{T_T^-}^{T_T^+} \delta\lambda_T(T) \tilde{g}_t(T) dT = 0 \quad \forall \delta\lambda_T \in \mathbf{L}_T \Rightarrow \tag{144}$$
$$\tilde{g}_t(T) = 0 \quad \forall T \in [T_T^-, T_T^+] \Rightarrow \tilde{g}_t(\mathbf{x}_n) = 0 \quad \forall \mathbf{x}_n \in D^{(T)}$$

fulfilling the second of equations (97).

The equations above show that equations (90) to (97) are the Euler-Lagrange equations of the variational problem in equations (98) to (101). The proof for the frictionless case follows from the proof above and a null friction coefficient ($\mu = 0$).

APPENDIX II

Let us assume the proposition $D^{(T)} \cap D^{(N)} \neq D^{(T)}$. Therefore, from equations (126), and (127) there should exist some $\mathbf{x}_n$ such that:

$$\left.\begin{aligned} \mathbf{x}_n \in D^{(T)} &\Rightarrow F^{fric}(\mathbf{x}_n) < 0 \\ \mathbf{x}_n \notin D^{(N)} &\Rightarrow \lambda_N(\mathbf{x}_n) = 0 \end{aligned}\right\} \Rightarrow |\lambda_T(\mathbf{x}_n)| - \mu |\lambda_N(\mathbf{x}_n)| = |\lambda_T(\mathbf{x}_n)| < 0 \tag{145}$$

which is not possible. Therefore

$$D^{(T)} \cap D^{(N)} = D^{(T)} \Rightarrow D^{(T)} \subset D^{(N)} \tag{146}$$

PART 2: NUMERICAL ASPECTS

***Abstract**: This is the second part of the work, describing the numerical aspects of a new approach within the context of computational contact mechanics. The theoretical basis of the newly developed "Contact Domain Method" is detailed in the first part of this paper. Starting from this, the present contribution focuses on describing important algorithmic details that go along with the finite element implementation for two dimensional problems. Important aspects are the construction of the contact domain mesh, via a constraint Delaunay triangulation, the linearization of the discretized contact contributions and some important technical aspects about the extrapolation procedure used for the predictive active set strategy. Finally a set of numerical examples is presented to demonstrate the performance of the developed contact strategy. Demanding static and dynamic contact problems in the context of large deformations, including frictional effects as well as self contact, show the wide applicability and the robustness of the proposed method.*

Keywords: contact domain, interior penalty method, frictional contact, self contact, contact searching, updated lagrangean approach, dynamic contact

1. INTRODUCTION

In the first part of this work [13] the theoretical aspects of the so called *contact domain method* have been presented. The method introduces a new computational contact strategy based on the following elements: 1) the use of an updated lagrangean approach to describe the motion of the contacting bodies, 2) consideration of a two-dimensional contact domain, where the contact/friction restrictions are imposed, and construction of a one layer triangulation in this domain, 3) a Lagrange multiplier method to impose the contact/friction constraints, 4) an interior penalty procedure, allowing condensation of the Lagrange multipliers, ensuring the stability of the discretized problem and 5) an active set strategy, for determining the subsets of the contact domain were contact/friction conditions have to be applied.

Since the approach brings new and very specific ingredients with respect to more classical contact methods [9, 16], the corresponding numerical and algorithmic treatment is far from being trivial. In this sense, and in order to provide to the interested reader suitable information to ensure the reproducibility of the method, this second part of the work concentrates on these numerical and algorithmic aspects, provides detailed information about its finite element implementation and supplies a representative set of examples displaying the performance of the proposed methodology in a number of different contact scenarios.

The remaining of this paper is organized as follows: section 2 shortly describes the problem to be analyzed, summarizes some basic notations and restates the variational problem for the contact domain method derived in [13]. The construction of the contact domain mesh, which can, in turn, be interpreted as a contact searching strategy, is illustrated in section 3. In section 4 the spatial discretization of the contact virtual work and the contact constraint variational equations is given, followed by the necessary linearization of these contributions. Important technical aspects of the predictive active set strategy, introduced in [13] are described in section 5. The performance of the

proposed algorithms is analyzed, in section 6, by means of various numerical examples. Finally, section 7 provides some concluding remarks.

2. PROBLEM DESCRIPTION

In this section a frictional large deformation contact problem will be very briefly recalled to introduce some notations subsequently used in this paper. The contact domain, the utilized gap definitions and the variational problem of the frictional contact problem are summarized. For a detailed derivation of these expressions, the reader is referred to the first part of this work [13].

2.1. Basic notations

Dealing with contact problems, one might need to face scenarios of numerous deformable bodies coming into contact with each other (*multiple contact*), as well as the possibility, that parts of the boundary of one specific body might come into contact with another part of the boundary of the same body (*self contact*). Without lacking generality, the subsequent description will be done on basis of one contact pair. A two-dimensional, large deformation contact problem of two deformable bodies $\Omega^{(1)}$ and $\Omega^{(2)}$ eventually coming into contact within a specific timestep $[t_n, t_{n+1}]$ is shown in Figure 2.

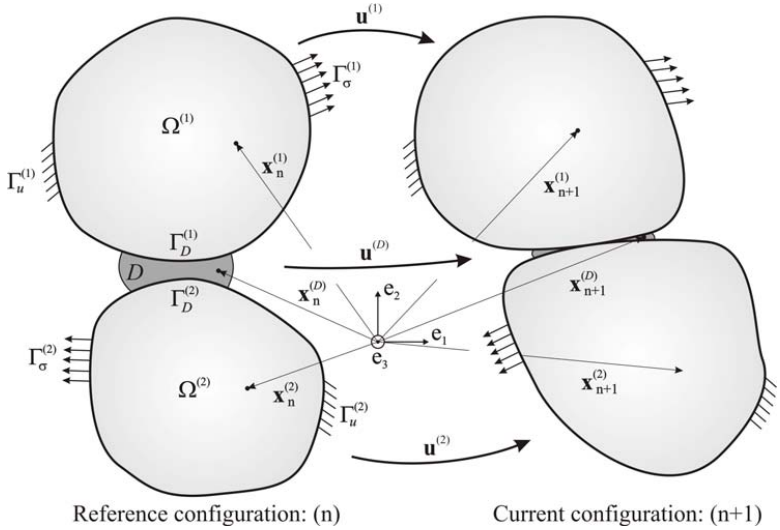

Figure 7: Notation for a two body large deformation contact problem in an updated Lagrangean scheme

Using an *updated Lagrangean approach* [10], the reference (material) configuration will be updated after every timestep, and thus coincides with the configuration at time t_n. Subsequently the index $\alpha = 1,2$ will be used to distinguish between the two bodies. The incremental motion of the bodies can then be written as

$$\mathbf{u}^{(\alpha)} = \mathbf{x}_{n+1}^{(\alpha)} - \mathbf{x}_n^{(\alpha)} \quad . \tag{147}$$

The boundaries $\partial\Omega^{(\alpha)}$ of $\Omega^{(\alpha)}$ are divided into $\Gamma_u^{(\alpha)}$, where displacements are prescribed, $\Gamma_\sigma^{(\alpha)}$ where tractions are prescribed and a part $\Gamma_D^{(\alpha)}$ where the bodies might be in contact at the end of the time interval. It is assumed that the following conditions are satisfied:

$$\Gamma_u^{(\alpha)} \cup \Gamma_\sigma^{(\alpha)} \cup \Gamma_D^{(\alpha)} = \partial\Omega^{(\alpha)} \text{ and} \tag{148}$$

$$\Gamma_\sigma^{(\alpha)} \cap \Gamma_u^{(\alpha)} = \Gamma_\sigma^{(\alpha)} \cap \Gamma_D^{(\alpha)} = \Gamma_u^{(\alpha)} \cap \Gamma_D^{(\alpha)} = \varnothing. \tag{148}$$

In addition to the displacement fields of the contacting bodies, a displacement field $\mathbf{u}^{(D)}$ is defined, which describes the motion of a point in the so-called contact domain. This displacement is linearly interpolated from the corresponding displacements at the contacting boundaries (see Part 1 [13], section 2.1).

2.2. The contact domain

The most relevant feature of the presented contact formulation is the definition of an additional domain, pairing the two potential contact boundaries $\Gamma_D^{(\alpha)}$. A typical contact domain D is shown in Figure 5. It is assumed that the active contact and friction domains, fulfilling the appropriate constraints at the end of the considered time step are known in advance by means of an active set strategy (see Part1, section 5). Therefore the active contact domain $D^{(N)} \subset D$ is subdivided into a part $D^{(T)}$, where stick conditions have to be applied and into the remaining part $D^{(N)} \setminus D^{(T)}$, where slip conditions, fulfilling an appropriate friction law, have to be enforced.

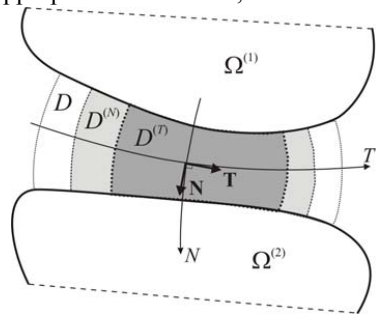

Figure 8: Geometrical definition of the contact domain for the frictional case, accounting for the stick condition (in $D^{(T)}$) and the slip condition (in $D^{(N)} \setminus D^{(T)}$).

2.3. Definition of the normalized gaps

Different to other contact formulations, dimensionless, extrapolation based normalized gap definitions are introduced, which have the property of being contact indicators:

$$\tilde{g}_n(\mathbf{u}^{(D)}) = \tilde{\mathbf{n}} \cdot (\mathbf{N} + \nabla\mathbf{u}^{(D)} \cdot \mathbf{N}) \tag{149}$$

$$\tilde{g}_t(\mathbf{u}^{(D)}) = \tilde{\mathbf{t}} \cdot (\mathbf{N} + \nabla\mathbf{u}^{(D)} \cdot \mathbf{N}) \tag{149}$$

Herein $\tilde{\mathbf{n}}$ and $\tilde{\mathbf{t}}$ are first order approximations of the current (spatial) normal and tangent vectors, $\mathbf{N}$ is the reference (material) normal vector and $\nabla\mathbf{u}^{(D)}$ displays the material gradient of the incremental displacement field. It has to be emphasized, that $\tilde{\mathbf{n}}$ and $\tilde{\mathbf{t}}$, as well as $\mathbf{N}$, are independent of the current incremental deformation and thus the utilized gap definitions in equation (149) display a linear dependence on $\mathbf{u}$. In Part 1

[13], section 2.2, this specific gap definition is deeply explained and the similarity to traditional gap definitions is pointed out.

2.4. Variational problem of frictional contact domain method

Applying a finite element discretization scheme to solve contact problems, an appropriate weak form of the underlying boundary value problem is needed. The *contact domain method* presented in [13] enforces the contact constraints using a generalization of the stabilized Lagrange multiplier method used in [7]. This allows for the condensation of the introduced Lagrange multipliers (λ_N, λ_T), which represent the normal and tangential contact tractions at the contacting boundaries. Assuming, that the active normal and frictional contact domains $D^{(N)}$ and $D^{(T)}$ are known for the present time step $\left[\mathrm{t_n}, \mathrm{t_{n+1}}\right]$, the initial inequality constrained problem can be translated into an equality constrained one (see Part 1, section 4.2). Using appropriate spaces for the displacements, $\mathbf{u} = \left[\mathbf{u}^{(\alpha)}, \mathbf{u}^{(D)}\right]$, and their variations, $\delta\mathbf{u} = \left[\delta\mathbf{u}^{(\alpha)}, \delta\mathbf{u}^{(D)}\right]$ (virtual displacements), as well as for the introduced Lagrange multipliers, $\boldsymbol{\lambda} = \left[\lambda_N, \lambda_T\right]$, and their variations, $\delta\boldsymbol{\lambda} = \left[\delta\lambda_N, \delta\lambda_T\right]$, the utilized variational equations can be summarized. The virtual work principle (see Part 1, section 4.4, equation (104)) reads

$$\delta\Pi_u\left(\mathbf{u}, \delta\mathbf{u}, \boldsymbol{\lambda}\right) = \delta\Pi_{\mathrm{int},ext}\left(\mathbf{u}^{(\alpha)}, \delta\mathbf{u}^{(\alpha)}\right) + \delta\Pi_{cont}\left(\delta\mathbf{u}^{(D)}, \boldsymbol{\lambda}\right) = 0 \tag{150}$$

where $\delta\Pi_{\mathrm{int},ext}\left(\mathbf{u}^{(\alpha)}, \delta\mathbf{u}^{(\alpha)}\right)$ denotes the sum of the virtual work arising from the internal and external forces of the contacting bodies. Various variational energy principles can be utilized to derive an expression for the virtual work done by the internal and external forces of the respective body. As the present work concentrates on the description of the contact phenomena, this will not be detailed any further. The main focus of this work will be on the second contribution in equation (150), namely the contact virtual work. Utilizing the variations of the normal and tangential gap in equation (149), the contact virtual work expression can be written as

$$\delta\Pi_{cont}\left(\delta\mathbf{u}^{(D)}, \boldsymbol{\lambda}\right) = \underbrace{\int_{D^{(N)}} \delta\tilde{g}_n\, \lambda_N dD}_{\text{active normal contact}} + \underbrace{\int_{D^{(T)}} \delta\tilde{g}_t\, \lambda_T dD}_{\text{active stick}} + \underbrace{\int_{D^{(N)}\setminus D^{(T)}} \delta\tilde{g}_t\, \mathcal{T}\, dD}_{\text{active slip}}. \tag{151}$$

Herein, $\mathcal{T} = \mu\, sign\left(\tilde{g}_t\right) |\, \lambda_N\, |$ represents the classical coulomb friction law, with μ being the coefficient of friction. As can be seen in equation (151), the contact virtual work expression consists of three different portions. An integral over the active normal contact domain $D^{(N)}$, the active stick domain $D^{(T)}$ and the active slip domain $D^{(N)} \setminus D^{(T)}$, respectively. For the enforcement of the contact constraints, two additional variational equations (see Part 1 [13], section 4.4, equation (105))

$$\begin{aligned}
\delta\Pi_{\lambda_N}\left(\mathbf{u}^{(\alpha)}, \mathbf{u}^{(D)}, \lambda_N, \delta\lambda_N\right) &= \int_{D^{(N)}} \delta\lambda_N \tilde{g}_n dD + \underbrace{\int_{\Gamma_N} \delta\lambda_N \tau(P_{\tilde{n}N} - \lambda_N) d\Gamma}_{\text{additional term}} = 0 \\
\delta\Pi_{\lambda_T}\left(\mathbf{u}^{(\alpha)}, \mathbf{u}^{(D)}, \lambda_T, \delta\lambda_T\right) &= \int_{D^{(T)}} \delta\lambda_T \tilde{g}_t dD + \underbrace{\int_{\Gamma_T} \delta\lambda_T \tau(P_{\tilde{t}N} - \lambda_T) d\Gamma}_{\text{additional term}} = 0
\end{aligned} \tag{152}$$

are derived, split into a normal and tangential part. Equations $(28)_1$ and $(28)_2$ are the (stabilized) variational constraint equations to enforce the normal and frictional (stick) contact conditions within the appropriate active contact domains $D^{(N)}$ and $D^{(T)}$. The

added terms can be interpreted as stabilization terms, which allow condensing the introduced Lagrange multipliers, where τ is a user defined stabilization parameter, which will be discussed later. Furthermore, $P_{\tilde{n}N}$ and $P_{\tilde{t}N}$ are the projections of the traction vector at the boundaries of the contacting bodies onto the approximated normal and tangential directions, given with

$$P_{\tilde{n}N} = \tilde{\mathbf{n}} \cdot \mathbf{P} \cdot \mathbf{N} \quad \text{and} \quad P_{\tilde{t}N} = \tilde{\mathbf{t}} \cdot \mathbf{P} \cdot \mathbf{N} \,, \tag{153}$$

where $\mathbf{P}$ is the first Piola-Kirchhoff stress tensor. It is worth noting, that the normal and tangential tractions defined in equation (153) live in the body $\Omega^{(\alpha)}$ and not in the contact domain D.

3. CONTACT PAIRING ALGORITHM

Finding the appropriate contact pairs is generally a difficult task, which has lead to various proposals for effective contact searching algorithms (e.g. [1], [12], [18], [19], [17], [2], [21], [15]). Yang and Laursen [19] extend their contact searching algorithm for finite sliding mortar formulations [18] to the case of self contact. In order to achieve a comparable computational cost in their self contact searching algorithm, they need to add some special criterions to their basic algorithm. In this work, a general contact pairing strategy is presented, which can naturally be applied to any contact scenario, including self contact. It is based on a so-called constraint Delaunay triangulation, producing at the same time the necessary contact domain mesh between potential contact pairs. The technical aspects of this procedure are detailed in the following.

3.1. Construction of the contact domain mesh

In Figure 9 the basic steps of the construction of the contact domain mesh are shown. Figure 9a) displays two discretized bodies, eventually being in contact. The contact domain mesh to be constructed should have the property to connect the boundary nodes of the discretized bodies. Therefore all the interior nodes of the discretized bodies are removed. A key step in the generation process is the shrinkage of the outer boundary, taking into account the outward normals. With this shrinkage it is guaranteed, that the boundary nodes are separated sufficiently far enough from each other, such that the automatic mesh generation algorithm can generate a domain mesh. The removal of the interior nodes, as well as the shrinkage or offset of the boundary nodes is displayed in Figure 9b). Subsequently only the position of the modified boundary nodes and their specific outward normal are needed for the remaining steps. This information is then given to an automatic mesh generation algorithm, which connects the boundary nodes within a user defined tolerance of distance. The result of this is the contact domain mesh, given in Figure 9c). It is worth noting, that for the implementation of the presented contact strategy, only the *connectivity* of the boundary nodes, defining a contact domain element, is needed and it will be worked with the original spatial position of the finite element nodes placed at the boundaries of the contacting bodies (see Figure 9d). That means that the important step of repositioning the boundary nodes (shrinkage) is only a technical necessity to allow the meshing algorithm to build up the connectivity, and does not introduce any form of modifying the geometrical description of the contacting bodies.

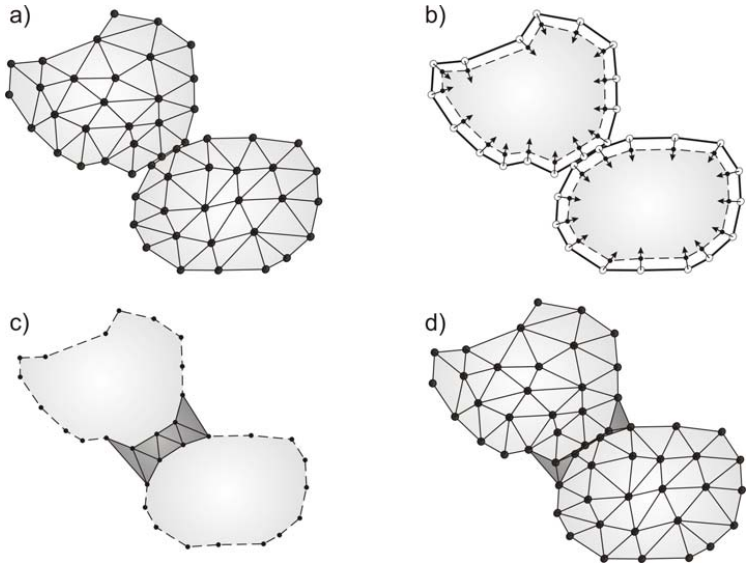

Figure 9: Generating the contact domain mesh: a) two meshed bodies, b) removal of the interior nodes and shrinkage of the boundary, c) construction of the contact domain mesh, d) retrieve of original boundary and mesh

4. FINITE ELEMENT APPROXIMATION

To solve the variational problem in equation (150), the deformable bodies $\Omega^{(\alpha)}$ as well as the contact domain D are discretized using finite elements. The discretization of the contacting bodies is done using standard, linear CST (constant strain triangle) elements and will not be further explained.

4.1. Discretization of a contact domain element

Concentrating on the contact part, suitable approximations for the displacement field $\mathbf{u}^{(D)}$ and for the introduced Lagrange multipliers have to be chosen. The construction of the contact domain mesh, explained in section 3.1, guarantees a triangulation, which consists of a unique layer of triangles that connect the boundary nodes of the finite element mesh of the contacting bodies.

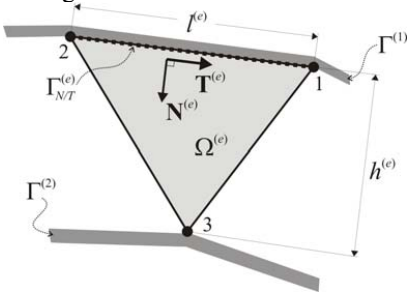

Figure 10: A typical contact domain element

A typical contact domain element is shown in Figure 10. It is obvious, that every of these elements has one node placed on the boundary of one contacting body and two on the boundary of the other. To ease the further documentation, the local numbering of the finite element nodes within one contact domain element, as shown in Figure 10, will be used. Therefore node 3 is always the individual node and the nodes 1 and 2 are placed on a shared edge with an adjacent finite element of a contacting body. A linear approximation for the elemental displacement field

$$\mathbf{u}^{(e)} \approx \mathbf{u}^{(e)_h} = \sum_{I=1}^{3} N_I \mathbf{d}_I \tag{154}$$

is used, where N_I are standard linear interpolation functions and $\mathbf{d}_I$ are the nodal displacements. For the interpolation of the Lagrange multipliers λ_N and λ_T, an element-wise constant approximation is utilized:

$$\lambda_N^{(e)} \approx \lambda_N^{(e)_h} = \Phi^{(e)}(\mathbf{x}_n)\Lambda_N^{(e)} \quad ; \quad \lambda_T^{(e)} \approx \lambda_T^{(e)_h} = \Phi^{(e)}(\mathbf{x}_n)\Lambda_T^{(e)} \tag{155}$$

with

$$\Phi^{(e)}(\mathbf{x}_n) = \begin{cases} 1 & \forall \mathbf{x}_n \in \Omega^{(e)} \\ 0 & \forall \mathbf{x}_n \notin \Omega^{(e)} \end{cases} \tag{156}$$

Some of the beneficial consequences of these choices have already been discussed in the first part of this paper and the direct consequences will be shown subsequently. The element-wise constant unit normal and tangential vector as well as the length of the common edge $l^{(e)}$ and the element height $h^{(e)}$ are easily calculated on basis of the element geometry.

$$\mathbf{T}^{(e)} = \frac{1}{l^{(e)}}\left(\mathbf{x}_1 - \mathbf{x}_2\right) \quad ; \quad \mathbf{N}^{(e)} = \begin{pmatrix} \mathrm{T}_y^{(e)} \\ -\mathrm{T}_x^{(e)} \end{pmatrix} \tag{157}$$

with

$$l^{(e)} = \left\| \mathbf{x}_1 - \mathbf{x}_2 \right\| \tag{158}$$

and

$$h^{(e)} = \left(\mathbf{x}_3 - \mathbf{x}_1\right) \cdot \mathbf{N}^{(e)} \quad \text{or} \quad h^{(e)} = \left(\mathbf{x}_3 - \mathbf{x}_2\right) \cdot \mathbf{N}^{(e)} \tag{159}$$

As the subsequent explanations are based on one contact domain element, the superscript $(\bullet)^{(e)}$ will be omitted in the following.

4.2. Local constraint enforcement

Due to the element-wise approximation of the Lagrange multipliers, the enforcement of the contact constraints in equation (28) can be decoupled and thus enforced separately for every single contact domain element. In fact, every single contact domain element can be interpreted as an individual contact domain itself, such that the definition of the normal and tangential vectors does not need to be conforming across the elements. Furthermore, one contact domain element, which is identified as being active for normal contact, has either to fulfill a stick or a slip condition. Assuming that a specific contact domain element needs to enforce a stick condition, the following two constraints have to be fulfilled:

$$\delta\Pi^{h}_{\lambda_N}\left(\mathbf{d},\Lambda_N,\delta\Lambda_N\right)=\int_{D^{(N)}}\delta\Lambda_N\tilde{g}_n dD+\int_{\Gamma_N}\delta\Lambda_N\tau\ (P_{\bar{n}N}-\Lambda_N)d\Gamma=0$$
$$\delta\Pi^{h}_{\lambda_T}\left(\mathbf{d},\Lambda_T,\delta\Lambda_T\right)=\int_{D^{(T)}}\delta\Lambda_T\tilde{g}_t dD+\int_{\Gamma_T}\delta\Lambda_T\tau\ (P_{\bar{t}N}-\Lambda_T)d\Gamma=0 \tag{160}$$

Herein $P_{\bar{n}N}$ and $P_{\bar{t}N}$ are the normal and tangential tractions in the finite element of the contacting body sharing the common edge with the contact domain element (see equation (153)). As the spatial discretization of the contacting bodies is done with CST elements, the stresses are constant within one finite element and therefore the tractions are constant along the common edge. Furthermore all the other arguments within the integrals are constant as well and thus the integration can be done analytically which leads to the following constraint equations:

$$\frac{1}{2}\tilde{g}_n l\ h+\tau\ (P_{\bar{n}N}-\Lambda_N)l=0$$
$$\frac{1}{2}\tilde{g}_t l\ h\ \ +\tau\ (P_{\bar{t}N}-\Lambda_T)l=0 \tag{161}$$

Recalling the normalized gap definitions from equation (149) and dividing by l gives

$$\frac{1}{2}\tilde{G}_n+\tau(P_{\bar{n}N}-\Lambda_N)=0$$
$$\frac{1}{2}\tilde{G}_t+\tau(P_{\bar{t}N}-\Lambda_T)=0 \tag{162}$$

where the definitions of the (extrapolation based) normal and tangential gaps

$$\tilde{G}_n=h\,\tilde{g}_n=h\ \tilde{\mathbf{n}}\cdot(\mathbf{N}+\nabla\mathbf{u}\cdot\mathbf{N})$$
$$\tilde{G}_t=h\,\tilde{g}_t=h\ \tilde{\mathbf{t}}\cdot(\mathbf{N}+\nabla\mathbf{u}\cdot\mathbf{N}) \tag{163}$$

has been used.

4.3. Exact evaluation of the discrete constraint equations

Having a closer look at the normal and tangential gap definitions in equation (163) might give rise to some concerns. What happens if the height h of a contact domain element, actually measuring the distance between contacting boundaries, tends to zero? The first part of the dot product will tend to zero, but at the same time, the gradient of the displacement field in normal direction will tend to infinity. Due to this problem an assumed regularization was considered in REMARK 2-1 of the first part of this work [13]. However, in the following it will be shown, that the gap definitions in equation (163) can be exactly computed, independent of the value of such a regularization parameter and thus independent of the height h. Using

$$\nabla\mathbf{u}\cdot\mathbf{N}=\frac{\partial\mathbf{u}}{\partial N} \tag{164}$$

and the linear discretization of the displacement field within a contact domain element in equation (154), the interesting part of equation (163) can be written as:

$$h\ \nabla\mathbf{u}\cdot\mathbf{N}=h\ \sum_{I=1}^{3}\frac{\partial N_I}{\partial N}\mathbf{d}_I \tag{165}$$

In Figure 11 a geometrical interpretation of the first part in equation (165) is shown. Multiplying the shape functions with the element height h allows for a direct evaluation of this term, which is totally independent of h.

$$h\frac{\partial N_1}{\partial N} = -\frac{a}{l} \quad ; \quad h\frac{\partial N_2}{\partial N} = -\frac{b}{l} \quad ; \quad h\frac{\partial N_3}{\partial N} = 1 \tag{166}$$

Therefore the evaluation of this term can be cut down to a pure geometric problem. It is only necessary to get the ratios of how the normal projection of node 3 intersects the baseline, which is defined by the nodes 1 and 2. This can be uniquely evaluated no matter of how distorted the contact domain element is, even if the normal projection of node 3 onto the baseline lies outside of the edge 1-2 (see Figure 12). Thus the (extrapolation based) normal and tangential gaps (see equation (163)) can be evaluated with:

$$\begin{aligned} \tilde{G}_n &= h\,\tilde{\mathbf{n}}\cdot\mathbf{N} + \tilde{\mathbf{n}}\cdot\sum_{I=1}^{3}\left(h\frac{\partial N_I}{\partial N}\right)\mathbf{d}_I \\ \tilde{G}_t &= h\,\tilde{\mathbf{t}}\cdot\mathbf{N} + \tilde{\mathbf{t}}\cdot\sum_{I=1}^{3}\left(h\frac{\partial N_I}{\partial N}\right)\mathbf{d}_I \end{aligned} \tag{167}$$

Knowing the normal and tangential gaps, the constraint equations in (162) can be directly solved for the discrete, element-wise constant Lagrange multipliers:

$$\Lambda_N = \frac{1}{2\tau}\tilde{G}_n + P_{\tilde{n}N} \quad ; \quad \Lambda_T = \frac{1}{2\tau}\tilde{G}_t + P_{\tilde{t}N} \tag{168}$$

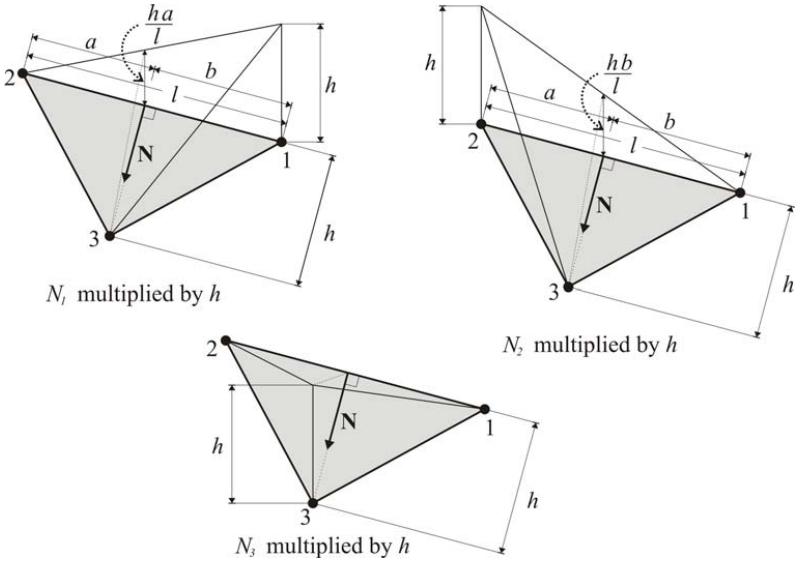

Figure 11: Normal direction derivative of the shape functions (regular element)

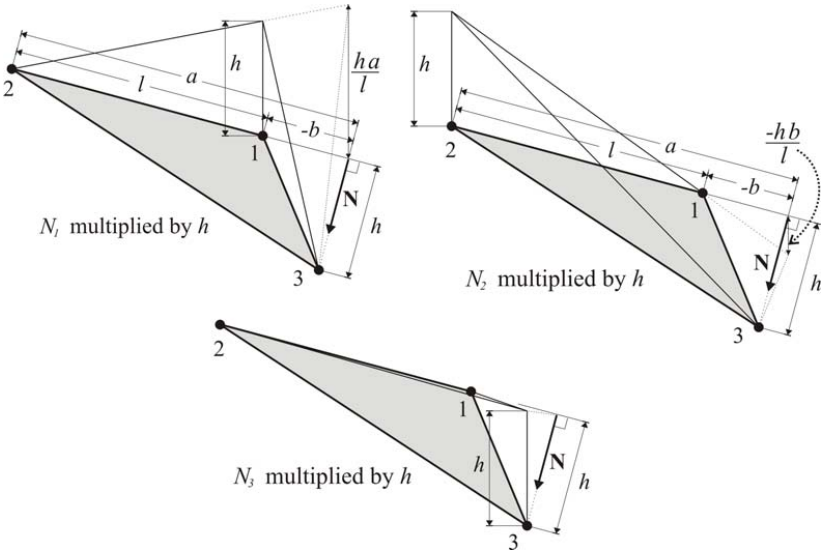

Figure 12: Normal direction derivative of the shape functions (distorted element)

4.4. Contact forces

After the determination of the discrete Lagrange multipliers, by enforcing the contact constraints, the resulting contact forces can be computed. Therefore the contact virtual work expression in equation (151) is discretized using the introduced approximations. Again, all arguments within the integrals turn out to be constant and the integrals can be evaluated analytically. Similar expressions as detailed in section 4.3 appear, such that the definitions introduced there can be reused. To shorten the expressions, the contact forces will be split in a normal contact, a stick and a slip part, respectively.

$$\mathbf{F}_{\text{cont}} = \underbrace{\mathbf{F}^{(N)}}_{\text{normal}} + \underbrace{\mathbf{F}^{(T)}}_{\text{stick}} + \underbrace{\mathbf{F}^{(N\setminus T)}}_{\text{slip}} \tag{169}$$

Inserting the approximations of the variations of the elemental normalized gaps (see equation (149))

$$\begin{aligned} \delta\tilde{g}_n &= \tilde{\mathbf{n}} \cdot \nabla\delta\mathbf{u} \cdot \mathbf{N} = \tilde{\mathbf{n}} \cdot \sum_{I=1}^{3} \frac{\partial N_I}{\partial N} \delta\mathbf{d}_I \\ \delta\tilde{g}_t &= \tilde{\mathbf{t}} \cdot \nabla\delta\mathbf{u} \cdot \mathbf{N} = \tilde{\mathbf{t}} \cdot \sum_{I=1}^{3} \frac{\partial N_I}{\partial N} \delta\mathbf{d}_I \end{aligned} \tag{170}$$

as well as the approximations of the Lagrange multipliers (see equations (116) and (156)) into the contact virtual work expression from equation (151) leads to the different parts of the contact forces (see equation (169)). The contributions to the nodal contact forces within one contact domain element can then be expressed as follows:

$$\mathbf{F}_I^{(N)} = \frac{1}{2} l \, \Lambda_N \left(h \frac{\partial N_I}{\partial N} \right) \tilde{\mathbf{n}}$$

$$\mathbf{F}_I^{(T)} = \frac{1}{2} l \, \Lambda_T \left(h \frac{\partial N_I}{\partial N} \right) \tilde{\mathbf{t}} \qquad (171)$$

$$\mathbf{F}_I^{(N\backslash T)} = \frac{1}{2} l \, T \left(h \frac{\partial N_I}{\partial N} \right) \tilde{\mathbf{t}} = \frac{1}{2} l \, \mu \, sign\left(\tilde{G}_t \right) \left| \Lambda_N \right| \left(h \frac{\partial N_I}{\partial N} \right) \tilde{\mathbf{t}}$$

REMARK 4-1. For the evaluation of the *sign* function in equation $(171)_3$, the extrapolation based, normalized tangential gap $\tilde{g}_t$ has been replaced with the real geometric tangential gap $\tilde{G}_t$. These two gap definitions are related via (see Part1 [13], section 2.2.2):

$$\tilde{G}_t = h \, \tilde{g}_t \qquad (172)$$

In the theoretical derivations for the continuum formulation, it was assumed, that the initial gap $G_N^{(0)}$ of a point in the contact domain is always positive (see [13], REMARK 2-1 and 2-4) and therefore the equivalence of $sign(g_t) = sign(G_t)$ could be used. After the discretization procedure, the height h of a contact domain element plays the role of the initial gap. In the previous section 4.3 it has been shown, that all necessary gap definitions can be exactly evaluated regardless of the elemental height h (see equation (166)). Therefore the restriction made in [13] (REMARK 2-1) is no longer necessary for the discretized counterpart. In fact, in numerical calculations the initial gap h might be negative (interpenetration), as can be seen in the example in section 6.2.

4.5. Effective structural equation

Starting from the variational form (150) of the entire problem the semi-discrete equation of motion is derived introducing the spatial discretization of the contacting bodies. This leads to a compact notation of the semi-discrete initial value problem

$$\mathbf{M}\ddot{\mathbf{d}} + \mathbf{F}_{\text{int}}\left(\mathbf{d}\right) + \mathbf{F}_{\text{cont}}\left(\mathbf{d}\right) = \mathbf{F}_{\text{ext}} \qquad (173)$$

where $\mathbf{M}$ is the mass matrix, $\mathbf{F}_{\text{int}}\left(\mathbf{d}\right)$ is the vector of the deformation dependent internal forces, $\mathbf{F}_{\text{cont}}\left(\mathbf{d}\right)$ is the vector of contact forces (see section 4.4) and $\mathbf{F}_{\text{ext}}$ is the vector of external forces. The vectors $\mathbf{d}$ and $\ddot{\mathbf{d}}$ represent the discrete nodal displacements and accelerations, respectively. To integrate the semi-discrete problem (173) in time, the Generalized-α method [3] is used, which applies the equilibrium equation at a generalized mid-point configuration.

$$\mathbf{M}\ddot{\mathbf{d}}_{\text{n+1-}\alpha_m} + \mathbf{F}_{\text{int}}\left(\mathbf{d}_{\text{n+1-}\alpha_f}\right) + \mathbf{F}_{\text{cont}}\left(\mathbf{d}_{\text{n+1-}\alpha_f}\right) = \mathbf{F}_{\text{ext}}\big|_{\text{n+1-}\alpha_f} \qquad (174)$$

Herein α_m and α_f are interpolation parameters that allow to control the numerical dissipation. Inserting the classical Newmark approximations [11] leads to a fully discretized non-linear equation, which will be solved by means of a Newton-Raphson

scheme. The necessary linearization yields the effective incremental structural equation to be solved within every iteration step k .

$$\mathbf{K}_T^{eff}\,\Delta\mathbf{d} = \mathbf{F}^{eff} \tag{175}$$

where

$$\mathbf{K}_T^{eff} = \frac{1-\alpha_m}{\beta\Delta t^2}\mathbf{M} + \left(1-\alpha_f\right)\frac{\partial\mathbf{F}_{\text{int}}\left(\mathbf{d}_{\text{n+1}}^k\right)}{\partial\mathbf{d}_{\text{n+1}}^k} + \left(1-\alpha_f\right)\frac{\partial\mathbf{F}_{\text{cont}}\left(\mathbf{d}_{\text{n+1}}^k\right)}{\partial\mathbf{d}_{\text{n+1}}^k} \tag{176}$$

is the effective tangential stiffness matrix and

$$\mathbf{F}^{eff} = \mathbf{F}_{\text{ext}}\big|_{\text{n+1-}\alpha_f} - \frac{1-\alpha_m}{\beta\Delta t^2}\mathbf{M}\mathbf{d}_{\text{n+1}}^k + \mathbf{h}\left(\mathbf{d}_{\text{n}},\dot{\mathbf{d}}_{\text{n}},\ddot{\mathbf{d}}_{\text{n}}\right) - \mathbf{F}_{\text{int}}\left(\mathbf{d}_{\text{n+1-}\alpha_f}\right) - \mathbf{F}_{\text{cont}}\left(\mathbf{d}_{\text{n+1-}\alpha_f}\right) \tag{177}$$

is the effective load vector. Herein $\mathbf{h}\left(\mathbf{d}_{\text{n}},\dot{\mathbf{d}}_{\text{n}},\ddot{\mathbf{d}}_{\text{n}}\right)$ is a history term, that only depends on given state variables at time t_{n} .

$$\mathbf{h}\left(\mathbf{d}_{\text{n}},\dot{\mathbf{d}}_{\text{n}},\ddot{\mathbf{d}}_{\text{n}}\right) = \mathbf{M}\left[\frac{1-\alpha_m}{\beta\Delta\text{t}^2}\mathbf{d}_{\text{n}} + \frac{1-\alpha_m}{\beta\Delta\text{t}}\dot{\mathbf{d}}_{\text{n}} + \frac{1-\alpha_m-2\beta}{2\beta}\ddot{\mathbf{d}}_{\text{n}}\right] \tag{178}$$

4.6. Contact stiffness contributions

The construction of the effective tangential stiffness matrix in equation (176) necessitates the linearization of the vectors of internal and contact forces. As the linearization of the internal forces is quite standard and has been documented in numerous publications and textbooks, only the linearization of the contact forces will be addressed. The main part of the linearization involves the derivative of the discretized contact forces with respect to the vector of discrete nodal displacements

$$\frac{\partial\mathbf{F}_{\text{cont}}\left(\mathbf{d}\right)}{\partial\mathbf{d}} \tag{179}$$

This derivative will be detailed in the following for a given contact domain element. The derivative will be derived separately for the different parts of contact forces.

4.4.1. Contact stiffness for active normal contact

The contact forces acting at the degrees of freedom of one contact domain node is given in equation $(171)_1$, where the discrete normal Lagrange multiplier $\Lambda_N\left(\mathbf{d}\right)$ is the only displacement dependent part. Therefore the normal contact stiffness contributions can be computed with

$$\mathbf{K}_{IJ}^{(N)} = \frac{\partial\mathbf{F}_I^{(N)}}{\partial\mathbf{d}_J} = \frac{1}{2}l\left(h\frac{\partial N_I}{\partial N}\right)\tilde{\mathbf{n}}\otimes\frac{\partial\Lambda_N}{\partial\mathbf{d}_J} \tag{180}$$

Using equations (168) and (167), the derivative of the normal Lagrange multiplier reads

$$\frac{\partial\Lambda_N}{\partial\mathbf{d}_J} = \frac{1}{2\tau}\frac{\partial\tilde{G}_n}{\partial\mathbf{d}_J} + \frac{\partial P_{\tilde{n}N}}{\partial\mathbf{d}_J} = \underbrace{\frac{1}{2\tau}\left(h\frac{\partial N_I}{\partial N}\right)\tilde{\mathbf{n}}}_{\text{Part I}} + \underbrace{\frac{\partial P_{\tilde{n}N}}{\partial\mathbf{d}_J}}_{\text{Part II}} \tag{181}$$

Inserting equation (181) into equation (180) shows, that the resulting contact stiffness matrix can be decomposed in two parts.

$$ {}^{I}\mathbf{K}_{IK}^{(N)} = \frac{l}{4\tau}\left(h\frac{\partial N_I}{\partial N} \right)\left(h\frac{\partial N_K}{\partial N} \right)\tilde{\mathbf{n}}\otimes\tilde{\mathbf{n}} $$
$$ {}^{II}\mathbf{K}_{IL}^{(N)} = \frac{l}{2}\left(h\frac{\partial N_I}{\partial N} \right)\tilde{\mathbf{n}}\otimes\frac{\partial P_{\tilde{n}N}}{\partial \mathbf{d}_L} \tag{182} $$

where the nodal counters (I, J, K, L) are specified as follows (see Figure 13).

$$ I=[1,2,3] \quad ; \quad J=[1,2,3,4] \quad ; \quad K=[1,2,3] \quad ; \quad L=[1,2,4] \tag{183} $$

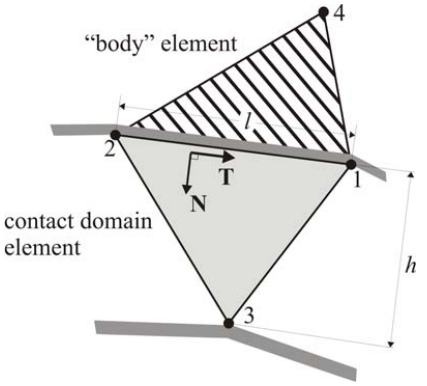

Figure 13: Contact domain element with adjacent "body" element

The first part of the stiffness matrix in equation (182) can already be computed. It gives rise to a symmetric contribution to the contact stiffness, affecting only degrees of freedom of the contact domain element nodes. However, the second part needs to be explored a little further, as the computation of the normal contact traction $P_{\tilde{n}N}$ is based on the deformation of the adjacent finite element in the contacting body ("body" element, see Figure 13). The derivation of the normal contact traction (equation (153)) is as follows:

$$ \frac{\partial P_{\tilde{n}N}}{\partial \mathbf{d}_L} = \frac{\partial\left(\tilde{\mathbf{n}}\cdot\mathbf{P}\cdot\mathbf{N}\right)}{\partial \mathbf{d}_L} = \tilde{\mathbf{n}}\cdot\frac{\partial \mathbf{P}}{\partial \mathbf{d}_L}\cdot\mathbf{N} \tag{184} $$

with

$$ \frac{\partial \mathbf{P}}{\partial \mathbf{d}_L} = \frac{\partial\left(\mathbf{F}\cdot\mathbf{S}\right)}{\partial \mathbf{d}_L} = \frac{\partial \mathbf{F}}{\partial \mathbf{d}_L}\cdot\mathbf{S} + \mathbf{F}\cdot\frac{\partial \mathbf{S}}{\partial \mathbf{d}_L} \tag{185} $$

where $\mathbf{F}$ is the material deformation gradient and $\mathbf{S}$ is the second Piola-Kirchhoff stress tensor, both defined in the adjacent "body" element. Further specifications of how to calculate the derivative in equation (185) in a two-dimensional finite element implementation, are given in the APPENDIX.

4.4.2. Contact stiffness for active tangent stick condition

Taking the derivative of the associated nodal contact forces given in equation $(171)_2$ with respect to the discrete nodal displacements, leads to the contact stiffness contribution for an active stick element. It exhibits a very similar structure than the one derived in section 4.4.1 for the active normal contact part (see equation (180)), since now the discrete tangential Lagrange multiplier $\Lambda_T(\mathbf{d})$ displays the only displacement

dependent part in the computation of the contact forces (see equation $(171)_2$). Hence the contact contribution for an active stick element reads

$$\mathbf{K}_{IJ}^{(T)} = \frac{\partial \mathbf{F}_I^{(T)}}{\partial \mathbf{d}_J} = \frac{1}{2} l \left(h \frac{\partial N_I}{\partial N} \right) \tilde{\mathbf{t}} \otimes \frac{\partial \Lambda_T}{\partial \mathbf{d}_J} \tag{186}$$

Utilizing equation (168) together with equation (167), the derivative of the discrete tangential Lagrange multiplier can be specified.

$$\frac{\partial \Lambda_T}{\partial \mathbf{d}_J} = \frac{1}{2\tau} \frac{\partial \tilde{G}_t}{\partial \mathbf{d}_J} + \frac{P_{\tilde{t}N}}{\partial \mathbf{d}_J} = \underbrace{\frac{1}{2\tau} \left(h \frac{\partial N_I}{\partial N} \right) \tilde{\mathbf{t}}}_{\text{Part I}} + \underbrace{\frac{\partial P_{\tilde{t}N}}{\partial \mathbf{d}_J}}_{\text{Part II}} \tag{187}$$

Inserting equation (187) into (186) yields the stiffness contribution, which, similarly to equations (180) to (182) will be split into two parts:

$$\begin{aligned} {}^{I}\mathbf{K}_{IK}^{(T)} &= \frac{l}{4\tau} \left(h \frac{\partial N_I}{\partial N} \right) \left(h \frac{\partial N_K}{\partial N} \right) \tilde{\mathbf{t}} \otimes \tilde{\mathbf{t}} \\ {}^{II}\mathbf{K}_{IL}^{(T)} &= \frac{l}{2} \left(h \frac{\partial N_I}{\partial N} \right) \tilde{\mathbf{t}} \otimes \frac{\partial P_{\tilde{t}N}}{\partial \mathbf{d}_L} \end{aligned} \tag{188}$$

Again, the first one constitutes a symmetric contribution to the contact stiffness and can readily be computed, whereas the second one causes unsymmetric entries into the contact stiffness matrix. For the evaluation of the second part of the contact stiffness contribution given in equation $(188)_2$, the derivative of the tangential traction has to be carried out. It is given with

$$\frac{\partial P_{\tilde{t}N}}{\partial \mathbf{d}_L} = \frac{\partial \left(\tilde{\mathbf{t}} \cdot \mathbf{P} \cdot \mathbf{N} \right)}{\partial \mathbf{d}_L} = \tilde{\mathbf{t}} \cdot \frac{\partial \mathbf{P}}{\partial \mathbf{d}_L} \cdot \mathbf{N} \tag{189}$$

where the derivative of the first Piola-Kirchhoff stress tensor in equation (185) can be reused.

4.4.3. Contact stiffness for active tangent slip condition

Starting from the nodal contact forces given in equation $(171)_3$, the contact stiffness contribution for an active slip element can be expressed in a similar manner than for the first two contact stiffness parts outlined in sections 4.4.1 and 4.4.2. Neglecting the (quasi-zero) derivative of $sign\left(\tilde{G}_t\right)$, the contact stiffness contribution for an active slip element gives

$$\mathbf{K}_{IJ}^{(N\setminus T)} = \frac{\partial \mathbf{F}_I^{(N\setminus T)}}{\partial \mathbf{d}_J} = \frac{1}{2} l \, \mu \, sign\left(\tilde{G}_t\right) \left(h \frac{\partial N_I}{\partial N} \right) \tilde{\mathbf{t}} \otimes \frac{\partial \left| \Lambda_N \right|}{\partial \mathbf{d}_J} \tag{190}$$

Using

$$\frac{\partial \left| \Lambda_N \right|}{\partial \mathbf{d}_J} = sign\left(\Lambda_N \right) \frac{\partial \Lambda_N}{\partial \mathbf{d}_J} \tag{191}$$

and the derivative of the discrete normal Lagrange multiplier in equation (181), the two parts of the resulting stiffness contribution can be summarized:

$$\begin{aligned} {}^{I}\mathbf{K}_{IK}^{(N\setminus T)} &= \frac{l}{4\tau} \, \mu \, sign\left(\tilde{G}_t\right) sign\left(\Lambda_N \right) \left(h \frac{\partial N_I}{\partial N} \right) \left(h \frac{\partial N_K}{\partial N} \right) \tilde{\mathbf{t}} \otimes \tilde{\mathbf{n}} \\ {}^{II}\mathbf{K}_{IL}^{(N\setminus T)} &= \frac{l}{2} \mu \, sign\left(\tilde{G}_t\right) sign\left(\Lambda_N \right) \left(h \frac{\partial N_I}{\partial N} \right) \tilde{\mathbf{t}} \otimes \frac{\partial P_{\tilde{n}N}}{\partial \mathbf{d}_L} \end{aligned} \tag{192}$$

For the calculation of the unsymmetric second part, the derivative of the normal traction, given in equation (184), is used.

5. ACTIVE SET STRATEGY – TECHNICAL ASPECTS

The contact formulation presented so far is based on the assumption that the active set of contact domain elements being in contact at the end one specific time step is known "a priori". This includes the active normal contact condition as well as the frictional conditions, distinguishing between stick or slip. In the first part of this paper [13] a predictive active set strategy, based on so-called *active constraint indicators* is presented. In the following, some important technical details about the important extrapolation procedure are discussed.

5.1. Prediction of effective gaps

For the proposed active set strategy, the so-called effective normal and tangential gaps

$$\bar{G}_n \equiv \tilde{G}_n + 2\tau\ P_{\tilde{n}N} \tag{193}$$

$$\bar{G}_t \equiv \tilde{G}_t + 2\tau\ P_{\tilde{t}N} \tag{193}$$

and suitable (displacement based) active constraint indicators

$$e \in D^{(N)} \Leftrightarrow \beta_N \overset{def}{=} \bar{G}_n < 0 \tag{194}$$

$$e \in D^{(T)} \Leftrightarrow \beta_T \overset{def}{=} \left|\bar{G}_t\right| - \mu\left|\bar{G}_n\right| < 0 \tag{194}$$

are defined for every contact domain element. In order to predict the active contact/friction element set for the next time step, a first order approximation of these indicators is performed on basis of the evolution of the effective normal and tangential gaps in previous time steps.

$$\left(\bar{G}_{n/t}\right)^{(0)}_{n+1} = (\bar{G}_{n/t})_n + \frac{\Delta t_{n+1}}{\Delta t_n}(\Delta\bar{G}_{n/t})_n \tag{195}$$

with

$$\left(\Delta\bar{G}_{n/t}\right)_n = \left(\bar{G}_{n/t}\right)_n - \left(\bar{G}_{n/t}\right)_{n-1} \tag{196}$$

where the subscripts $(\bullet)_n$ and $(\bullet)_{n-1}$ refer to the time steps n and $n-1$. Therefore, the effective normal and tangential gaps of the previous time steps need to be appropriately stored.

5.2. History of effective gaps

Keeping history of the effective gaps is not a trivial task. The effective gaps are defined for every contact domain element, providing information about this specific set of finite element nodes on the contacting boundaries. One specific feature of the presented contact strategy is the reconstruction of the contact domain mesh, whenever the relative motion of the contacting surfaces exceeds some tolerances. In fact, contact problems involving large relative sliding require a reconnection of boundary nodes very frequently, sometimes even after every time step. Consequently it is not possible to just store the effective gaps within the contact domain element, as this element may not exist anymore in the ensuing time step. Furthermore, the values of the effective gaps strongly depend on the connectivity of the contact domain mesh. If the connectivity changes from one time step to the other (see Figure 14), it might happen, that the height h, as a main part for the calculation of the effective gaps, alters erratic. The effective gaps would not vary smoothly and the extrapolation of these values would not be beneficial.

To overcome this, a different procedure for keeping track of the evolution of the effective gaps is necessary.

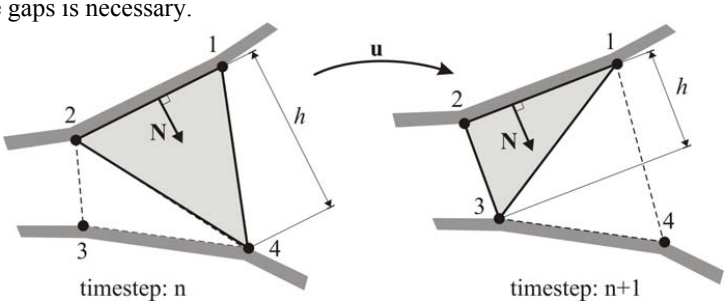

Figure 14: Change of connectivity – Influence on gaps

For the presented contact algorithm the following approach is used. Instead of storing the effective gaps themselves, the placement of the finite element nodes on the contact boundary, as well as the normal and tangential surface tractions $\left(P_{\bar{n}N},\, P_{\bar{t}N}\right)$ at the boundary of the "body" elements, are stored for the previous time steps n and $\mathrm{n}-1$. Based on the connectivity of a contact domain element in the considered time step, the effective gaps are calculated retrospective.

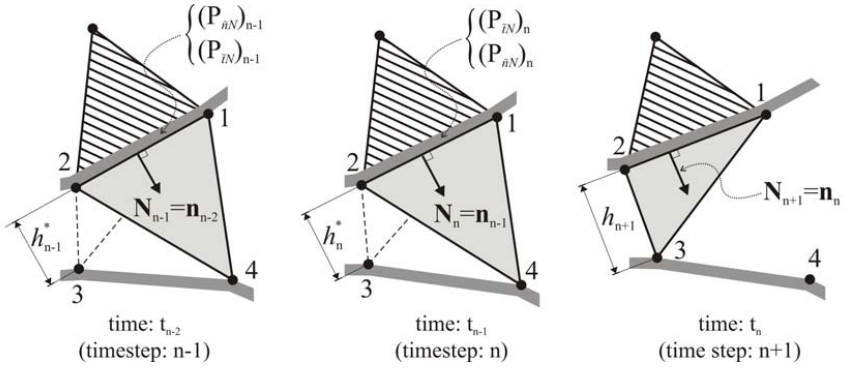

Figure 15: Reference configuration of different time steps

In Figure 15 the placement of a contact domain element is shown at the beginning of three consecutive time steps, thus representing in each case the reference configuration. Based on the connectivity of the considered contact domain element at the present time step $\mathrm{n}+1$ (nodes 1-2-3), the fictive heights h^* at the beginning of the two previous time steps are calculated using equation $(159)_2$.

$$h^*_{\mathrm{n-1}} = \left[\left(\mathbf{x}_3\right)_{\mathrm{n-2}} - \left(\mathbf{x}_2\right)_{\mathrm{n-2}}\right] \cdot \mathbf{N}_{\mathrm{n-1}} \quad \text{and} \quad h^*_{\mathrm{n}} = \left[\left(\mathbf{x}_3\right)_{\mathrm{n-1}} - \left(\mathbf{x}_2\right)_{\mathrm{n-1}}\right] \cdot \mathbf{N}_{\mathrm{n}} \tag{197}$$

With this, the (extrapolation based) normal and tangential gaps $\tilde{G}_n$ and $\tilde{G}_t$ (see equation (167)) are evaluated for the two previous time steps

$$\left(\tilde{G}_n\right)_{\text{n-1}} = h^*_{\text{n-1}} \underbrace{\mathbf{n}_{\text{n-1}}}_{\mathbf{N}_{\text{n}}} \cdot \mathbf{N}_{\text{n-1}} + \underbrace{\mathbf{n}_{\text{n-1}}}_{\mathbf{N}_{\text{n}}} \cdot \sum_{I=1}^{3} \left(h^*_{\text{n-1}} \frac{\partial N_I}{\partial \mathbf{N}_{\text{n-1}}} \right) \left(\mathbf{d}_I\right)_{\text{n-1}}$$

$$\left(\tilde{G}_t\right)_{\text{n-1}} = h^*_{\text{n-1}} \underbrace{\mathbf{t}_{\text{n-1}}}_{\mathbf{T}_{\text{n}}} \cdot \mathbf{N}_{\text{n-1}} + \underbrace{\mathbf{t}_{\text{n-1}}}_{\mathbf{T}_{\text{n}}} \cdot \sum_{I=1}^{3} \left(h^*_{\text{n-1}} \frac{\partial N_I}{\partial \mathbf{N}_{\text{n-1}}} \right) \left(\mathbf{d}_I\right)_{\text{n-1}} \tag{198}$$

and

$$\left(\tilde{G}_n\right)_{\text{n}} = h^*_{\text{n}} \underbrace{\mathbf{n}_{\text{n}}}_{\mathbf{N}_{\text{n+1}}} \cdot \mathbf{N}_{\text{n}} + \underbrace{\mathbf{n}_{\text{n}}}_{\mathbf{N}_{\text{n+1}}} \cdot \sum_{I=1}^{3} \left(h^*_{\text{n}} \frac{\partial N_I}{\partial \mathbf{N}_{\text{n}}} \right) \left(\mathbf{d}_I\right)_{\text{n}}$$

$$\left(\tilde{G}_t\right)_{\text{n}} = h^*_{\text{n}} \underbrace{\mathbf{t}_{\text{n}}}_{\mathbf{T}_{\text{n+1}}} \cdot \mathbf{N}_{\text{n}} + \underbrace{\mathbf{t}_{\text{n}}}_{\mathbf{T}_{\text{n+1}}} \cdot \sum_{I=1}^{3} \left(h^*_{\text{n}} \frac{\partial N_I}{\partial \mathbf{N}_{\text{n}}} \right) \left(\mathbf{d}_I\right)_{\text{n}} \tag{199}$$

with

$$\left(\mathbf{d}_I\right)_{\text{n-1}} = \left(\mathbf{x}_I\right)_{\text{n-1}} - \left(\mathbf{x}_I\right)_{\text{n-2}} \quad \text{and} \quad \left(\mathbf{d}_I\right)_{\text{n}} = \left(\mathbf{x}_I\right)_{\text{n}} - \left(\mathbf{x}_I\right)_{\text{n-1}} \tag{200}$$

Instead of using the approximations $\tilde{\mathbf{n}}$ and $\tilde{\mathbf{t}}$ for the spatial normal and tangential vectors within one time step, the real spatial normal and tangential vectors, which coincide with the material normal and tangential vectors of the subsequent time step (e.g. $\mathbf{n}_{\text{n}} = \mathbf{N}_{\text{n+1}}$ and $\mathbf{t}_{\text{n}} = \mathbf{T}_{\text{n+1}}$) are used in the calculations for the normal and tangential gaps in equations (198) and (199).

Together with the stored normal and tangential tractions $\left(P_{\tilde{n}N},\ P_{\tilde{t}N}\right)$, at the boundary of the adjacent "body" element (see Figure 15), the effective gaps for the previous time steps can be calculated using equation (193). Having these quantities at hand, the extrapolation of the effective normal and tangential gaps can be performed as described in the first part of this paper [13].

6. NUMERICAL EXAMPLES

The performance of the newly developed contact strategy is evaluated by means of a set of numerical examples. All the examples are computed under the assumption of a plane strain condition using a compressible neo-Hookean, hyperelastic material. For the element-wise constant stability parameter τ the relation

$$\tau = \frac{\alpha_{\text{stab}}}{E_{\min}} l \tag{201}$$

is used, where $E_{\min}$ is the minimal Young's modulus of the contacting bodies, l is the characteristic length of the contact domain element and α_{stab} is a dimensionless, user defined parameter. For the static analyses performed, the inertia term $\mathbf{M}\ddot{\mathbf{d}}$ in equation (173) drops out of the effective structural equation and therefore the non-linear static problem can be solved without using the described time integration scheme. Dealing with dynamic problems, the Generalized-α time integration scheme, described very briefly in section 0 is utilized, where the so-called spectral radius ρ_∞ defines the values of the introduced interpolation and Newmark parameters:

$$\alpha_m = \frac{2\rho_\infty - 1}{\rho_\infty + 1} \ ; \ \alpha_f = \frac{\rho_\infty}{\rho_\infty + 1} \ ; \ \beta = \frac{1}{4}\left(1 - \alpha_m + \alpha_f\right)^2 \ ; \ \gamma = \frac{1}{2} - \alpha_m + \alpha_f \tag{202}$$

6.1. Frictional Hertzian contact

To investigate the accuracy of the proposed contact formulation a cylinder on cylinder Hertzian contact problem is analyzed. The underlying analytical solution dates back to the work of Hertz [8], which assumes infinitesimal small deformation. In order to compare the results with the proposed large deformation contact strategy a very little load is applied. The geometric setup as well as the utilized finite element discretization is shown in Figure 1. Two elastic half cylinders ($E = 200.0\ [N/mm^2], \nu = 0.3$) are first pressed together with a compressive normal force $P = \int p(x)ds = 10.0\ [N]$. Subsequently a tangential force $Q = \int q(x)ds = 1.0\ [N]$ is applied which causes tangential contact tractions in the contact zone. The width b, being the half of the contact zone, can then be calculated analytically with

$$b = 2\sqrt{PR\frac{1-\nu^2}{\pi E}} = 0.6808\ [mm] \tag{203}$$

where R is the radius of the two cylinders. The normal pressure distribution in the contact zone is given with

$$\sigma_n = \sigma_n^{\max}\sqrt{1-\left(\frac{x}{b}\right)^2} \tag{204}$$

where $\sigma_n^{\max}$ is the maximum normal pressure computed via

$$\sigma_n^{\max} = \sqrt{\frac{PE}{\pi\left(1-\nu^2\right)R}} = 9.351\ [N/mm^2] \tag{205}$$

For the frictional contact part a Coulomb friction coefficient of $\mu = 0.2$ is assumed. Increasing the applied tangential forces q from zero to the maximal value, micro-slip evolves starting from the edges of the contact zone. Therefore the contact zone is subdivided into a stick part $|x| \leq |c|$ and two areas of slip $|c| \leq |x| \leq |b|$. The size of the stick region is given by

$$c = b\sqrt{1-\frac{Q}{\mu P}} = 0.481\ [mm] \tag{206}$$

Thus the distribution of the tangential contact tractions can be calculated as follows:

$$\begin{aligned} \sigma_t(x) &= \frac{\mu\sigma_n^{\max}}{b}\left(\sqrt{b^2-x^2}-\sqrt{c^2-x^2}\right) \quad : \quad |x| \leq |c| \\ \sigma_t(x) &= \mu\sigma_n(x) \qquad\qquad\qquad\qquad\qquad\quad : \quad |c| \leq |x| \leq |b| \end{aligned} \tag{207}$$

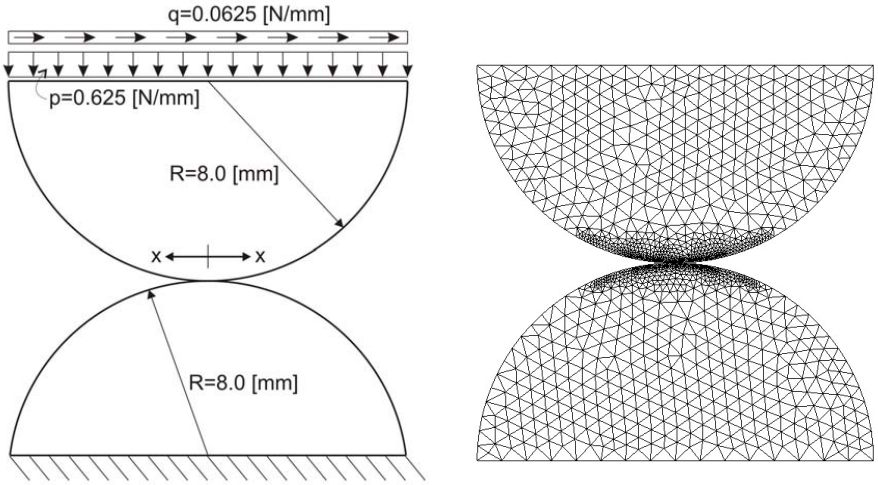

Figure 16: Cylinder on cylinder Hertzian contact problem and utilized discretization

In Figure 17 the numerical solution is plotted against the analytical solution, where the fine dashed line indicates the maximum tangential traction $\mu\sigma_n$. The abrupt change in the tangential traction stems from the transition from stick to slip. The shown numerical results are calculated using a stabilization parameter $\alpha_{\text{stab}} = 0.5$ (see equation (201)). It should be mentioned, that the influence of the stabilization parameter in this example is very little. A variation of this parameter between $\alpha_{\text{stab}} = [0.1 \rightarrow 5.0]$ produces qualitatively and quantitatively comparable results, as the deformations are very small and therefore the contact is very well imposed regardless of the utilized stabilization parameter. When the geometrical contact condition is very well imposed, the normal and tangential gaps defined in equation (167) tend to zero and thus the discrete normal and tangential Lagrange multipliers (see equation (168)) have the property of representing the normal and tangential surface tractions at the boundaries of the contacting bodies ($\Lambda_N \approx P_{\bar{n}N}$ and $\Lambda_T \approx P_{\bar{t}N}$). Therefore, the discrete Lagrange multipliers are utilized to check the normal and tangential contact tractions against the exact analytical solution. As the introduced Lagrange multipliers are element-wise constant values, they will be discontinuous at the boundary nodes. Therefore nodal values of the Lagrange multipliers are calculated, using the weighted nodal sum of the discrete, constant elemental values of the introduced Lagrange multipliers at the adjacent contact elements to one contacting node:

$$\Lambda^{node} = \frac{\sum_{e=1}^{n_e} \Lambda^{(e)} l^{(e)}}{\sum_{e=1}^{n_e} l^{(e)}} \tag{208}$$

Herein Λ^{node} depicts the average nodal Lagrange multiplier, n_e is the number of adjacent active contact domain elements to this specific boundary node and $\Lambda^{(e)}$ and $l^{(e)}$ are the elemental constant Lagrange multiplier and the elemental length of a contact domain element, respectively. In general one would weigh the elemental Lagrange multipliers with the area of the element, but as the elemental height $h^{(e)}$ denotes a measure of the actual gap, this tends to zero for active contact elements and thus has no

significant meaning. Therefore only the elemental length $l^{(e)}$ of a contact element is taken into account.
Looking at the results plotted in Figure 17 one can observe, that the contact tractions are quite well represented by the present contact algorithm. Particularly the calculated tangential contact tractions fit very well with the analytical solution. The normal contact tractions display some little differences and the maximum normal contact traction in the middle of the contact zone is a little bit overestimated. This is probably due to the fact, that the actual contact zone is not perfectly captured by the used discretization. Utilizing a large strain formulation for this example may also have some influence on the quantitative results.

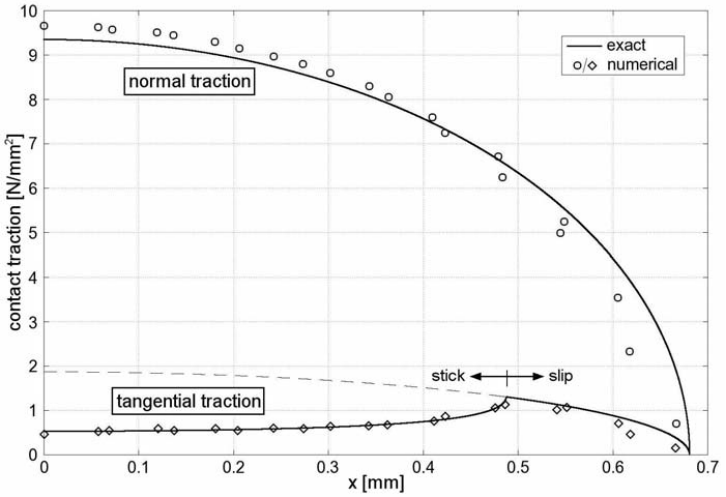

Figure 17: Computed contact traction for frictional cylinder on cylinder contact problem

6.2. Rotating discs

This example, analyzed by Puso and Laursen [14] in a three-dimensional setting, is chosen to demonstrate the locking-free behavior of the proposed contact domain method. Two concentric discs ($E = 1.0\ [N/mm^2], \nu = 0.0$) are first pressurized together with $p = 0.1\ [N/mm^2]$ and then rotated relative to each other, while a frictionless contact ($\mu = 0.0$) is assumed between the two bodies. A relatively rough discretization is used for the two discs, which initially display a conforming mesh along the contact interface. The problem is analyzed neglecting inertia effects, using three different values of the stabilization parameter α_{stab}. In Figure 18 the initial mesh and the deformed configurations for different values of α_{stab} are shown. From the equations (201) and (193) it is quite obvious, that the parameter α_{stab} is responsible for the admissible amount of interpenetration of one specific node. A very small value of the stabilization parameter ($\alpha_{\text{stab}} = 0.01$) is equivalent to a very strict enforcement of the geometric contact constraint, whereas a larger magnitude ($\alpha_{\text{stab}} = 1.0$) actually allows for some interpenetration.

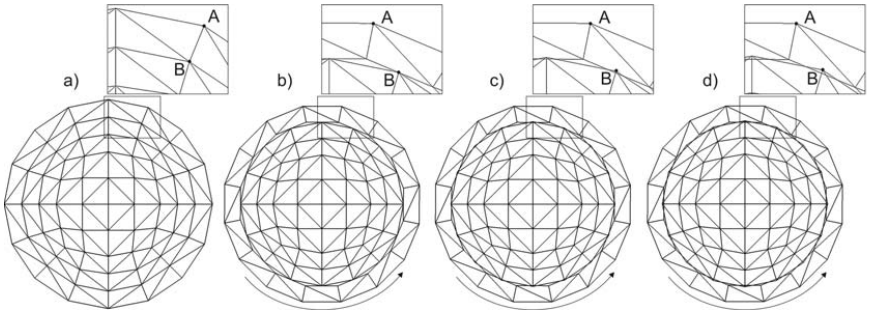

Figure 18: a) initially conforming mesh; b) deformation with $\alpha_{\text{stab}} = 0.01$; c) deformation with $\alpha_{\text{stab}} = 0.1$; d) deformation with $\alpha_{\text{stab}} = 1.0$

That means, that for this specific example, the proposed contact methods tends to lock for small values of α_{stab}, but tends to display a looking-free behavior for an appropriate magnitude of the stabilization parameter. This is nicely displayed in Figure 19, where the maximum pressure in the discs versus the applied rotation is shown. The calculation with $\alpha_{\text{stab}} = 1.0$ matches very good the theoretical exact solution.

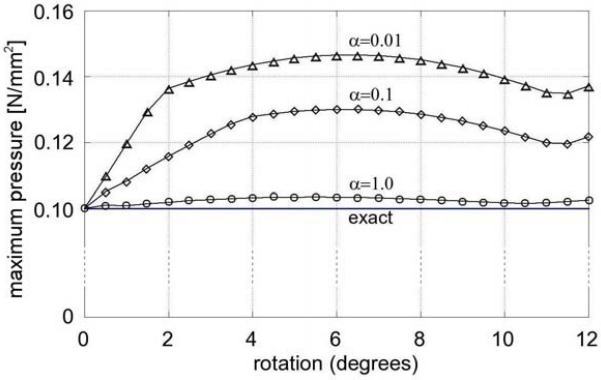

Figure 19: Maximum pressure versus rotation for different values of the stabilization parameter

6.3. Disc in Disc

The following example was discussed in a three-dimensional setting by Puso and Laursen [14] and later for the two-dimensional case by Fischer [4], Fischer and Wriggers [5] and Wriggers [16], respectively. For their analysis they use a large deformation, mortar based, frictionless contact formulation. A solid disc with a radius of $r = 0.6\ [mm]$ is placed within a hollow disc, having an inner radius of $r_i = 0.7\ [mm]$ and an outer radius of $r_o = 2.0\ [mm]$. Geometry and material data are given in Figure 20. The solid disc is pressed into the hollow disc by applying a uniform prescribed vertical displacement of $u = 1.15\ [mm]$ to all finite element nodes of the discretized solid disc. This is applied in 25 equal displacement increments while the outer boundary of the hollow disc is fixed. Due to the very large compressions occurring in the contact

zone, a relatively small stabilization parameter $\alpha_{\text{stab}} = 0.01$ is utilized for this example to ensure an appropriate enforcement of the geometrical contact constraint.

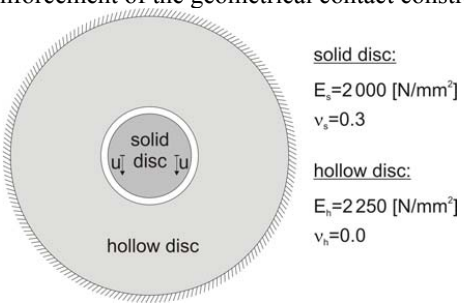

Figure 20: Disc in Disc: Geometry and material parameters

During the prescribed vertical displacement process, the inner boundary of the hollow disc undergoes substantial deformations, while the inner solid disc loses its circular shape. In Figure 21 the deformed configuration is plotted for different displacement steps, where the anticipating contact domain mesh (cdm) is shown always on the right side of the symmetry line. Puso and Laursen [14] report, that a classical node-to-segment contact formulation will fail in this example at a very early state of deformation. The contact domain method presented in this work is able to represent the large changes of size and position of the contact area in a very robust manner, using only 25 displacement increments. Its performance in this example is thus similar to the best mortar contact formulations and superior to classical node-to-segment contact strategies.

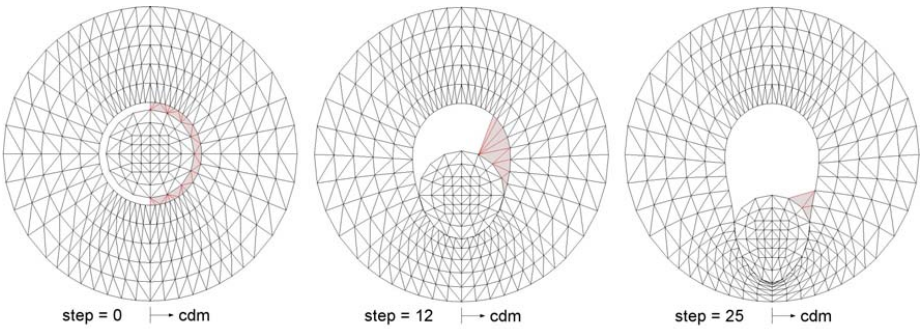

Figure 21: Disc in Disc: Deformed configuration at different steps
(cdm: plotting the contact domain mesh)

6.4. Ironing

In this example a frictional contact problem is analyzed, where both bodies undergo finite deformations. A block is pressed into an elastic slab and then slid over the surface. The slab is fixed at its bottom and is ten times softer than the indenting block. Vertical and horizontal displacements of the block are prescribed at its top edge. In the following two different ironing problems are discussed, which differ slightly in the geometry of the block and the amount of indentation u_V of the punch into the slab (see Figure 22).

The material properties used for the block ($E_b = 68.96 \times 10^8$ $[N/mm^2]$, $\nu_b = 0.32$) and the slab ($E_s = 68.96 \times 10^7$ $[N/mm^2]$, $\nu_s = 0.32$) are the same in both cases. Friction is considered between all contacting faces, with the coefficient of friction being $\mu = 0.3$. In both cases, the prescribed vertical displacement u_V is applied between $t = 0.0$ and $t = 1.0$. The subsequent prescribed horizontal displacement is applied between $t = 1.0$ and $t = 2.0$, where the time has no physical meaning, as the calculation was carried out neglecting dynamical effects.

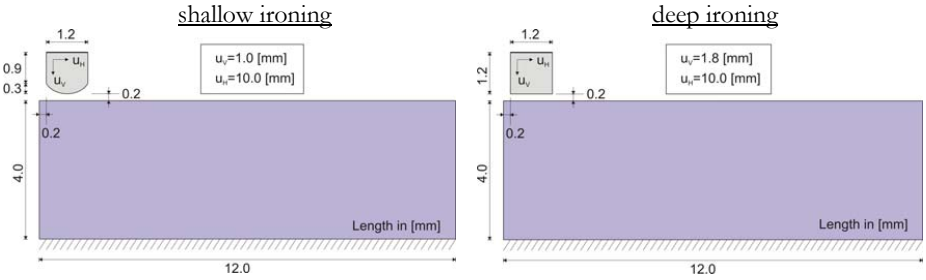

Figure 22: Ironing: Geometry for two different versions

2.2.66.4.1 Shallow ironing

The first version of this example is analyzed in Fischer [4], Fischer and Wriggers [6] and Wriggers [16]. They use a mortar based contact formulation with a penalty regularization scheme together with quadratic 9-node-elements. As they report that the quality of the computed vertical and horizontal reactions depends on the utilized finite element discretization, a comparable triangulation is used in the present study. Using the same number of finite element nodes, one quadratic 9-node-element is being replaced with eight linear 3-node-elements, which will lead to the same number of degrees of freedom involved in the problem. As in the reference works, the vertical displacement is applied in 10 time steps and the horizontal displacement is prescribed within 500 time steps. For the present calculation a stabilization parameter of $\alpha_{\text{stab}} = 0.3$ is used.

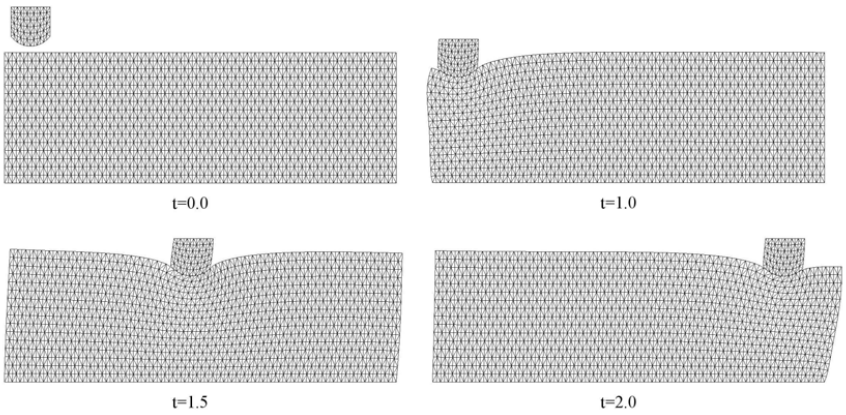

Figure 23: Shallow ironing: Deformed configurations at different time steps

The initial and three deformed configurations of the computation are shown in Figure 23, which demonstrate the finite deformations involved in the ironing process. In Figure 24 the total vertical and horizontal reaction forces, computed at the top of the indenting block, are plotted versus time. Together with the results of the present study, the graphs reported by Fischer and Wriggers [6] are displayed. While pressing the block into the slab, the curves are smooth and the two bodies stick together. Starting the horizontal movement, the vertical as well as the horizontal reaction forces increase until a limit is reached. At this stage the block starts sliding over the slab. While the vertical reaction force remains nearly constant, the horizontal reaction force oscillates. This is due to the fact that the finite element mesh of the slab has to slip around the right corner of the indenting block. Comparing the results of the present study with the ones reported in [6] one can note, that the qualitative behavior is very well captured, whereas the absolute values do not match. Quantitative differences in the computed reaction forces may stem from the usage of different finite elements used for the discretization of the contacting bodies. Due to Fischer and Wriggers [6] the computation of this problem using a node-to-segment approach fails around time step $t = 1.2$. Thus, the present contact strategy behaves again much better than a classical node-to-segment formulation and produces confidential results compared with mortar based contact methods.

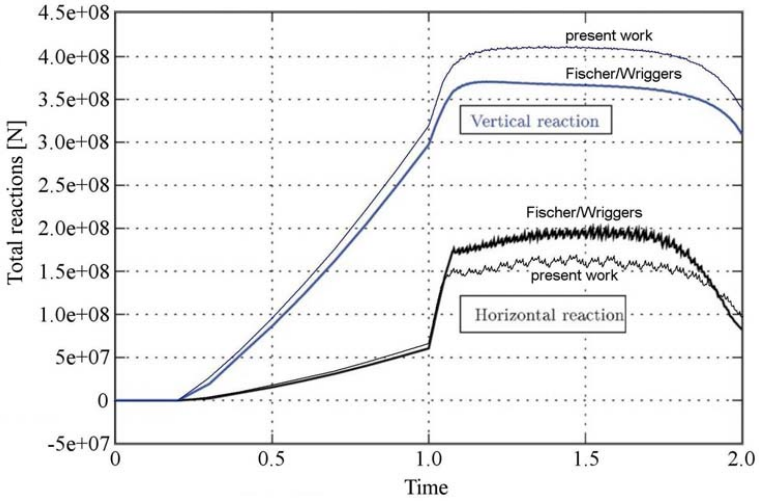

Figure 24: Shallow ironing: Computed total reaction forces versus time

2.2.76.4.2 Deep ironing

The second version of the ironing problem is analyzed in Yang et al. [20], where they use again a large deformation mortar contact formulation. For two reasons, this version is a lot more demanding to compute than the first one. First, the geometry of the upper block is just a square, having sharp corners at the indenting side as well. This produces very large contact pressures at the lower right corner of the indenting block. Second, the amount of indentation is nearly twice as big as in the first version, making it very difficult for the finite elements in the slab to slide around the sharp edge of the punch. In fact, due to [20], a node-to-segment formulation fails in analyzing this example at $t = 0.66$, being not even able to run the computation until the punch has fully indented.

In their calculation, Yang et al. [20] discretized the contacting bodies using bi-linear 4-node-elements. For reasons of comparison, again a comparable finite element triangulation is used for the present calculations, dividing one bi-linear 4-node-element into two linear 3-node-elements, leading to the same degrees of freedom. In [20] the number of load increments used for the vertical indentation and the horizontal sliding is not given. Here, the vertical displacement is prescribed in 20 time steps and the horizontal displacement is applied in 1500 time steps. A stabilization parameter of $\alpha_{\text{stab}} = 0.1$ is used.

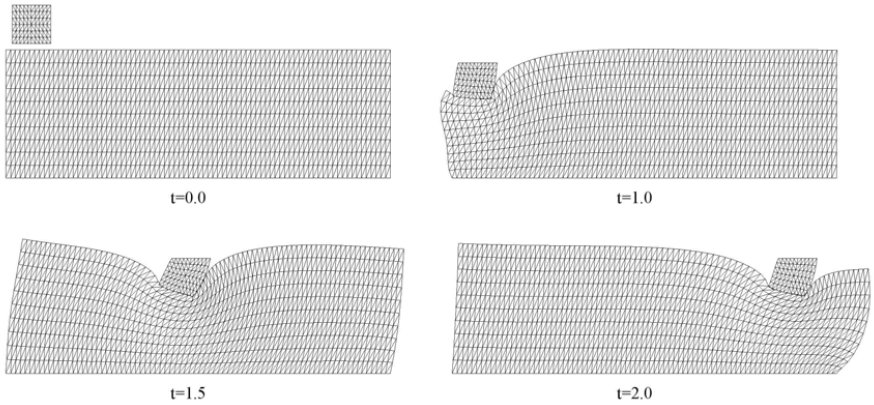

Figure 25: Deep ironing: Deformed configurations at different time steps

The deformed configuration of the ironing problem is depicted in Figure 25. In here, the appearance of finite deformations is even more pronounced than in the first version. The deformation of the slab is so large that even contact of the right side of the upper block has to be considered. In contrast to [20] frictional effects are considered in this part as well. Figure 26 depicts again the total vertical and horizontal reactions, computed at the top edge of the punch. A similar behavior than in the first ironing version can be observed, but it seems that the amplitudes of the oscillating horizontal reactions are significant smaller. This is most probably due to the fact, that the horizontal displacements are applied in three times more displacement increments. The differences in the absolute values of the reaction forces are due to the usage of different finite elements for the discretization of the contacting bodies and due to the different treatment of the friction coefficient at the right side of the block with the slab.

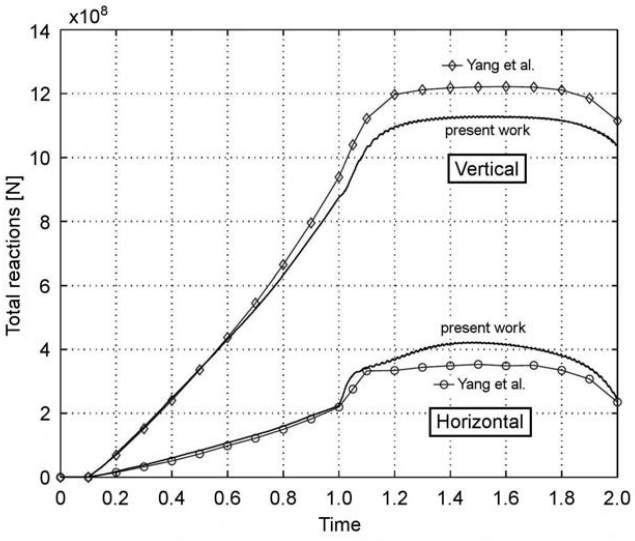

Figure 26: Deep ironing: Computed total reaction forces versus time

6.5. Ring impact

This example was published by Yang and Laursen [19] to show the performance of their presented self-contact search algorithm. In this work, the example is chosen, to demonstrate, that the presented contact strategy can automatically deal with self-contact problems without any further modifications.

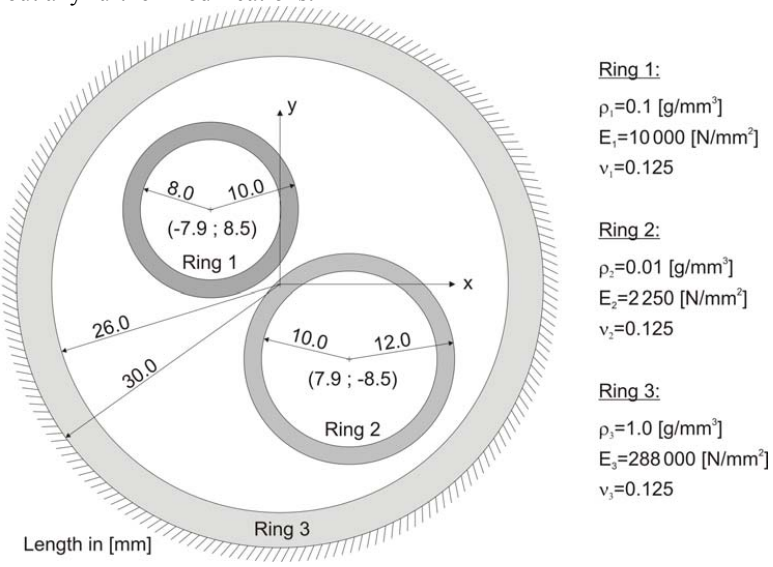

Figure 27: Ring impact: Geometry and material properties

The geometry setup and the utilized material properties for the elastic rings are shown in Figure 27. A fixed Dirichlet boundary condition is assigned to the external boundary of

the largest ring (Ring 3). Two smaller rings are located within Ring 3, where the smallest ring (Ring 1) is given an initial velocity of $\mathbf{v} = \left[30.0\ [mm/ms], -30.0\ [mm/ms]\right]^T$ to hit the medium sized ring (Ring 2). After hitting Ring 2, the two inner rings move together towards the inner surface of Ring 3. As the stiffness of the medium sized ring is very low, it gets pressed together between the two other rings in such a way, that self contact of the inner boundary of Ring 2 occurs. Between all possible contact pairings a frictional coefficient of $\mu = 0.3$ is utilized. For the stabilization parameter a value of $\alpha_{\text{stab}} = 0.1$ is chosen. To better compare the deformations with the ones shown in [19], the same time integration method and time step size are utilized. A Newmark time integration method is applied with $\beta = 0.25$ and $\gamma = 0.5$, which is included in the general framework of the Generalized-α method by setting the interpolation parameters to $\alpha_f = 0.0$ and $\alpha_m = 0.0$. The time step size is chosen to be constant with $\Delta t = 0.001\ [ms]$.

In Figure 28 a comparison of the deformed configurations at different time steps is shown. On the left hand side the results from Yang and Laursen [19] are plotted, who use a large deformation mortar contact method and on the right hand side the results from the present work is displayed. The results obtained with the newly developed contact domain method match very well with the ones obtained with the mortar method. In contrast to the "reference" solution, the present algorithm does not need a special contact search algorithm, optimized and adjusted for the treatment of self contact. The detection of possible contact pairs, including self contact, is automatically done with the contact pairing algorithm detailed in section 3.1 without any modifications.

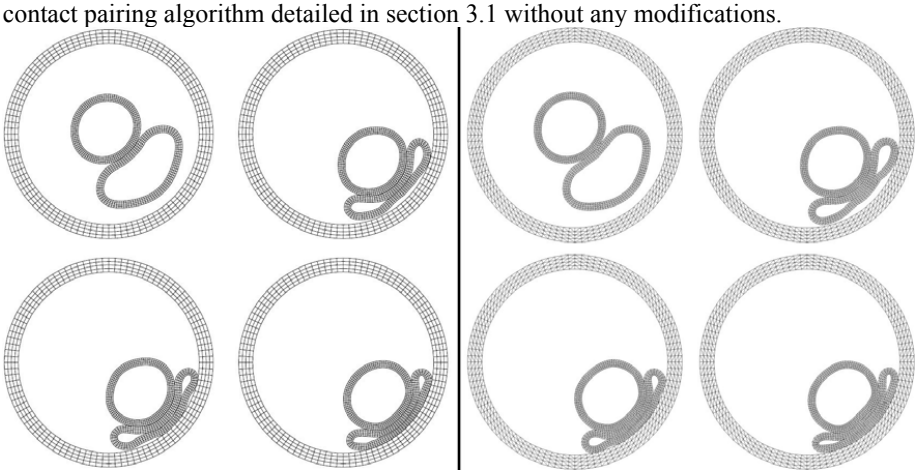

Figure 28: Ring impact: Comparison of deformed configurations at different time steps
Left: Yang and Laursen [19] / right: present work

6.6. Flipper

This example is devised to demonstrate the possibility to capture complex, highly dynamic contact scenarios including various regions with self-contact. In Figure 29 the geometric setup as well as the material properties of the problem is shown. First the tip of the cantilever is moved horizontally by a prescribed displacement $u = 5.0\,\text{mm}$, which is then suddenly released at $t = 10.0\,\text{ms}$. Now the cantilever is free to move and starts swinging around its initial position. On the way back to its initial position, the cantilever hits the elastic disc, which will be accelerated towards the very flexible strip. When the disc gets into contact with the thin strip, this deforms significantly, such that it will get into contact with its own parts. Both the disc and the highly deformed strip are then hitting against the rigid wall, again producing a very difficult contact scenario. The dynamic analysis is performed using the Generalized-α scheme with a spectral radius of $\rho_\infty = 0.85$, which introduces a little bit of numerical dissipation. As the numerical analysis is quite demanding, the time step size was adjusted several times during the calculation in order to capture the physics of the different contact scenarios (cantilever-to-disc, disc-to-strip, strip-to-strip, strip-to-wall). Friction is assumed between all possible contact pairs using $\mu = 0.1$ and the stabilization parameter is set to $\alpha_{\text{stab}} = 0.3$.

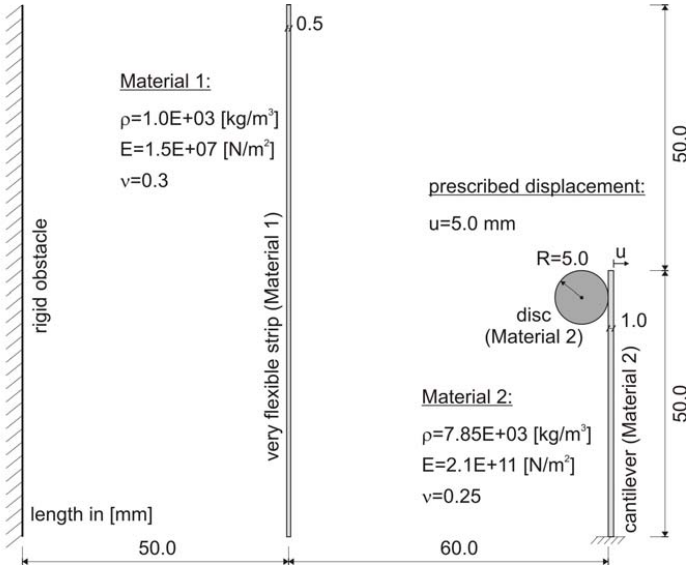

Figure 29: Flipper: Geometry and material properties

In Figure 30 and Figure 31 the complex motion of the problem is shown at different time steps, without and with displaying the constructed contact domain triangulation, respectively. The presented contact algorithm performs very well in this complex dynamic contact problem and can deal with self-contact without any additional difficulty by construction.

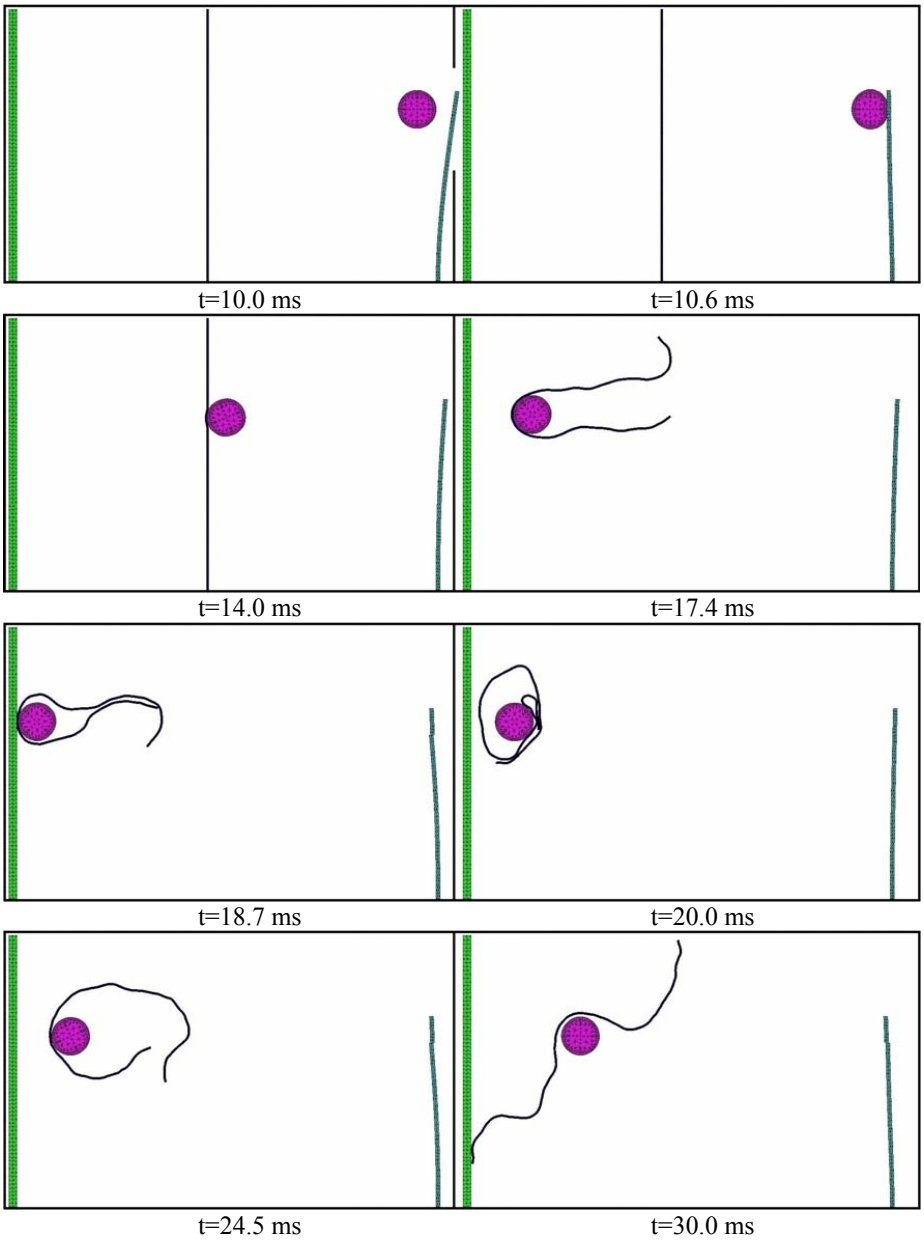

Figure 30: Flipper - Motion: without plotting the contact domain mesh

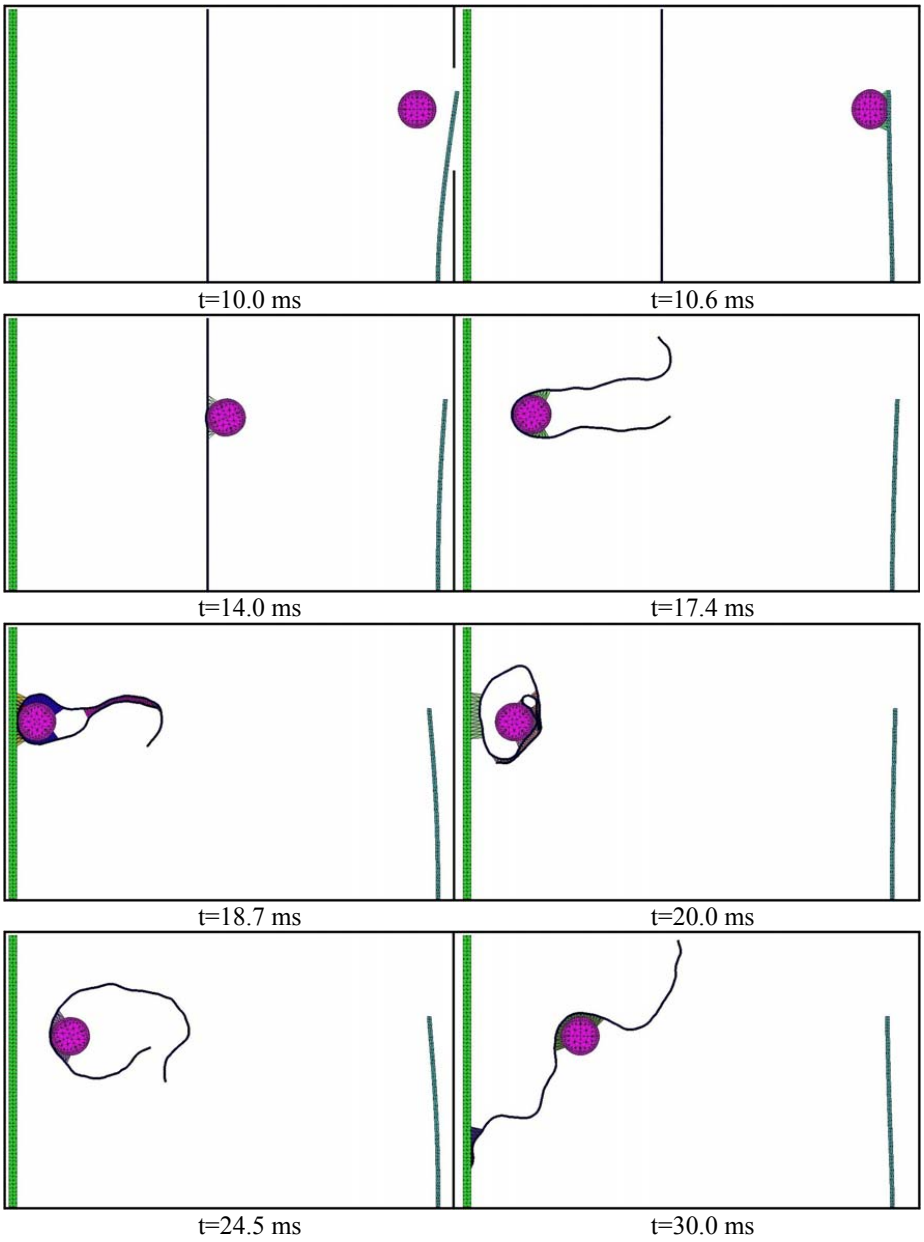

Figure 31: Flipper - Motion: with plotting the contact domain mesh

6.7. Spiral

In this problem, a thin strip is pushed through a tight form in order to be rolled up like a spiral. Therefore large relative tangential sliding as well as multiple self-contact has to be captured by the contact algorithm. The setup of the example, as well as the material

properties of the strip, is shown in Figure 32. Although the form is discretized with finite elements, it is assumed to be rigid, as its all finite element nodes are fixed throughout the whole calculation. The strip is pushed by a prescribed horizontal displacement u_H at its right edge. A dynamic analysis is carried out using the Generalized-α time integration scheme with a spectral radius of $\rho_\infty = 1.0$. In a total calculation time of $t = 60.0$ [ms] a horizontal displacement of $u_H = 60.0\,[mm]$ is prescribed. A constant time step size is chosen to be $\Delta t = 0.05$ [ms]. In the analysis a stabilization parameter of $\alpha_{\text{stab}} = 0.1$ is utilized. Between the contacting boundaries a frictionless contact behavior is assumed.

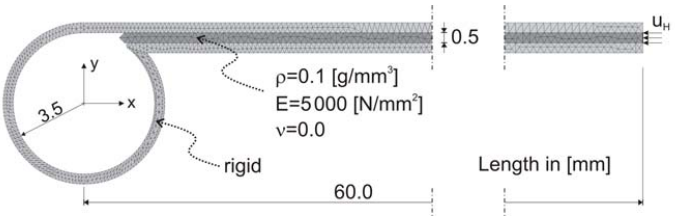

Figure 32: Spiral: Geometry and material properties

The deformed configurations of the spiral problem are shown in Figure 33. It can be seen, that the contact strategy is able to capture the very large relative tangential sliding between the strip and the form as well as between different parts of the strip. Self contact of the strip, even being in contact on both sides of the strip at the same time, is tracked reliably by the present contact formulation.

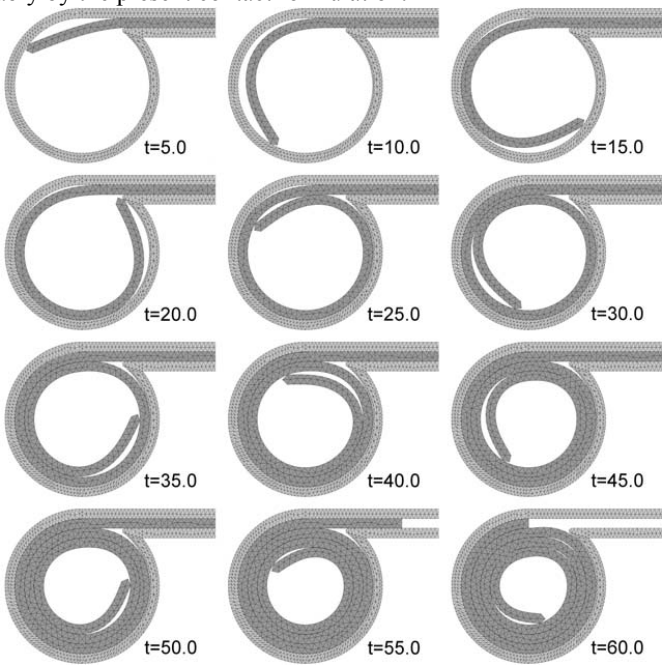

Figure 33: Spiral: Deformed configurations at different time steps (t in [ms])

6.8. Multiple contact

The last example is devised just to demonstrate, that the proposed contact strategy can handle contact scenarios between many contacting bodies without any further modification. Nine geometrical objects are placed randomly as can be seen in Figure 34 inside an elastic boundary. All objects and the boundary have the same elastic properties, given in Figure 34. Some of the objects are arbitrarily accelerated to get into contact with the others. The dynamic calculation is done using the Generalized-α scheme with $\rho_\infty = 1.0$, a stabilization parameter $\alpha_{\text{stab}} = 0.3$, a friction coefficient of $\mu = 0.2$ between all occurring contact pairs and a constant time step of $\Delta t = 0.01\ [ms]$.

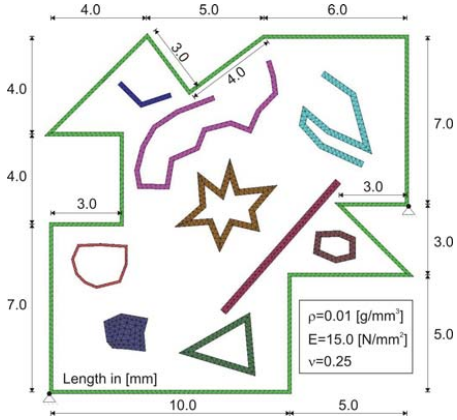

Figure 34: Multiple contacts: Geometry and material properties

In Figure 35 the deformed configurations of the multiple contact problem at different times steps are depicted. The contact algorithm can handle at no difficulty the contact of sharp edges as well as multiple contact pairings of one object with others and with itself. This underlines the powerful contact pairing strategy introduced in section 3.1.

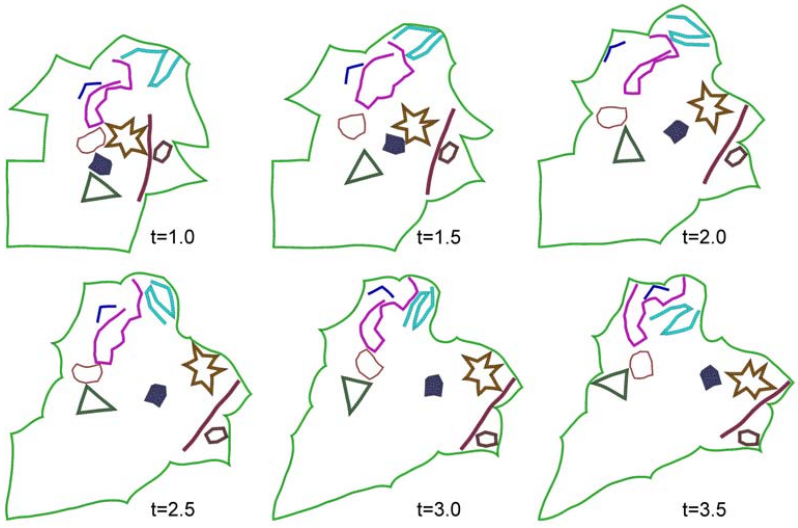

Figure 35: Multiple contact: Deformed configurations at different time steps (t in [ms])

7. CONCLUDING REMARKS

Together with the first part of this paper [13] a new contact strategy is developed to analyze large deformation static and dynamic (self) contact problems. Compared to many existing contact formulations, the presented *contact domain method* varies in many ways. The present formulation produces a solution, which does not dependent on the choice of *slave* and *master* sides, as the contact pairing is uniquely defined via a constraint Delaunay triangulation. Thus, no projections of slave nodes/segments onto master segments have to be performed, circumventing the problem of possible pathological cases. As the Lagrange multipliers are introduced on the newly defined contact domain, the time consuming numerical procedure to evaluate integrals of products of shape functions living on different surface grids involved in the mortar method is omitted. Due to the element-wise constant approximation of the Lagrange multipliers, the stabilized constraint equations can be decoupled and the necessary integrations can be performed analytically. This allows for a very easy implementation of the algorithm and speeds up the computation. The utilized contact pairing strategy displays a unified approach in the context of contact searching algorithms, which does not necessitate any modifications in the treatment of self contact or multiple contacts.

The numerical examples have shown that the *contact domain method* will produce reliable and accurate results. Challenging problems, so far only captured by recently developed mortar based methods, can be calculated with much less numerical costs. Highly dynamic problems involving multiple contacts as well as self contact can be analyzed without any additional modification to the algorithm.

Due to the experience in numerous numerical examples, a stabilization parameter $\alpha_{\text{stab}} \in [0.1 - 0.5]$ can be recommended to produce very good results for most applications. In the case of having very large contact stresses, the stabilization parameter needs to be chosen a little bit smaller to guarantee a sufficiently well enforced geometric contact constraint (see example in section 6.3). However it can be reported, that the numerical analysis is not very sensible to the variations of the stabilization parameter unlike to classical penalty methods. This is due to the fact, that the introduced stabilization displays a consistent, interior penalty method, not suffering from the drawbacks of classical penalty strategies.

Despite the necessary linearization of the first Piola-Kirchhoff stress tensor, the implementation of this contact method is quite simple. The introduced stabilization term, together with an element-wise constant approximation of the introduced Lagrange multipliers allow the local elimination of the discrete Lagrange multipliers on element level. All the necessary integrations can be done analytically, circumventing possible difficulties in performing demanding numerical quadratures. Furthermore, the calculation of the contact forces and the contact stiffness contributions can be carried out locally for every individual contact domain element, which only necessitates some information of the adjacent “body” element. Therefore a parallel implementation of this contact algorithm seems to be quite natural and simple to undertake. This would even speed up this already quite cheap contact formulation.

As the performance of the presented contact strategy is superior to classical node-to-segment formulations, comparable to recently developed mortar based contact algorithms while being less costly, the *contact domain method* displays a sound alternative in the field of computation contact methods.

Acknowledgements

The first author gratefully acknowledges the support of the German Research Foundation through the grant HA 5433/1-1. Furthermore the financial support from the Spanish Ministry of Science and Technology through grant BIA2005-09250-C03-03 is acknowledged.

REFERENCES

[1] Benson D.,Hallquist J. A single surface contact algorithm for the post-buckling analysis of shell structures. *Computer Methods in Applied Mechanics and Engineering*. **78**, 141-163, 1990.

[2] Bruneel H.C.J.,De Rycke I. QuickTrace: a fast algorithm to detect contact. *International Journal for Numerical Methods in Engineering*. **54**, 299-316, 2002.

[3] Chung J.,Hulbert G.M. A Time Integration Algorithm for Structural Dynamics With Improved Numerical Dissipation: The Generalized-alpha method. *Journal of Applied Mechanics*. **60**, 371-375, 1993.

[4] Fischer K.A., Mortar Type Methods Applied to Nonlinear Contact Mechanics, Ph.D. Thesis, Research Report F05/2, Institut für Baumechanik und Numerische Mechanik, Universtität Hannover, Germany. 2005.

[5] Fischer K.A.,Wriggers P. Frictionless 2D Contact formulations for finite deformations based on the mortar method. *Computational Mechanics*. **36**, 226-244, 2005.

[6] Fischer K.A.,Wriggers P. Mortar based frictional contact formulation for higher order interpolations using the moving friction cone. *Computer Methods in Applied Mechanics and Engineering*. **195**, 5020-5036, 2006.

[7] Heintz P.,Hansbo P. Stabilized Lagrange multiplier method for bilateral elastic contact with friction. *Comput. Methods Appl. Mech. Engrg.* **195**, 4323-4333, 2006.

[8] Hertz H. Über die Berührung fester elastischer Körper. *Journal für die reine und angewandte Mathematik*. **92**, 156-171, 1881.

[9] Laursen T.A. *Computational Contact and Impact Mechanics*: Springer, 2002.

[10] Malvern L.E.E. *Introduction to the Mechanics of a Continuous Medium* Prentice-Hall, 1997.

[11] Newmark N. A method of computation for structural dynamics. *Journal of the Engineering Mechanics Division*. **85**, 67-94, 1959.

[12] Oldenburg M.,Larsgunnar N. The position code algorithm for contact searching. *International Journal for Numerical Methods in Engineering*. **37**, 359-386, 1994.

[13] Oliver J.,Hartmann S.,Cante J.C.,Weyler R.,Hernández J. A new approach in computational contact mechanics: the contact domain method. Part 1: thoeretical basis. *Computer Methods in Applied Mechanics and Engineering*. **(submitted)**, 2009.

[14] Puso M.,Laursen T. A mortar segment-to-segment contact method for large deformation solid mechanics. *Computer Methods in Applied Mechanics and Engineering*. **193**, 601-629, 2004.

[15] Wang S.P.,Nakamacki E. The inside-outside contact search algorithm for finite element analysis. *International Journal for Numerical Methods in Engineering*. **40**, 3665-3685, 1997.
[16] Wriggers P. *Computational Contact Mechanics*. 2nd ed. New York: Springer Berlin / Heidelberg, 2006.
[17] Wu J.-H.,Juang C.H.,Lin H.-M. Vertex-to-face contact searching algorithm for three dimensional frictionless contact problems. *International Journal for Numerical Methods in Engineering*. **63**, 876-897, 2005.
[18] Yang B.,Laursen T. A contact searching algorithm including bounding volume trees applied to finite sliding mortar formulations. *Computational Mechanics*. **41**, 189-205, 2008.
[19] Yang B.,Laursen T. A large deformation mortar formulation of self contact with finite sliding. *Computer Methods in Applied Mechanics and Engineering*. **197**, 756-772, 2008.
[20] Yang B.,Laursen T.,Meng X. Two dimensional mortar contact methods for large deformation frictional sliding. *International Journal for Numerical Methods in Engineering*. **62**, 1183-1225, 2005.
[21] Zhong Z.-H.,Nilsson L. A contact searching algorithm for general contact problems. *Computers and Structures*. **33**, 197-209, 1989.

APPENDIX

SPECIFICATION OF THE DERIVATIVE OF THE FIRST PIOLA-KIRCHHOFF STRESS TENSOR FOR A TWO DIMENSIONAL IMPLEMENTATION

The derivative of the first Piola-Kirchhoff stress tensor $\mathbf{P}$ with respect to the discrete nodal displacements $\mathbf{d}_L$ (see equation (185)) reads

$$\frac{\partial \mathbf{P}}{\partial \mathbf{d}_L} = \frac{\partial \left(\mathbf{F} \cdot \mathbf{S} \right)}{\partial \mathbf{d}_L} = \frac{\partial \mathbf{F}}{\partial \mathbf{d}_L} \cdot \mathbf{S} + \mathbf{F} \cdot \frac{\partial \mathbf{S}}{\partial \mathbf{d}_L} \tag{209}$$

It involves the derivative of the material deformation gradient $\mathbf{F}$ as well as the derivative of the second Piola-Kirchhoff stress tensor $\mathbf{S}$. The linearization of the second Piola-Kirchhoff stress tensor can be written as

$$\Delta \mathbf{S} = \square^{\text{tang}} : \Delta \mathbf{E} \;\rightarrow\; \frac{\partial \mathbf{S}}{\partial \mathbf{d}} \cdot \Delta \mathbf{d} = \square^{\text{tang}} : \frac{\partial \mathbf{E}}{\partial \mathbf{d}} \cdot \Delta \mathbf{d} \tag{210}$$

where $\square^{\text{tang}}$ is the 4th order constitutive tangent operator, which relates the incremental second Piola-Kirchhoff stresses $\Delta \mathbf{S}$ with the incremental non-linear Green-Lagrange strains $\Delta \mathbf{E}$. With equation (210) the derivative of $\mathbf{P}$ in equation (209) may be expressed with

$$\frac{\partial \mathbf{P}}{\partial \mathbf{d}_L} = \frac{\partial \mathbf{F}}{\partial \mathbf{d}_L} \cdot \mathbf{S} + \mathbf{F} \cdot \square^{\text{tang}} : \frac{\partial \mathbf{E}}{\partial \mathbf{d}_L} \tag{211}$$

and in indicial notation with

$$\frac{\partial P_{ij}}{\partial d_{L_p}} = \frac{\partial F_{ik}}{\partial d_{L_p}} S_{kj} + F_{il} \square^{\text{tang}}_{ljno} \frac{\partial E_{no}}{\partial d_{L_p}} \tag{212}$$

Using a two dimensional, 3-noded finite element formulation, the approximations of the Green-Lagrange strain tensor for a finite element Ω_e is

$$\mathbf{E} = \begin{pmatrix} E_{11} & E_{12} \\ E_{21} & E_{22} \end{pmatrix} = \frac{1}{2}\left(\mathbf{F}_e^T \mathbf{F}_e - \mathbf{1}\right) \tag{213}$$

with the elemental material deformation gradient

$$\mathbf{F}_e = \begin{pmatrix} F_{11} & F_{12} \\ F_{21} & F_{22} \end{pmatrix} = \sum_{L=1}^{3} \begin{pmatrix} x_{L_1} N_{L,1} & x_{L_1} N_{L,2} \\ x_{L_2} N_{L,1} & x_{L_2} N_{L,2} \end{pmatrix} \tag{214}$$

Herein $N_{L,\alpha}$ are the derivatives of the shape functions with respect to α, and $x_{L_\alpha} = X_{L_\alpha} + d_{L_\alpha}$ are the nodal coordinates of the current (spatial) configuration, where X_{L_α} are the nodal coordinates of the reference (material) configuration and d_{L_α} are the nodal displacements. Thus the derivatives of the deformation gradient are

$$\begin{aligned} &\frac{\partial F_{11}}{\partial d_{L_1}} = N_{L,1} \;\; ; \;\; \frac{\partial F_{11}}{\partial d_{L_2}} = 0 \\ &\frac{\partial F_{12}}{\partial d_{L_1}} = N_{L,2} \;\; ; \;\; \frac{\partial F_{12}}{\partial d_{L_2}} = 0 \\ &\frac{\partial F_{21}}{\partial d_{L_1}} = 0 \;\; ; \;\; \frac{\partial F_{21}}{\partial d_{L_2}} = N_{L,1} \\ &\frac{\partial F_{22}}{\partial d_{L_1}} = 0 \;\; ; \;\; \frac{\partial F_{22}}{\partial d_{L_2}} = N_{L,2} \end{aligned} \tag{215}$$

The components of the Green-Lagrange strains (see equation (213)) are

$$\begin{aligned} E_{11} &= \frac{1}{2}\left(F_{11}^2 + F_{21}^2 - 1\right) \\ E_{12} = E_{21} &= \frac{1}{2}\left(F_{11}F_{12} + F_{21}F_{22}\right) \\ E_{22} &= \frac{1}{2}\left(F_{12}^2 + F_{22}^2 - 1\right) \end{aligned} \tag{216}$$

and their derivatives are

$$\begin{aligned} \frac{\partial E_{11}}{\partial d_{L_\alpha}} &= \frac{1}{2}\left(2F_{11}\frac{\partial F_{11}}{\partial d_{L_\alpha}} + 2F_{21}\frac{\partial F_{21}}{\partial d_{L_\alpha}}\right) \\ \frac{\partial E_{12}}{\partial d_{L_\alpha}} = \frac{\partial E_{21}}{\partial d_{L_\alpha}} &= \frac{1}{2}\left(\frac{\partial F_{11}}{\partial d_{L_\alpha}}F_{12} + F_{11}\frac{\partial F_{12}}{\partial d_{L_\alpha}} + \frac{\partial F_{21}}{\partial d_{L_\alpha}}F_{22} + F_{21}\frac{\partial F_{22}}{\partial d_{L_\alpha}}\right) \\ \frac{\partial E_{22}}{\partial d_{L_\alpha}} &= \frac{1}{2}\left(2F_{12}\frac{\partial F_{12}}{\partial d_{L_\alpha}} + 2F_{22}\frac{\partial F_{22}}{\partial d_{L_\alpha}}\right) \end{aligned} \tag{217}$$

Inserting equation (215) into (217) yields

$$\begin{aligned} &\frac{\partial E_{11}}{\partial d_{L_1}} = F_{11}N_{L,1} \;\; ; \;\; \frac{\partial E_{11}}{\partial d_{L_2}} = F_{21}N_{L,1} \\ &\frac{\partial E_{12}}{\partial d_{L_1}} = \frac{\partial E_{21}}{\partial d_{L_1}} = \frac{1}{2}\left(F_{11}N_{L,2} + F_{12}N_{L,1}\right) \;\; ; \;\; \frac{\partial E_{12}}{\partial d_{L_2}} = \frac{\partial E_{21}}{\partial d_{L_2}} = \frac{1}{2}\left(F_{21}N_{L,2} + F_{22}N_{L,1}\right) \\ &\frac{\partial E_{22}}{\partial d_{L_1}} = F_{12}N_{L,2} \;\; ; \;\; \frac{\partial E_{22}}{\partial d_{L_2}} = F_{22}N_{L,2} \end{aligned} \tag{218}$$

With these specifications, the derivative of the first Piola-Kirchhoff stress tensor, given in equation (212) can be computed.